Stony Brook University

An *ex vivo* femoral artery model to demonstrate inflammatory response and monocyte response following increased vascular wall shear stress

A Dissertation Presented

by

Aparna Kadam Baldwin

In completion of Requirements

for the Degree of

Doctor of Philosophy

in

Biomedical Engineering

Stony Brook University

December 2013

Stony Brook University

The Graduate School

Aparna Kadam Baldwin

We, the dissertation committee for the above candidate for the

Doctor of Philosophy degree, hereby recommend

acceptance of this dissertation.

Dr. Mary D Frame – Dissertation Advisor
Biomedical Engineering

Dr. Richard A F Clark - Chairperson of Defense
Biomedical Engineering

Dr. David Rubenstein
Biomedical Engineering

Dr. Todd K Rosengart
Cardiothoracic Surgery, Baylor College of Medicine

This dissertation is accepted by the Graduate School

Charles Taber
Interim Dean of the Graduate School

Abstract of the Dissertation

An *ex vivo* femoral artery model to demonstrate inflammatory response and monocyte response following increased vascular wall shear stress

by

Aparna Kadam Baldwin

Doctor of Philosophy

in

Biomedical Engineering

Stony Brook University

2013

Background Vascular remodeling reestablishes blood flow in the case of occlusions and can save tissue that would otherwise become hypoxic and necrotic. Vascular growth in an adult can occur in two ways: angiogenesis and/or arteriogenesis. While some pathways that govern the two are similar, the triggers have been found to be distinct. This study focuses on arteriogenesis- believed to be triggered by increases in wall shear stress (WSS) due to arterial occlusion. **Hypothesis** Inflammatory response will be initiated in an *ex vivo* femoral artery model in response to an increase in WSS. The inflammatory response will be detected by increases in TNFα, MCP-1, IL-2, P-Selectin, ICAM-1 and VCAM-1 expression. Inflammation alone (TNFα or shear stress induced) is not sufficient to initiate collateral vessel growth; monocyte recruitment and adhesion are required to see changes in vasculogenic growth factors VEGF, FGF-2, TGFβ and Egr-1. **Methodology** C57BL/6 mice will be used in an *in vivo* femoral artery excision model to study inflammatory response, monocyte recruitment, and vascular remodeling over 3 days post-occlusion. *Ex vivo* studies will then use isolated perfused femoral artery to show the monocyte adhesion cascade and collateral vessel initiation under inflammatory conditions, specifically inflammation caused by an increase in vascular WSS. **Results/Conclusions:** *In vivo* femoral artery excision (FAE) studies show significant increases in cytokines, adhesion molecules, monocytes and growth factors in the FAE samples over the contralateral. Inflammatory cytokines are expressed almost immediately after FAE in mouse. The resulting monocyte recruitment gives way to extravasation and proliferative arteriogenesis. The following *ex vivo* studies successfully defined a model for studying changes in WSS *ex vivo*, and show that the artery behaves by upregulating markers consistent with *in vivo* when subject to increases in WSS. Finally the perfusion of monocytes through the vessel results in adhesion when the endothelium is expressing inflammatory markers. The *ex vivo* femoral artery model can be used in future studies for longer time course analysis for vessel sprouting, as well as for studying inflammatory conditions initiated and treated in many different ways other than WSS.

Dedication

To family, teachers, and friends
who taught me to be curious, ask questions,
seek answers and follow dreams

TABLE OF CONTENTS

ABBREVIATIONS AND SYMBOLS

CAD	coronary artery disease
CVD	cardiovascular disease
DMEM	Dulbecco's Modified Eagle Medium
Egr-1	early growth response protein-1
eNOS	endothelial nitric oxide synthase
FACS	Fluorescence-activated cell sorting
FAE	femoral artery excision
FBS	fetal bovine serum
FGF-2	fibroblast growth factor-2
GM-CSF	Granulocyte-macrophage colony-stimulating factor
GPCR	G-protein coupled receptor
HA	hyaluronan
HABP	hyaluronan binding protein
HBSS	HEPES buffered salt solution
HEPES	4-2-hydroxyethyl-1-piperazineethanesulfonic acid
HS	heparan sulfate
ICAM-1,2	intracellular adhesion molecule-1,2
IL-2	interleukin-2
IPA	isopropyl alcohol
JAM-A,B,C	junctional adhesion molecule-A,B,C
LDI	Laser Doppler imaging
LDL	low-density lipoprotein
LFA1	lymphocyte function associated antigen-1
MCP-1	monocyte chemoattractant protein-1
MMP	matrix metalloproteinases
NO	nitric oxide
PAD	peripheral artery disease
PDGF	platelet derived growth factor
PECAM-1	platelet endothelial cell adhesion molecule-1
PFA	paraformaldehyde
qPCR	quantitative polymerase chain reaction
RPM	revolutions per minute
RT	reverse transcriptase
SMA	smooth muscle actin
TBS	tris buffered saline
TBST	tris buffered saline + 0.1% tween-20
TGFβ	transforming growth factor-β
TNFα	tumor necrosis factor-α
TRPV4	transient receptor potential vanilliod-4
VLA4	very late angtigen-4
VCAM-1	vascular cell adhesion molecule-1
VEGF	vascular endothelial growth factor
VSMC	vascular smooth muscle cell
WSS	wall shear stress
A	area= πR^2
$\dot{m}$	flow rate
η	viscosity
ρ	density
P	pressure
$\dot{Q}$	flow rate
R	radius = ½ diameter
τ_θ	circumferential shear stress
τ_w	wall shear stress
U	universal heat transfer coefficient

LIST OF FIGURES

LIST OF TABLES

ACKNOWLEDGEMENTS

First and foremost I would like to acknowledge Dr. Mary Frame, my ever patient and encouraging thesis advisor. I came into her lab thinking I wanted to do one thing, and this here is the *third* project that finally stuck. She let me find my way giving all the appropriate nudges as needed. She let me be lost and figure problems out for myself, while always making her support clear. I am a better student, teacher, scientist, engineer and overall thinker because of her tutelage.

Along the path to being here presenting this dissertation, there were many people that influenced, inspired and drove me to become who I am today. Dr. Michael Hadjiargyrou, for teaching a young high school student to question and wonder. David Konatsu and Robert Gersch for being excellent graduate student mentors. All my fellow graduate students, especially Danielle, Andrea, Gabriel, Dana- this process is one that requires support and commiseration that can only be understood by those in the "same boat" and you have all been there for all those times.

An extra thank you to Robert Gersch, for his guidance and mentorship specifically throughout this thesis study. Also, through my research endeavors from high school though my doctorate Rob has shown me that science as a whole is an exciting place that can stay fun for a long time, and something that will keep teaching you forever.

A huge thank you to my family both immediate and extended. I am fortunate enough to have grown up with parents and siblings who have been supportive through every endeavor I have undertaken and this is no exception. Also, thank you to Travis and my in-laws for the continued support.

There are really too many people to thank along the road of getting to this point—family, friends, teachers, mentors. I am grateful for everyone who has played a role in encouraging, pushing, and questioning me so that I could have faith in my abilities to attain the goal that I set so many years ago of being a scientist when I "grew up".

CHAPTER 1
LITERATURE REVIEW AND INTRODUCTION

CARDIOVASCULAR DISEASE AND BLOCKAGES

An estimated 82.6 million American adults have 1 or more types of cardiovascular disease (CVD), of which 16.3 million have coronary artery disease (CAD) and 8 million have peripheral arterial disease (PAD), according to the American Heart Association 2012 Heart Disease and Stroke Update[3]. CVD was the underlying cause of over 30% of all deaths in 2008, and has been the leading cause of deaths every year since 1900[3]. Of the deaths caused by CVD, nearly 50% are attributed to CAD and another 3.4% to other diseases of the arteries, which includes PAD. In the United States 7% of adults ≥ 20 years of age have CAD and 12-20% of adults ≥ 65 years of age have PAD[3]. Collateral vessel formation is critical to the survival of patients with CVD, and the reason that many of them survive to the point of diagnosis. Describing the mechanisms behind collateral vessel growth is important in their implications for therapeutic potential.

Arteriosclerosis

CAD and PAD, although classified as distinct diseases, have the same pathology in that they refer to arteriosclerosis. The difference is that in CAD the affected arteries feed the heart directly, while in PAD the arteries supply the peripheral circulation. Arteriosclerosis, also called, atherosclerosis, occurs when fat, cholesterol, and other substances build up in the arteries forming plaques[4]. Specifically, low-density lipoprotein (LDL) is retained in artery walls and the lipid portion begins to oxidize[5]. This atherosclerotic, or pre-atherosclerotic, tissue recruits monocytes (but not neutrophils) that bind to the endothelial cells. The monocytes differentiate into macrophages and lend their oxidative capacity to further oxidize the lipid and also the protein in LDL[4,6]. The modified protein becomes unrecognizable to the LDL receptor and shift to recognition by scavenger receptors (macrophages). This change results in the cellular uptake by receptors that are unable to moderate the cholesterol content of the cell and thus a massive accumulation of

cholesterol[4]. These fatty macrophages are what initially comprise what is called the "fatty streak". These lesions progress towards plaque formation and their arterial calcification which changes the mechanical characteristics of the artery wall predisposing it to rupture[7]. When these plaques rupture they release tissue factor, which is a potent coagulant that when exposed to the flowing blood will result in clotting that will induce a clinical event[4].

The chronic state of inflammation by macrophage accumulation, along with increased cholesterol deposition and clotting causes a thickening and constriction of the vessel and ultimately thrombosis[4]. The resulting hardening and narrowing of the arteries reduces or blocks blood flow to downstream vessels, depriving the target tissue of needed oxygen and nutrients. This type of occlusions can result in tissue damage and death of muscle or nerves and can cause heart attacks or loss of function in the extremities. Collateral blood vessels are arteries that naturally grow to by-pass these types of occlusion sites; these are the focus of this study. For the purpose of this study arterioles will be defined as preexisting blood vessels with a smooth muscle cell sheath, and collaterals as blood vessels that form via angio/arteriogenesis to circumvent arterial occlusion and reestablish blood flow; these vessel can be capillaries or arterioles

Current Treatments

Current treatments include both medication and surgical options coupled with lifestyle changes in diet and exercise[8]. Cholesterol medications that aggressively reduce LDL levels are often prescribed and can help slow or even reverse the arteriosclerosis[9]. Statins are a class of drugs that inhibit the synthesis of cholesterol in the liver and increase the uptake of LDL to draw it out of the circulation. Fibrates also draw out LDL from the circulation by forming LDL with a higher affinity for LDL receptor, additionally they increase plasma HDL levels and facilitate more efficient

reverse cholesterol transport. While these drugs are effective they do come with side effects such as diabetes, myopathy, risk of gall stones, and acute renal failure.

Anti-platelet, beta blockers, angiotensin-converting enzyme inhibitors, and calcium channel blockers all aim to mitigate the risks involved with arteriosclerotic conditions[9]. They reduce the chances of increased blockage, control blood pressure, and reduce heart rate, to lower the chances of embolisms, heart rhythm issues and heart attacks. They are not able to reverse the arteriosclerotic condition.

In the cases of severe occlusions, surgical interventions are employed. Angioplasty and stent placement compresses the deposits outward into the vessel wall expanding the passage and a stent is left in place to keep the vessel open[9]. While this is effective, restenosis is a major and common downstream risk. Endarterectomy and thrombolytic therapy are the surgical removal of fatty deposits and blood clots from the walls of the artery, respectively[9]. These again, are susceptible to reoccurrence if not coupled effectively with lifestyle changes.

Finally, by-pass, is the option to use a synthetic or grafted vessel to create a route for blood flow around the occluded artery[9,8]. This is the intervention that mimics the body's natural response to occlusion of creating collateral vessels. This is an effective route when a major occlusion is identified and several by-passes can be done at one time. However, if the patient has multiple partial occlusions, especially in the periphery this is not a practical solution. This study aims to understand the mechanisms behind the generation of natural "by-pass" collaterals.

VASCULAR GROWTH

Vasculature in a developed postnatal mammal is thought to be relatively stable. In response to tissue injury or pathological conditions such as these arterial occlusions, the body has adaptive abilities to compensate for reduced blood flow by creating collateral vessels[2]. The process for vasculogenesis is seen in *figure 1*. It starts with endothelial proliferation dependent on FGF-2 and driven by VEGF. The proliferating endothelial cells then recruit mural cells (cells within the wall of the blood vessel) by secreting PDGF-B, and through the TGFβ signaling pathway form the smooth muscle cell vessel wall of mature arteries, arterioles, veins and venules[2,10].

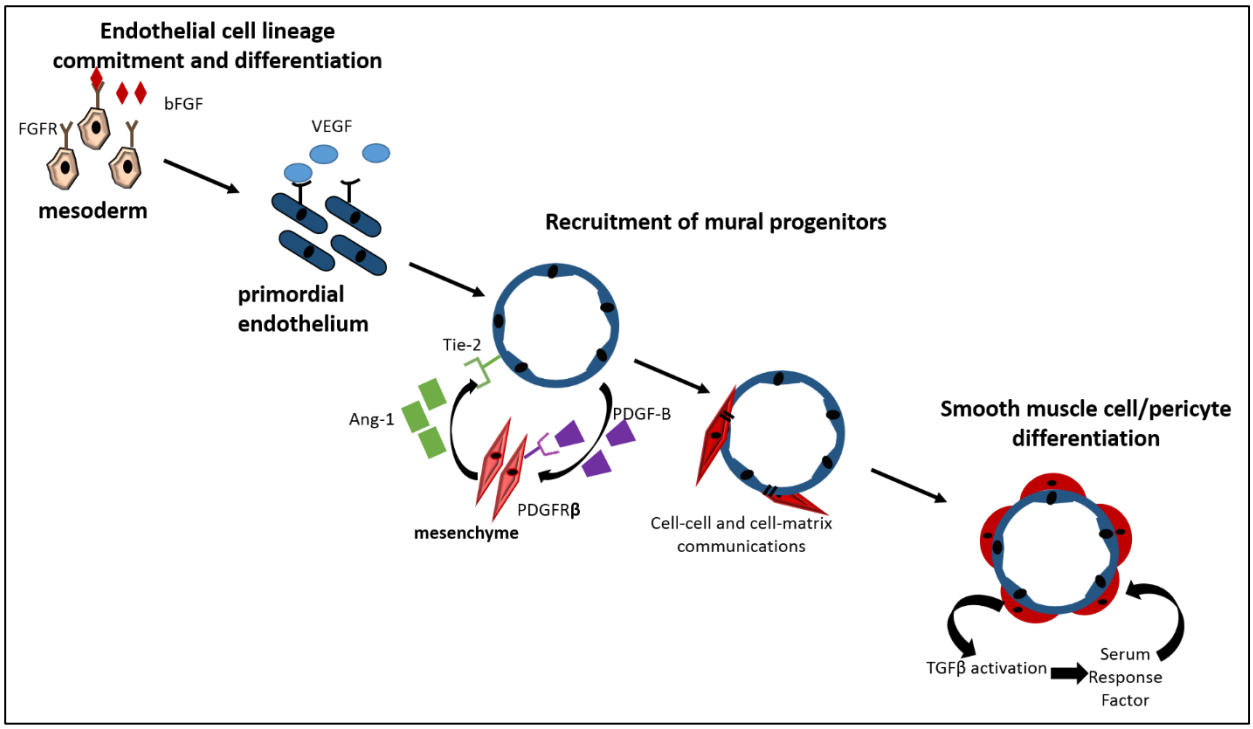

Figure 1. *This schematic shows the embryonic development of vessels [2]. The presence of FGF-2 (bFGF) in the mesoderm cells commits the cells towards the endothelium lineage. VEGF then mediates the cell migration and tube formation. PGF-B then acts as a chemoattractant for mural cells. Through TGFβ the mural cells interact with the endothelial cells to mature to a smooth muscle cell/pericyte phenotype.*

Angiogenesis

In an adult, vascular growth occurs in one of two ways; angiogenesis and arteriogenesis. **Angiogenesis** is characterized by the hypoxia induced, VEGF signaling driven, *de novo* sprouting of capillaries that are formed from endothelial cells. These initial capillaries then elongate and sprout to generate capillary networks[11,12]. **Arteriogenesis (collateralization)** is vascular growth stemming from the remodeling of pre-existing arterioles with multiple triggers and signaling pathways that remain to be defined. Collaterals form primarily via the process of arteriogenesis. The growth factors involved with angiogenesis and arteriogenesis do overlap, specifically VEGF, FGF-2 and TGFβ, but the conditions that initiate the processes distinguish the two. Further, vessels formed via angiogenesis start as capillaries (lacking smooth muscle cell sheath), whereas arteriogenesis is the remodeling of mature blood vessel including smooth muscle sheath.

The femoral artery occlusion model has become a popular model for elucidating the mechanisms associated with vascular growth at occlusion sites[13-20]. These models induce an occlusion in the femoral artery of a murine model downstream of the inguinal ligament either by ligation or excision[1]. Femoral artery occlusion studies distinctly show that the location of angiogenesis and arteriogenesis have disparate locations and independent triggers[21]. Specifically, arteriogenesis/collateral vessels form in the upper leg close to the site of occlusion between proximal and side branches, whereas angiogenesis occurs in the lower leg and foot, a great distance distal to the site of occlusion in regions of ischemia[13,19,20,22]. Further, capillaries formed by angiogenesis, regardless of number, will be limited by their lumen size in providing adequate relief—they can maximally increase blood flow by 1.5 to 1.7 fold[21]. On the other hand arteriogenesis can maximally increase blood flow by 10 to 20 fold, indicating that only collateral

vessels that form from the proliferation of preexisting arteriolar connections, may reestablish enough blood flow to the compensate for the occluded artery[21].

Arteriogenesis/Collateral formation

The trigger for angiogenesis is largely accepted to be ischemia; the trigger for arteriogenesis is still a subject of much debate and is more complicated. There are three major schools of thought behind arteriogenic growth—*de novo* sprouting, differentiation of capillaries into arteries, and remodeling of pre-existing collateral networks,

Speculation regarding the *de novo* formation of collateral vessels stems from studies in occlusion models where there was a transient increase in capillary density that was followed by an increase in arterioles. This implies that the new collateral vasculature started as angiogenic capillaries that quickly matured into arteries[23,24]. Other evidence suggests that capillaries recruit smooth muscle cells to mature into arterioles in the skeletal muscle surrounding the occlusion[25]. Perhaps the strongest support for collateral growth originating from capillaries is the development of angiographically visible bridging collateral vessels[23]. In all these cases, however, is it possible that the vessels seen are related to pre-exiting arteriole vessels since prior to the insult/occlusion the vessels would have been very small (not angiographically visible), and conducting minimal flow[23]. While there is some *de novo* growth of collateral vessels, the significance of its contribution to the revascularization and restoration of blood flow versus the arterialization of the existing collateral networks still remains to be seen[23].

Pre-existing arteriolar collateral networks are known to exist and are potential sites for full collateral growth. In the absence of stimulus, these networks receive minimal nutritive flow until they are needed[23]. Mechanical effects of increased blood flow comprise the leading hypotheses

regarding triggers for collateral growth in these collateral networks. The focus of this study will be on the collateral growth of existing networks and vessels, the driving mechanisms for the growth, and models to use in order to study them.

MECHANOTRANSDUCTION

Mechanical stimuli of arteriogenesis

In the case of a partial or full occlusion of an artery, distally the transmural (static) arterial blood pressure drops, resulting in a dynamic pressure gradient axially along the preexisting collateral vessels which increases the flow in the these arteries[23]. The increase in blood flow causes an increase in wall shear stress which is defined by equation *(1)* derived from the Hagen-Poisseuille equation:

$$\tau_{\omega} = \frac{4\eta\dot{Q}}{\pi R^3} \quad (1)$$

where τ_{ω}= wall shear stress (WSS) η= viscosity, $\dot{Q}$= flow rate, and R= internal radius of the vessel[26,27]. Physiological wall shear stress (WSS) in an artery ranges from 10-40dynes/cm^2, depending on size and location of vessel, and is often used to emulate WSS of a normal vessel[28,29]. It has been suggested that an increase in WSS from this baseline stress triggers collateral remodeling, which continues until the WSS is normalized; implying that WSS is a major driving force for arterial remodeling[30-32].

Initially in response to chronically high WSS there is a thinning of the endothelial layer that activates the endothelium. With continued chronically elevated WSS there is an increased outward pressure (static pressure) on the vessel wall and overall thinning of the whole arterial vessel[33]. This

outward force is known as circumferential wall stress and is defined in equation *(2)* by Laplace's Law as:

$$\sigma_\theta = \frac{PR}{t} \quad (2)$$

where σ_θ= circumferential stress, P= is transmural pressure, R= internal radius of the vessel, and t= wall thickness[27]. From this it can be see that the initial thinning of the endothelium will result in an increase of circumferential stress. The sustained increase in WSS on the endothelium is a proliferative stimulus for outward remodeling, including endothelial growth (triggered by wall shear stress) and wall thickening by smooth muscle proliferation (triggered by circumferential stress)[27,30,32].

High shear stress has been further shown to have therapeutic potential. *In vivo* experiments by Shaper et. al. created an AV shunt that generated very high shear stress in the collaterals, the results showed that the high shear stress allowed the collateral conductance to reach 80% opposed to the 33% obtained from natural response to occlusion[21]. The increase of the flow in the arterial lumen, subsequent WSS is directly in contact with the endothelium, and resulting circumferential stress that activates the smooth muscle cells, all plays an important role in the remodeling process in detecting the mechanical stimuli[23,34]. The way in which the shear stress is translated to the endothelium is controversially discussed and includes protein kinases, stretch sensitive ion channels, and the phosphorylation of focal adhesions[19,33].

Mechanism of mechanosensing on the vascular endothelium

The central hypothesis to this study is that increasing wall shear stress results in collateral formation; key players in this type of mechanotransduction are the caveolae, endothelial

glycocalyx, and the transient receptor potential vanilliod-4 (TRPV4) Ca^{2+} channel [35]. When exposed to WSS, endothelial cells express varying amounts of adhesion molecules within the glycocalyx[36]. Shear stress also is known to cause endothelial cell release of nitric oxide (NO), which is largely accepted to be mediated by an increase in intracellular Ca^{2+} and the Ca^{2+}/calmodulin-dependent activation of endothelial nitric oxide synthase (eNOS)[37,38].

Caveolae are flask-shaped invaginations on the surface of many cells including endothelial cells and smooth muscle cells. In the presence of fluid shear stress induction there in an increase of caveolae density at the luminal plasma membrane. It is thought that the calveoli can directly activate shear sensitive molecules such as ERK and eNOS, or that through mechanotransmission by the cytoskeleton the signal is translated to other down-stream players.

Glycocalyx is a carbohydrate rich layer, of constantly dynamic self-assembling 3D mesh of polysaccharides that lines the endothelium[36]. Glycoproteins and proteoglycans are considered to be the backbone molecules of the glycocalyx[36]. Glycoproteins are largely endothelial cell adhesion molecules such as selectins, ICAM, VCAM-1, PECAM-1. The expression of these molecules is dynamic and dependent on the ever changing conditions of the vasculature. The dynamic abilities of the glycocalyx have been further shown to have vasculoprotective properties[39]. The core protein groups for proteoglycans are syndecans and glypicans, both of which can bind to five different of glycosaminoglycan chains-- heparan sulfate (HS), chondroitin sulfate, dermatan sulfate, keratan sulfate, and hyaluronan (HA)[36]. In vasculature, heparan sulfate proteoglycans represent roughly 50–90% of the total amount of proteoglycans present in the glycocalyx[40,41].

Studies suggest that the perturbation of endothelial glycocalyx by atherogenic stimuli increases vascular permeability and adhesiveness of platelets and leukocytes to the cell surface. *In vitro*

studies show that an increase in shear increases the amount of HA, which may be an indication of shear sensing by the endothelium[42]. Further, studies show that glycocalyx thins by almost 6 fold from ~400nm to ~70nm when comparing glycocalyx in a mouse common carotid artery with laminar flow versus at the carotid bifurcation where there is disturbed laminar and higher shear[43]. This thickness can be examined by measuring the distance between the proteoglycans and the nuclei. Since the glycocalyx houses adhesion molecules critical to vascular remodeling, how it changes in response to shear is very important.

TRPV4 channels are Ca^{2+} channels that can be activated in many ways which include osmotic stress and shear stress[44-46]. In quiescent endothelial cells TRPV4 has the important function of mediating vasomotion. Studies have found that the mRNA transcription for this channel is constantly upregulated in wall shear stress induced collaterals when there is arterio-venous shunting (AV-shunt) in place inducing prolonged high shear[47]. Without the AV-shunt increasing and prolonging the wall shear stress in a femoral ligation model, TRPV4 is still transiently expressed, but drops to control levels 5 days post occlusion[47]. The comparison between TRPV4 expression in artificially induced prolonged high fluid WSS versus WSS under normal occlusion conditions confirms the dependence of its expression on shear levels[47]. Further, chronic stimulation by TRPV4 is shown to cause the proliferation of vascular cells. This supports that the positive feedback of TRPV4 expression leads to an increase in responsiveness to WSS ultimately pushing the cells beyond vasodilation into the active growth of vasculature[47]. The importance of TRPV4 dependence on WSS lays in the downstream signaling. Upon activation various Ca^{2+} -dependent mechanisms play roles in transducing the signal for vasodilation; specific to collateral growth is nitric oxide (NO) derived from the Ca^{2+}/calmodulin-dependent activated eNOS[47]. In NO-knockout models, there is a strong anti-arteriogenic response recovery of blood flow after

hind-limb ischemia induction is impaired[48]. As a result, it stands that TRPV4 induced growth of smooth muscle cells in collateralization acts through NO by mediating the initial required increase in Ca^{2+} to activate the eNOS enzyme[49]. Thus, TRPV4 is an endothelial membrane bound protein that is a mediator of WSS, and when activated is a trigger for collateral growth.

Mechanotransduction of WSS stimuli occurs through endothelium based molecules in the glycocalyx to express adhesion molecules and TRVP4 Ca^{2+} channels to initiate the NO-pathway. These stimuli reach the nucleus and activate transcription factors such as *Egr-1* (early growth response protein-1) that then trigger chemokines (i.e. MCP-1) and adhesion molecules (i.e. ICAM-1, VCAM-1) that are needed to recruit monocytes to progress down the arteriogenic path.

Endothelial Cell and Smooth Muscle Cell Signal Transduction

While there are many paths of sensing WSS, it is widely accepted that the subsequent activation of eNOS and the production of NO by the endothelium leads to a signaling cascade (*figure 2*)[49]. Following NO production a complex of PECAM-1, VEGFR2 and Ecadherin is expressed called Tsima[50]. Between this complex, the NO induced production of VEGF, and the activated ion channels, the osmotic regulation of the endothelium is disturbed. The activated endothelium is more permeable and expresses various adhesion molecules (Selectins, VCAM, ICAM), chemoattractants (MCP-1, TNFα), growth factors (VEGF, TGFβ), and transcription factors (CARP, Klf2, EGR-1), defining a synthetic phenotype in endothelial cells[51].

The vascular smooth muscle cells, likewise, undergo a phenotypic change through a signaling cascade initiated by triggering FGFR or PDGFR. Specifically, the ligation of these receptors results in the activation of the Ras/MEK/ERK pathway and the upregulation of the transcription

factors CAPR, SRE and Egr-1[52]. Ultimately this results in a synthetic phenotype for VSMC including upregulation of Cx37 and Tmsb4 and a down regulation of desmin.

The link between the endothelium activation and the VSMC activation is of great interest in the absence of cell to cell junctions given the barrier of the internal elastic lumina and the short reach of NO[51]. It becomes important to note now, that the synthetic endothelium is upregulating uPa and

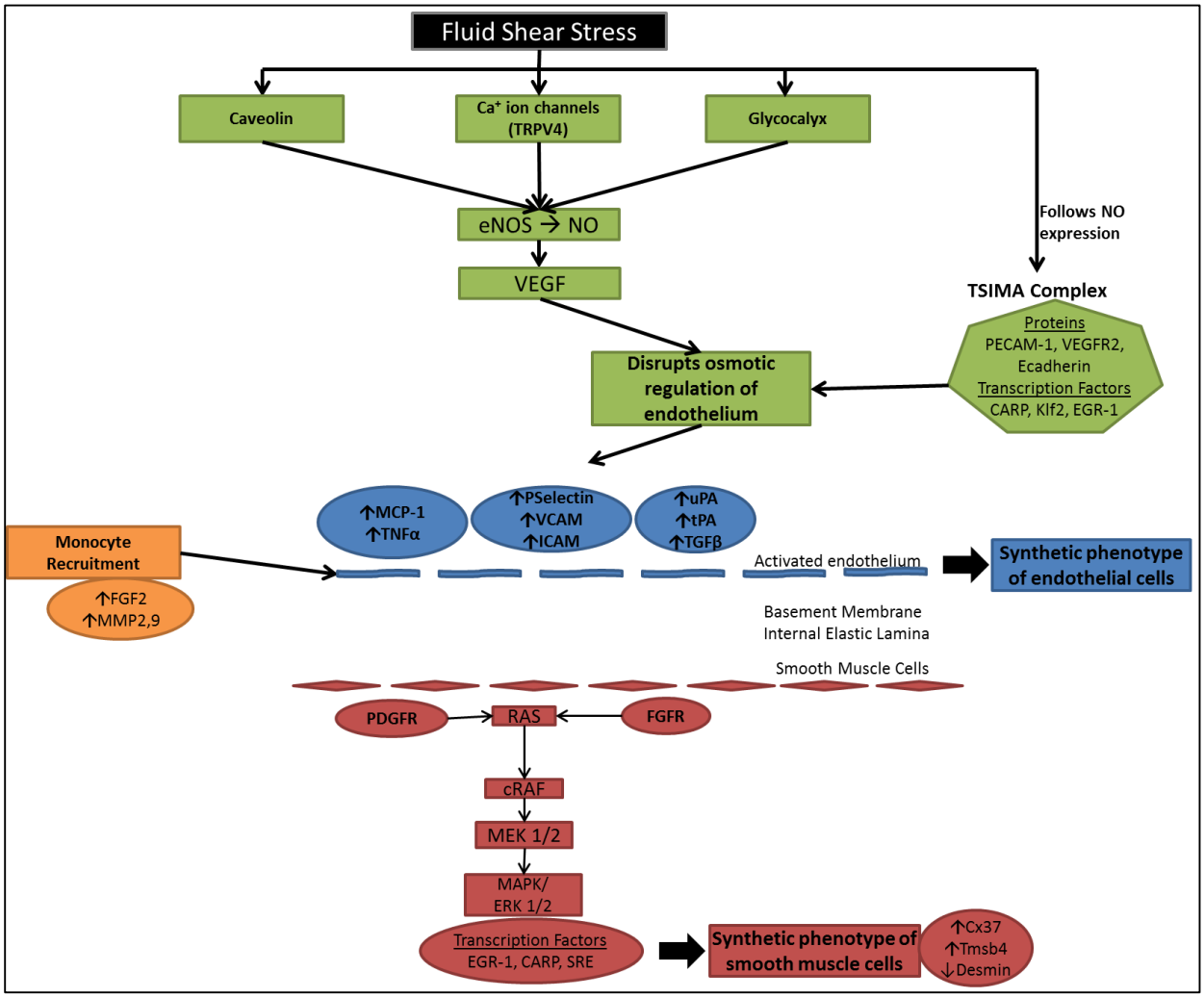

Figure 2. *Depicted is a proposed signaling cascade following detection of fluid shear stress.* ***Green:*** *Increase in fluid shear stress is detected directly by the endothelium and translated to NO production and causes the expression of the Tsima complex.* ***Blue:*** *This results in the activated synthetic phenotype of endothelial cells.* ***Orange:*** *The recruitment of monocytes (leukocytes) by the endothelium further progresses the degradation of the extracellular matrix as well as delivers FGF-2 necessary to progress the VSMC cascade.* ***Red:*** *VSMC changes pheynotype by activation of FGFR and the progression down the Ras/MEK/ERK pathway.*

tPa that both breakdown extracellular matrices to increase permeability. Further, it is recruiting leukocytes via MCP-1 and TNFα. These leukocytes, and specifically monocytes, bring more extracellular matrix degrading proteases (MMP2,9) and importantly, FGF-2. The increased permeability and delivery of FGF-2 by the monocytes makes them key players in linking the endothelium to the VSMC to allow for the progression of arteriogenesis.

LEUKOCYTE RECRUITMENT IN VASCULAR REMODELING

Leukocytes including neutrophil granulocytes, lymphocytes and monocytes all require adhesion and transmigration through blood vessel walls. The concepts of capture, rolling, slow rolling, arrest, adhesion strengthening, intraluminal crawling and paracellular and transcellular migration are accepted as steps in the adhesion cascade following inflammation[53].

Rolling is mediated by selectins (L-Selectin, E-Selectin, P-selectin) by interaction with P-selectin glycoprotein ligand 1 (PSGL1)[54]. L-Selectin is expressed by most leukocytes while E-selectin and P-selectin are expressed by activated endothelial cells. L-Selectin in particular enables leukocyte-leucokyte binding, and therefore secondary tethering, which enables leukocyte without domains to bind PSGL1 to reach sites of inflammation[55]. This binding is essential because they allow binding to inflamed endothelium under conditions of blood flow because they have very high on- and off- rates[56]. L-Selectin and P-selectin actually require shear stress for adhesion, the cells detach if flow is stopped[57]. This is attributed to the catch bond phenomenon of selectin, which strengthens as more pulling force is applied to the selectin[58]. Selectin mediated rolling allows activating signals to be transmitted through adjacent G-protein coupled receptors (GPCR) and directly through selectin ligation.

Activation and arrest is triggered by chemokines activating the endothelium to express adhesion molecules and mediated by integrins (VCAM-1 and ICAM-1) on the endothelial surface. The chemokines bind to specific GPCRs and activate these integrins by triggering a complex intracellular signaling network through a process referred to as inside-out signaling—which is when intracellular signaling results in the activation of a cell-surface receptor. These integrins, also involved in rolling, mediate the transition to firm adhesion. Specifically lymphocytes to VCAM-1 by very late antigen-4 (VLA4) and neutrophils via lymphocyte function associated antigen-1 (LFA1) to ICAM-1[59].

Transendothelial cell migration is thought to occur both paracellularly and transcellularly although paracellular is considered the more dominant pathway. Paracellular migration is made possible by the loosening of interendothelial contacts by the binding of surface adhesion molecules. Specifically inflamed endothelial cells can redistribute junction molecules to favor leukocyte migration. The redistribution moves molecules that present as an obstacle to emigrating cells, such as VE-cadherin, away from the junctions and will favor bringing leukocyte migration mediating molecules such as PECAM-1, ICAM-1, ICAM-2, JAM-A, JAM-B, JAM-C to the surface at junctions[60,61]. The ICAMs interact with the integrins, PECAM-1 supports hemophilic interactions, and JAMs do both[53]. This reorganization of adhesion molecules has more recently been called the endothelial lateral border recycling component (LBRC)[62]. Transcellular migration is route taken by less than 20% of migrating cells[63]. Recent studies believe that the same molecules and similar mechanisms that govern paracellular migration such as LBRC are involved[64]. *In vivo* it has been shown to be more likely to occur in areas of endothelial thinning, which would shorten the transmigration route, and potentially allow for mechanisms similar to the LBRC[65]

Monocyte Specific Recruitment

Although many leukocyte subsets are recruited to the site of inflammation, knock-out and exclusion studies have shown that deficiency of lymphocytes and neutrophil granuloytes do not alter downstream arteriogenic activity, whereas monocytes are critical[66,67,68].

The activated endothelial luminal surface participates in an immune response that includes the release of monocyte chemoattractant protein-1 (MCP-1) to recruit monocytes[66]. The subsequent monocyte localization is a complex multi-step process involving many endothelial adhesion molecules[69]. The first interaction of the monocytes with the vascular wall is rolling, which is regulated by various members of the selectin family (i.e. P-selectin and E-selectin) through a sialyl Lewis x counter receptor[33,34,70-72]. P-selectin in endogenously housed on the α-granule membrane of platelets and Weibel-Palade bodies of endothelial cells, but the stimulation of the endothelium initiates their phosphorylation and movement to be expressed on the plasma membrane[72,73]. The tight adhesion of the monocyte is then mediated by the Mac-1 and LFA-1 receptor binding to the adhesion molecules ICAM-1 and VCAM-1, which in response to activation are clustered in focal adhesion complexes[33,74]. The role of ICAM-1 has been validated by studies that show blocking ICAM-1 function inhibits monocyte adhesion and therefore arteriogenesis[75]. The tight adhesion then gives way to a monocyte "invasion" that is necessary for the dramatic remodeling of the arterioles that can result in a final vessel 20-fold increase in internal diameter diameter and 50-fold larger in tissue mass[33]. VCAM-1 is thought to be most likely responsible for guiding the monocytes through the endothelium into deeper regions of the vessel wall though the specific mechanisms remain unclear[33,76].

The monocytes themselves produce matrix metalloproteinases (MMP's) that are able to break down extracellular matrix on their progression through the vessel wall. It has specifically been

shown that the stimulation of arteriogenesis with MCP-1 augments the expression of several MMP's (MMP-1, 2,3,9)[33]. The MMPs aid in the breakdown of the extracellular matrix and skeletal muscle cells to create more space for the growth of the vessel. The recruited monocytes produce TNFα and FGF-2 that further aid in the proliferation of endothelial and smooth muscle cells. The significant role of monocyte extravasation in blood vessel growth gives way to a second hypothesis of this study, that without the recruitment of monocytes, endothelial activation will not result in progression towards arteriogenesis.

TIME COURSE OF ARTERIOGENESIS

Arteriogenesis is a process that can be classified into four stages- initiation, proliferation, synthesis/migration and maturation (*figure 3*). The initiation phase begins minutes after occlusion characterized by the activation of the endothelium (8-12 hours) and continues into hours later to include the upregulation of adhesion molecules and monocyte adhesion (12 hours)[19]. The

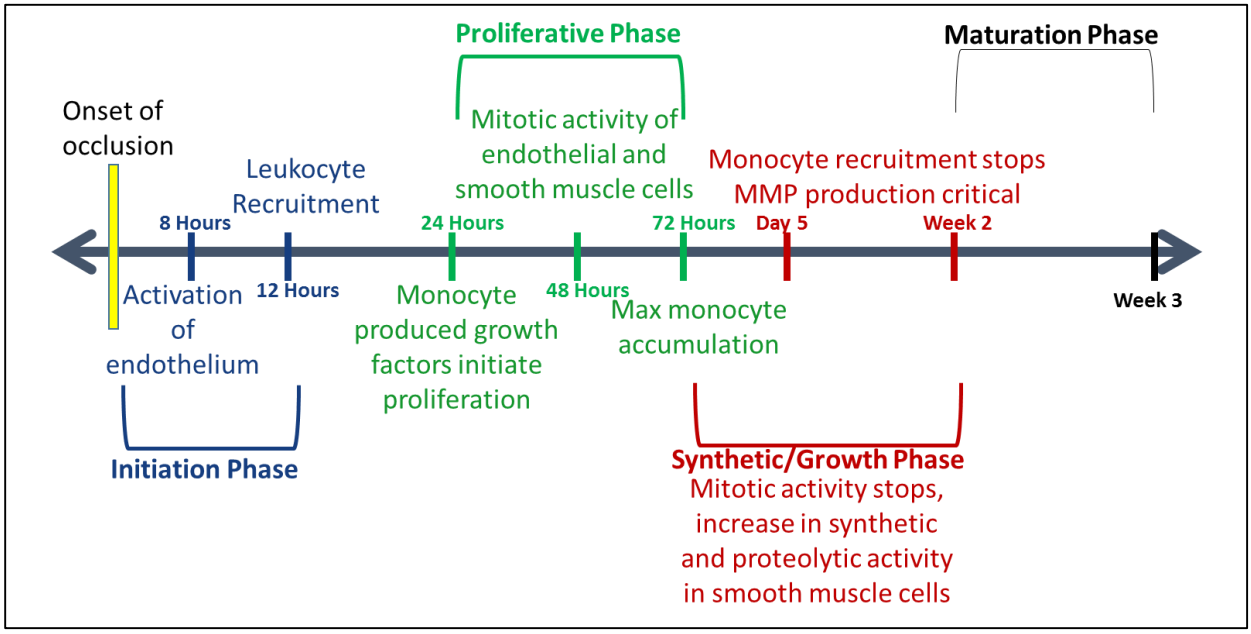

Figure 3. Time Course of Arteriogenesis. *After occlusion endothelium activation is almost instantaneous. The activation of the endothelium* ***(Blue)*** *recruits leukocytes within 24 hours initiating the proliferative phase that lasts over 3 days* ***(Green)****. The next week is attributed so the synthetic phase where the new arteries will become more established* ***(Red)*** *and then mature over the following weeks* ***(Orange)****.*

proliferation stage is initiated by the TNFα and FGF-2 produced by the monocytes/ macrophages both of which can initiate the mitotic activity of endothelial and smooth muscle cells[13]. This proliferation will start at 24 hours and peak at 2-3 days after occlusion, which is when monocyte accumulation is at its max[19]. The synthetic/growth phase is 3-14 day after occlusion and is characterized by a downregulation of mitotic activity but an increase in synthetic and proteolytic activity in smooth muscle cells[19]. While monocyte recruitment has stopped by this point, their role of supplying MMP's as previously described is necessary to digest the lamina elastic to allow for smooth muscle growth[33]. Finally the maturation phase that can take up to 21 days post occlusion is the stopping of all proliferative and proteolytic activity and restoring the smooth muscle cells to their contractile phenotype. This time line tells us that up to three days post occlusion there are molecular changes happening in short time periods after which the rate of change slows down to weeks[77]; I will use this information to select time points in our study.

RESEARCH QUESTION

In cases of vascular occlusion the ability to illicit a neovascular response (arteriogenesis) to form collateral vessels can protect blood flow by providing an alternate stable route for blood flow to underperfused regions. Understanding the mechanical factors and mechanisms that trigger and control arteriogenesis will allow for a targeted treatment to mediate the formation of these collateral networks when and where necessary.

Aims and Hypotheses

The overall objective of this dissertation was to design a viable *ex vivo* system for studying mechanical triggers leading to pro vasculogenic inflammatory conditions and to subsequently use this system to study arterial inflammatory conditions. This objective was addressed as three aims.

Aim 1: To design and validate an *ex vivo* femoral artery bioassay chamber as a model for testing vascular inflammatory conditions

Aim 2: To study the inflammatory response in a femoral artery due to induced increases in wall shear stress in an *ex vivo* femoral artery bioassay chamber.

Aim 3: To study monocyte recruitment and progression towards collateral vessel growth in an *ex vivo* femoral artery bioassay chamber.

The central hypothesis is that a*n inflammatory response will be initiated in an ex vivo femoral artery model in response to an increase in wall shear stress. The inflammatory response will be detected by increases in MCP-1, TNFα, IL-2, P-Selectin, VCAM-1, ICAM-1 expression. Inflammation alone (TNFα or shear stress induced) is not sufficient to initiate collateral vessel growth; monocyte recruitment and adhesion are required to see changes in vasculogenic growth factors VEGF, FGF-2, TGFβ and Egr-1*. This central hypothesis was addressed with experiments designed based on one design goal and three sub-hypothesis relating to each research aim.

Design Goal: To fabricate an *ex vivo* chamber that will be able to maintain the vessel's structural integrity on a gross and molecular scale while inducing a minimal inflammatory response.

Hypothesis 1: Compared to *in vivo* vessels, the *ex vivo* vessels will show similar distributions of endothelial and vascular smooth muscle markers. Further, *ex vivo* arteries will show similar distributions of cytokines, adhesion molecules and growth factors as *in vivo* arteries.

Hypothesis 2: The increase in vascular wall shear stress will induce inflammatory response increases in TNFα, MCP-1, and increases in endothelial adhesion molecules P-Selectin, ICAM-1 and VCAM-1. Growth factor expression will remain similar to *in vivo* baseline. These factors will

be upregulated in the positive control as well, and the level of upregulation will be dependent on wall shear stress.

Hypothesis 3: An inflammatory state is necessary for monocyte adhesion, and monocyte adhesion is further necessary for the upregulation of growth factors and transcription factors indicating progression towards collateral growth (FGF-2, TGFβ, Egr-1).

Animal Model and Research Design

C57BL/6 wild type mice were obtained from Taconic. These mice will be used because they have been routinely used for studies involving arterial occlusion models. Further when studying the effects of wall shear stress, the complex 3-D structure of a vessel cannot be compared to an *in vitro* monolayer of cells. For FAE surgeries, animals were anesthetized with 2-5% isoflurane with 100% oxygen, and given buprenex and ibuprofen by water as pain medication. When excising tissue for analysis the animals were first euthanized as described, and then the tissue removed. All procedures were approved by Stony Brook University‘s Institutional Animal Care and Use Committee. **Animal Care.** Animals were housed in Stony Brook University‘s Division of Laboratory Animal Resources facility. They were kept in cages with access to food and water, and their health monitored. If illness is noticed, the animals were properly euthanized. **Euthanasia:** Animals will be sedated with isoflurane and euthanized by cervical dislocation.

CHAPTER 2
IN VIVO MOUSE FEMORAL ARTERY EXCISION ARTERIOGENESIS STUDY

ABSTRACT

In this study we used an *in vivo* mouse femoral excision model to demonstrate which cytokines, adhesion molecules and growth factors are up- or down-regulated as well as monocyte recruitment as a result of peripheral vascular occlusion. We hypothesized that *the femoral occlusion will cause an increase in cytokine expression related to monocyte recruitment (MCP-1, TNFα, IL-2), endothelial adhesion molecule expression will show an upregulation of P-selectin,VCAM-1 and ICAM-1, Ly6c will be upregulated as monocytes are recruited, and an upregulation of the vascular factors FGF-2, TGFβ, Egr-1 will be seen.* Specifically, C57BL/6 mice underwent femoral excision surgeries of the left femoral artery to induce an occlusion of the femoral artery. The mice were sacrificed at 24, 48, and 72 hours post-surgery and the site of injury as well as the matching region from the contralateral control leg was excised for RNA analysis and immunohistochemistry (IHC). The results were analyzed for RNA expression via quantitative real-time PCR (qPCR) and for monocyte accumulation via IHC.

INTRODUCTION

Femoral occlusion studies have been widely used to study the progression of collateral vessel formation. The studies show that there is a marked decrease in flow perfusion immediately following the onset of occlusion. The perfusion in tissue downstream of the occlusion measured using laser Doppler imaging (LDI) over time, however, increases to almost 40% of original conductance in wild type mice, even without any treatment. The molecular mechanisms driving this perfusion have been studied using histology, protein analysis and quantified with real-time PCR. Studies to date, however, have focused on only a few parameters at a time[19,20,75,76,78]. This aim will analyze a panel of molecules spanning from cytokines, adhesion molecules and growth

factors concurrently in a single sample set providing paired quantitative data on the mechanism of collateral vessel formation at the site of occlusion.

MATERIALS AND METHODS

Experimental Design

Femoral arterial excisions were performed on C57BL/6 mice between 8-12 weeks of age. The time points for analysis were 24, 48, 72 hours, with n=6 at 24 and 72 hours and n=3 at 48 hours. Each time point was compared to naïve animals as baseline. At each time point quantitative real-time PCR show which mRNA markers have changed in expression. Specifically, I examined MCP-1, TNFα, IL-2 as cytokines, P-Selectin, VCAM-1, ICAM-1 as endothelial adhesion molecules, Ly6c as a monocyte marker, and TGFβ, FGF, VEGF, Egr-1 as vascular growth markers.

Femoral arterial excision (FAE)

Performed by a trained surgeon who removed approximately 3mm section of the left femoral artery (surgeries performed by Dr. Ahmed Nasser, Stony Brook University Hospital). Specifically, the proximal suture was tied on the artery just distal to the inguinal ligament and the distal suture tied

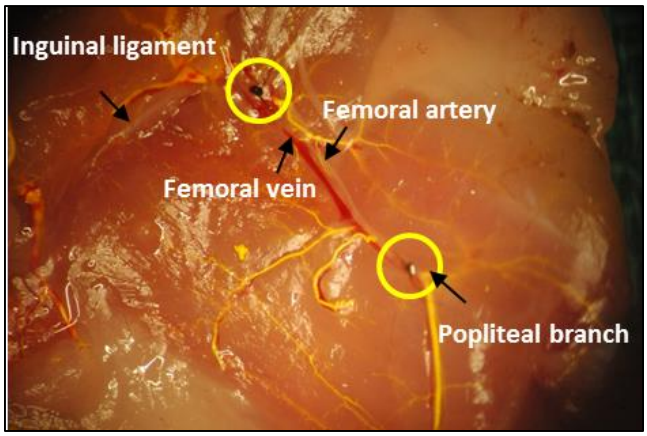

Figure 4. *Close up of mouse left "thigh". Two circles identify proximal (top) and distal (bottom) sutures on the femoral artery distal to the ingunal ligament and proximal to the deep femoral branch respectively. The length of the artery is excised without damaging the vein.*

just proximal to the deep femoral branch, the artery between the two ligation points was removed without disturbing the femoral vein (*figure 4*). The animal was maintained under anesthesia for the duration of the surgery, and administered pain medication (buprenex and ibuprofen in water) post-operatively. The day of FAE is day 0, and the animals were sacrificed at time points 24, 48 and 72 hours post-surgery. At sacrifice the semi-membranous muscle surrounding and including the site of FAE was removed, along with the respective segment from the contralateral leg (negative control) and placed in TRIzol at -80°C.

RNA Isolation

The frozen samples in TRIzol were thawed on the bench top, and the tissues homogenized using an immersion homogenizer. Chloroform was then added at 0.2mL/mL of TRIzol originally used and the samples incubated at room temperature for 10 min. After 15 minute centrifugation at 14,000g the sample were separates into 3 distinct layers; the top aqueous phase contains the RNA, the middle phase is DNA and the bottom organic layer is protein.

RNA was isolated by carefully pipetting the aqueous phase to a new tube and isopropyl alcohol (IPA) added. The sample was incubated at RT for 10 minutes and centrifuged at 14,000g for 10 min resulting in a RNA pellet. The pellet was then washed with 75% ethanol, air dried and resuspended in RNase free H_2O. RNA concentration was determined using a spectrophotometer and then samples were aliquoted and stored at -80°C.

Quantitative reverse transcriptase PCR (qPCR)

For analysis of cytokine, endothelial factor, monocyte and vascular factor expression from the isolated RNA. Specifically, the Qiagen Sybr-green one-step real time kit was be used. Reverse transcriptase (RT) PCR takes the unstable template RNA, converts it to a stable DNA template

exponentially greater number of template cDNA and therefore final double stranded DNA. Sybr Green fluorescent dye binds double stranded but no single stranded DNA, and its fluorescence is

Gene	Primer	Sequence	Product Size	Annealing Temp
GAPDH	Forward Reverse	5' actccactcacggcaaattc3' 5' tctccatggtggtgaagaca3'	223bp	60ºC
GMCSF	Forward Reverse	5' ggccttggaagcatgtagag 3' 5' ccgtagaccctgctcgaata 3'	161bp	60ºC
MCP-1	Forward Reverse	5' caagaaggaatgggtccaga 3' 5' aaggcatcacagtccgagtc 3'	237bp	60ºC
TNFα	Forward Reverse	5' atccgcgacgtggaactggc 3' 5' agaagagcgtggtggcccct 3'	127bp	66ºC
IL-2	Forward Reverse	5' cccacttcaagctccacttc 3' 5' atcctggggagtttcaggtt 3'	150bp	60ºC
P-Selectin	Forward Reverse	5' gtccacggagagtttggtgt 3' 5' aagtggtgttcggaccaaag 3'	241bp	60ºC
VCAM-1	Forward Reverse	5' gaaatgccaccctcacctta 3' 5' acgtcagaacaaccgaatcc 3'	189bp	60ºC
ICAM-1	Forward Reverse	5'agcacctccccacctacttt 3' 5'agcttgcacgacccttctaa 3'	160bp	60ºC
Ly6c	Forward Reverse	5' cactgtgcctgcaaccttg 3' 5' ggcactccatagcactcgta3'	150bp	59ºC
FGF-2	Forward Reverse	5' agcggctctactgcaagaac3' 5' gccgtccatcttccttcata 3'	183bp	60ºC
TGFβ	Forward Reverse	5' gtggaaatcaacgggatcag 3' 5'cgcacacagcagttcttctc 3'	186bp	60ºC
VEGF	Forward Reverse	5' caggctgctgtaacgatgaa 3' 5' aatgctttctccgctctgaa 3'	207bp	60ºC
Egr-1	Forward Reverse	5' gacgagttatcccagccaaa 3' 5' ggcagaggaagacgatgaag 3'	202bp	60ºC

Table 1. *13 primers used for SybrGreen qPCR. Designed using Primer3 program. All primers were tested via standard curves and denaturing protocol.*

the end of each cycle and is proportional to the amount of double stranded DNA. The specific primers for each gene of interest MCP-1, TNFα, IL-2, P-Selectin, VCAM-1, ICAM-1, Ly6c, FGF-2, TGFβ, VEGF, Egr-1 and the housekeeping gene GAPDH were designed using the online Primer3 program (*table 1*).

The data were collected in the form of CT which is the cycle number at which the Sybr-green fluorescence was detected over baseline. The ΔCT values for each gene were found by normalizing to the GAPDH housekeeper specific to each run ($\Delta CT = CT_{sample} - CT_{GAPDH}$)[79]. The expression fold change was then found by normalizing the ΔCT values for the experimental samples (Contralateral or FAE tissue) to the naïve tissue samples ($\Delta\Delta CT = \Delta CT$ experimental - ΔCT_{mean} naïve)[79]. The formula $2^{(-\Delta\Delta CT)}$ then equals the fold change in expression of each gene in respect to naïve tissue[79].

Statistical Analysis

All sample fold-changes were determined in respect to naïve tissue for each gene of interest. 1-Way ANOVA will determine any significant differences between Contralateral and naïve samples per gene at each time point. Unpaired t-tests with Welch's correction were used to analyze differences between contralateral and FAE for each independent gene at each time point. With an n=4 the experiments were calculated to have a power of 85% for determining significance at $p<0.05$.

Immunohistochemistry

For analysis of monocyte accumulation after FAE samples, muscle tissue proximal to the occlusion region, as shown in *figure 4*, was excised, fixed, and stained for CD11b a leukocyte marker, and counterstained with hematoxylin. Briefly, the muscle tissue was fixed overnight in 10% formalin, embedded in paraffin, and sectioned to reveal cross sectional views of the vessels in the occluded

region. The sections were deparaffinized, rehydrated, and antigen retrieval performed. The samples were blocked with normal horse serum and incubated with the CD11b primary antibody for 1 hour at -20°C. CDllb was visualized using the VectorLabs ABC DAB kit (#SK-4100), which involves consecutive secondary and tertiary incubation for 30min at 4°C. DAB was then added for 5 min, the brown color indicating CD11b became visually apparent. The reaction was stopped by rinsing with tris buffered saline with tween-20 (TBS-T). The samples were then counterstained with hematoxylin for 10 minutes, rinsed, dehydrated, and mounted under coverslips. The accumulation of CD11b indicates the recruitment, adhesion ad infiltration of CD11b into the vessel wall.

RESULTS

mRNA Expression

Results are shown for an n=6 for each gene of interest for *in vivo,* 24 and 72 hours; and n=3 at 48 hours (figure 5). The data are normalized to housekeeper GAPDH and then fold change calculated with respect to naïve tissue. Statistical differences are comparing FAE to contralateral, and fold changes are ± standard error. The first group of genes is the cytokines/chemoattractants (*figure 5a*). MCP-1 shows 12.07±3.53, 39.12±8.46, and 5.335±0.94 fold increases in the FAE samples at 24, 48 and 72 hours, respectively, which are all significantly greater than the contralateral counterpart ($p<0.05$, $p<0.05$, $p<0.01$). IL-2 shows increased expression at 48 hours with a 22.65±10.60 fold change in the contralateral and 20.79±9.39 fold change in the FAE sample. There is no difference detected between the FAE and contralateral, implying a systemic upregulation, and levels at 24 and 72 hours are comparable to naïve. TNFα shows no significant changes at the mRNA level.

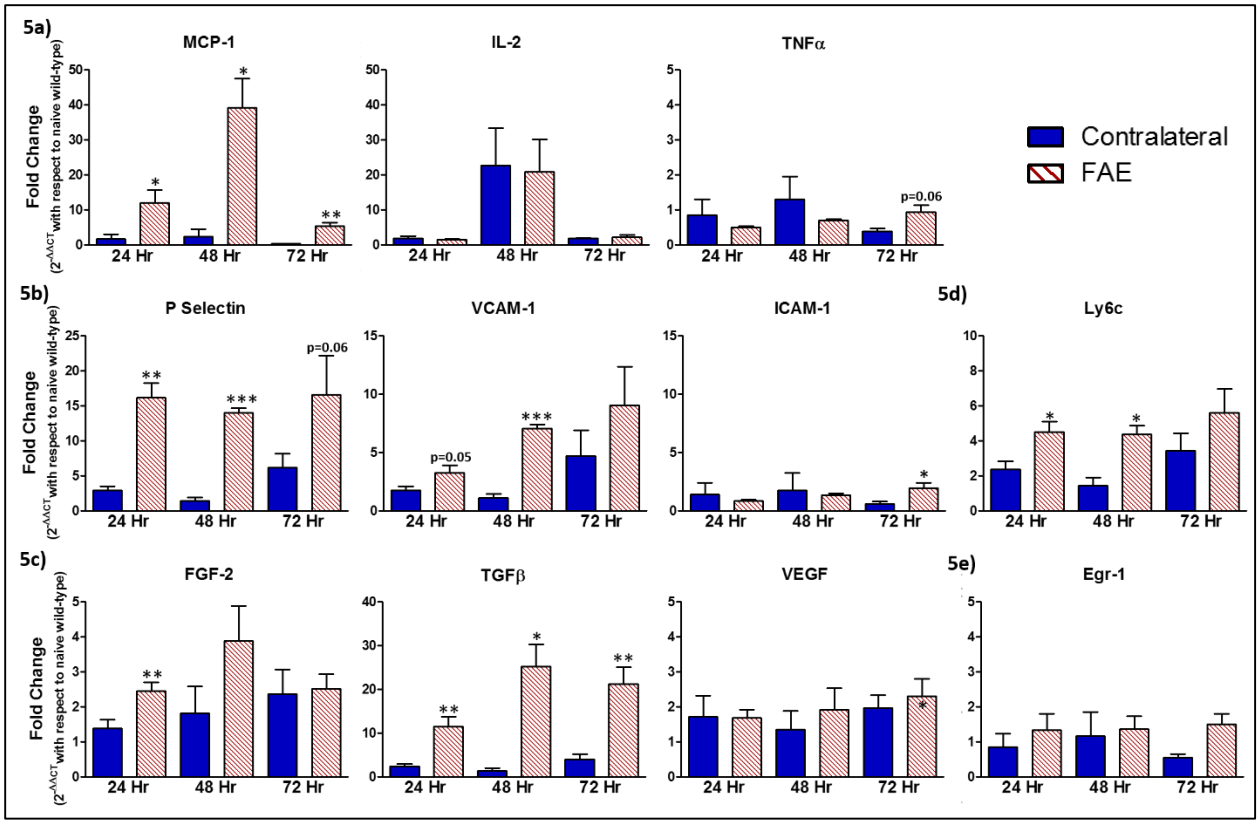

Figure 5. *All qPCR data is normalized to housekeeper gene GAPDH, and fold changes are values obtained as* $2^{-\Delta\Delta CT}$ *in reference to naïve samples, error bars represent SEM. Analysis and significance is of FAE in relation to contralateral samples.* ***a)*** *Cytokines MCP-1, IL-2 and TNFα. MCP-1 in significantly upregulated in FAE over contralateral as early as 24 hours. IL-2 is systemically upregulated by 48 hours.* ***b)*** *Adhesion molecules P-selectin, VCAM-1 and ICAM-1. P-selectin is significantly upregulated at 24Hr and sustained. VCAM-1is significantly upregulated at 24 and 48 hours.* ***c)*** *Growth factors FGF-2, TGFβ, and VEGF. FGF-2 is significantly increased at 24 hours and TGFβ is significantly increased throughout. VEGF shows no upregulation of mRNA throughout the time course.* ***d)*** *Monocyte marker Ly6c is consistantly upregulated through all time points and significantly at 24 and 48 hours.* ***e)*** *Transcription factor Egr-1 Egr-1 shows a modest yet significant increase at 72 hours. *p<0.05, **p<0.01, ***p<0.001.*

The next group of genes are adhesion molecules (*figure 5b*). P-Selectin is upregulated by 16.20±2.07, 14.00±0.68, and 16.60±5.53 fold at 24, 48 and 72 hours, respectively. Compared to contralateral samples these are significant changes ($p<0.01$, $p<0.001$, $p=0.06$). VCAM-1 has significant increases at 24 ($p=0.05$) and 48 ($p<0.001$) hours of 3.23±0.65 and 7.04±0.35 fold, respectively. ICAM-1 shows no significant changes until 72 hours where an increase of 1.95±0.45 is significant ($p<0.05$).

The next group of genes are growth factors (*figure 5c*). FGF-2 shows a significant increase of 2.45±0.25 fold ($p<0.01$) at 24 hours and an increase of 3.89±0.99 fold at 48 hours ($p=0.08$). TGFβ is significantly increased by 11.45±2.25, 25.18±5.07, and 21.18±3.93 fold at 24, 48 and 72 hours ($p<0.01$, $p<0.05$, $p<0.01$). VEGF show no significant changes at the mRNA level.

Figure 5d shows the monocyte marker Ly6c. The FAE leg has increased levels of Ly6c over contralateral at each time point, 4.50±0.59, 4.37±0.49 and 5.61±1.36 fold changes that are significant at 24 and 48 hours at $p<0.05$, respectively. While there is an increase at 72 hours, the change is not significatly different than contralateral because it also presents with an upregulation of 3.45±0.98 fold.

Finally *figure 5e* depicted Egr-1 is separated from the growth factors since it is a transcriptional factor. Egr-1 has modest increases in FAE over the time course, at 72 hours the 1.49±0.31 fold increase is signifant over contralateral ($p<0.05$). This is related directly to the growth factors as it is an umstream regulator of growth factor signalling cascade.

Immunohistochemistry

Figure 6 shows the IHC of the region proximal to the FAE region stained with CD11b, counterstained with hematoxylin. The region includes the femoral artery, vein and other smaller vessels as can be seen in *figure 6a*. A closer look at the femoral artery shows punctate CD11b staining, indicating the accumulation of leukocytes. The staining is at the endothelium but also into the tissue showing some transmigratory cells.

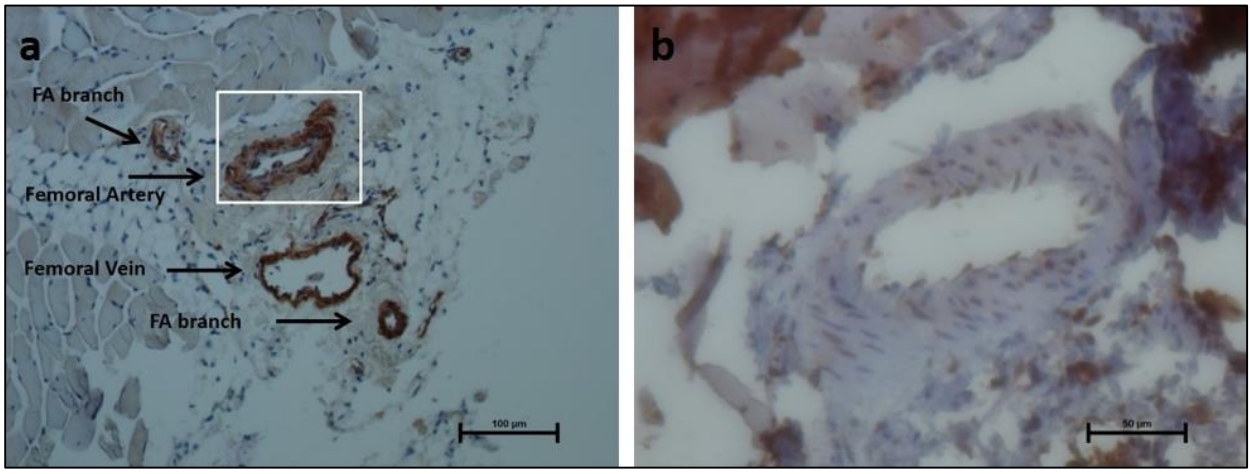

Figure 6. *IHC of muscle proximal to the FAE region. Wild type C57/B6 male mice (8-10weeks) underwent FAE. Throughout a 72hr time course animals were sacrificed and the occluded region of their left leg was isolated, fixed, embedded, and sectioned. Serial sections were then stained for SMA (abcam) or CD11b (leukocyte marker) and counterstained with hematoxylin.* ***a)*** *Micrograph was taken at 200x. IHC image of vasculature in the region arrows indicate femoral artery, vein and smaller vessel.* ***b)*** *400x image of the femoral artery where the arrows indicate punctate CD11b staining, leukocyte adhesion and transmigration.*

DISCUSSION

The data show that there is an inflammatory response as a result of severe vascular occlusion that is specific to the site of injury. As early as 24 hours there is a site specific increase in expression of cytokines as well as adhesion molecules, specifically MCP-1 and P-selectin. MCP-1 is vital to the recruitment of monocytes and its early and robust expression in the FAE region indicates the early involvement of monocytes. P-selectin is known to be constitutively expressed internally on the endothelium and externalized via phosphorylation when activated. As such, it is quick to respond to stimulus and is responsible for the early "rolling" and slowing down of monocytes to the site of inflammation. Following the initial recruitment of monocytes, as seen by Ly6c, the tight adhesion molecules and growth factors begin to be expressed. As the monocytes adhere, the release of MMP's allows the proliferation of both endothelial and smooth muscle cells, as seen by the upregulation of FGF-2 and TGFβ.

Previous work by Pagel et. al. showed an increase in MCP-1, macrophage, and ICAM-1 levels at 12 and 24 hours post-ligation[80]. The current data is in agreement with these findings, while suggesting that a longer time course will provide valuable information. Specifically, the tight adhesion molecules and growth factors do not show a discernable difference until at least 48 hours post occlusion. Further, we do not see a comparable increase in ICAM-1 as early that is likely due the excision model versus the ligation model. The excision model used in this study imparts a more severe occlusion making it more difficult for existing vessels to compensate blood flow as rapidly.

Egr-1 on the other hand, may provide more relevant information at an earlier time point. Since it is a transcription factor that is upstream of many growth factor signaling cascades. Since there is upregulation of growth factors being seen at the given time points, it is likely that Egr-1 expression was triggered earlier on.

In conclusion, we find the FAE model provides a severe occlusion model that allows the study of arteriogenesis without confounding results from existing by-pass vessels. The analysis of Ly6c mRNA expression corroborates the IHC data showing leukocyte accumulation. CD11b can be indicative of various leukocyte types, but together with the Ly6c data, we can be confident that specifically monocytes are accumulating at the site. The delayed expression of growth factors to after the recruitment of monocytes further solidifies their role in arteriogenic vessel proliferation and remodeling.

CHAPTER 3
THE DESIGN AND VALIDATION OF AN *EX VIVO* FEMORAL ARTERY MODEL FOR STUDYING INFLAMMATORY CONDITIONS

ABSTRACT

In this study the aim was to design and validate an *ex vivo* femoral artery bioassay chamber as a model for testing vascular inflammatory conditions. Through this aim, first, a bioassay chamber was designed and the pulsatile pump characterized. The perfusate for the artery was cell culture media (DMEM) and flow rate was calculated for imparting physiological WSS taking into consideration the fluid's viscosity. This study then compared naïve femoral arteries to arteries maintained *ex vivo* under the calculated physiological parameters to ensure that the *ex vivo* vessel did not have compromised structure, mechanosensors or endothelial adhesion molecules. Specifically, femoral arteries were excised from C56BL/6 mice and either analyzed immediately or set up in the bioassay chamber perfused with media at a physiological flow rate for 24 hours in a 37°C incubator. After 24 hours the arteries were analyzed and compared to the *in vivo* vessels. The analysis for both *in vivo* and *ex vivo* vessels included histological analysis of smooth muscle cells as well as endothelial cells, confocal analysis of the glycocalyx (mechanosensor), and RNA/Protein analysis of the adhesion molecules (P-Selectin, VCAM-1, ICAM-1) by qPCR and western blot respectively.

INTRODUCTION

The current methods for studies on vascular inflammatory conditions are primarily *in vivo* and *in vitro.* The *in vitro* models have the shortcomings of being a monolayer of cells rather than a complex 3-D tissue with structural and mechanical properties that are lost in translation. By creating an *ex vivo* femoral artery model, flow rates, wall shear stress, and inflammatory conditions will be controlled in a very localized and specific manner while maintaining tissue structure and organization and *in vivo*.

MATERIALS AND METHODS

Experimental Design

An *ex vivo* system was designed to sustain femoral arteries for at least 24 hours. The chamber design is comparable to previous *ex vivo* chambers, but designed to the specific needs of this study[81,82]. Specifically, the *ex vivo* arteries were compared to the *in vivo* (baseline control) to show that the endothelium and structural integrity was maintained. They were analyzed via histology (n=3), glycocalyx (n=2) and mRNA expression (n=6) for each analysis *in vivo* and *ex vivo*. In this case n equals the number of femoral arteries and each animal supplied two femoral arteries. The negative control (n=6) were vessels maintained in perfusion media but without any flow.

Chamber design

Shown in *figure 7*, the bottom is a glass slide and the mold is sylgard[81], there are two lengthwise ports leading out of the chamber that will hold the cannulated vessel and one port above the vessel level that acts as a passive drain for excess media. Perfused femoral arteries are cannulated with

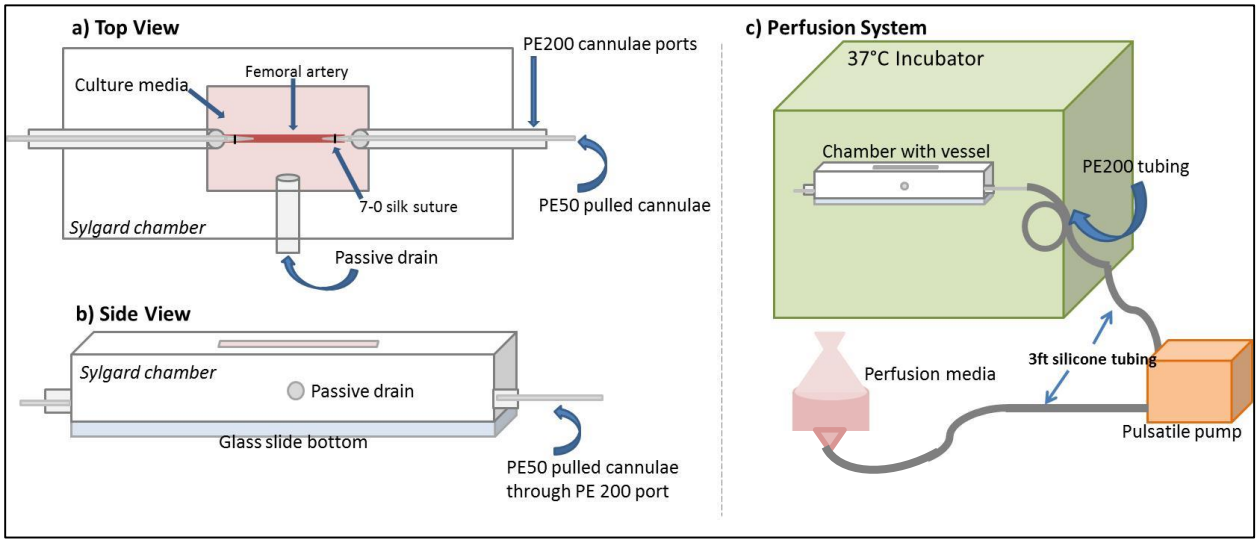

Figure 7. *Schematics showing the ex vivo set up for femoral artery perfusion a) the top view of the cannulation chamber where you can see silk sutures holding pulled PE50 tubing into the vessel. PE200 ports hold the PE50 pulled cannulae in place, b) the side view where you can see the cannulation ports are below the passive drain, and c) the whole set up where the pump and media are maintained outside the heated chamber. Chamber and media in chamber is kept at 37°C as checked by a temperature probe.*

pulled PE50 tubing and sutured in place with 7-0 silk suture. The vessel is then carefully lifted into the bioassay chamber where it is kept submerged in media while the cannula are stretched so the vessel is at its *in vivo* length (measured pre-extraction), submerged in perfusion media and attached to ports leading to longer PE200 tubing leading to a pulsatile pump (Watson Marlow 403U/VM2). The assay chamber is kept in an incubator at 37°C under sterile conditions. The PE200 tubing leaves the incubator to attach to the pump and receive media. A temperature probe within the incubator at the chamber location confirms that vessel chamber is being maintained at 37°C.

Perfusion media

Used for initial collection of aortas as well as perfusate during the study. The media consists of Dulbecco's Modified Eagle Medium (DMEM from Gibco) comprised of (mmol) NaCl 110.34, KCl 5.33, CaCl2 1.8, NaHCO3 44.05, MgSO4 0.814, NaH2PO4 0.906 supplemented with 10% fetal bovine serum (FBS)[83-87]. The osmolality of DMEM with 10% FBS is 300 mosmol/kg[88] which is comparable to the average plasma osmolality reported in male C57BL/6 mice of 315±6 mosmol/kg[89]. The viscosity is $\eta_{DMEM}= 8.9x10^{-4}$Pa·s, which is lower that the viscosity of blood which is $\eta_{blood}= 4.0x10^{-3}$Pa·s. This disparity was accounted for in the flow rate calculations.

Pulsatile Pump characterization

Performed on the Watson Marlow pulsatile pump. The pump has a setting for revolutions per minute (RPM). The pump was set at various RPM settings in a randomized manner and 1mL flow collected in a graduated cylinder while timing with a stopwatch. The flow rate at each setting was calculated by dividing the time by the volume collected. The data collected is shown in *figure 8*. The relationship is linear with $R^2= 0.996$. The equation of the line (y=0.0218x-0.0372) was used to determine what RPM setting will provide the correct flow rate.

The pulsatiliy of the pump was characterized using a pressure transducer[90]. A Matlab program was coded (*figure 10*) in order to collect the data from the pressure transducer. Representative screen shot of data collected via Matlab is shown in *figure 11*. The data output can present the original waveform as well as the frequency data on a power spectrum. The code allows the user to choose the file to analyze and is pre-selected as excel files. As shown in the code, the time data located in the Excel file must be in column 'A' and the pressure data must be in column 'B'. In line 6, the sampling frequency must be changed each time in order to reflect the sampling rate. Pulsatility is defined in *figure 9* by the given equation. Specifically; RPM=21.5 (physiological) = 104.92 beats/min, RPM=27.8 (1.4x physiological) = 136.38 beats/min, RPM=37.1 (2x physiological) = 182.83 beats/min. Compared to *in vivo* (~400beats/min) this is admittedly lower, more along the lines of a sedated mouse, but imparted the appropriate WSS which is the focus of this study.

As a given function of using a roller pulsatile pump, the pulsatility increased as flow rate and WSS increased. In *figure 12* the changes in frequency of the waveform can be seen as a function of RPM setting, which in turn is linearly related to the flow rate. The waveforms were drawn by determining the period at each setting by measuring the peak-to-peak distance and graphing the corresponding pressure values as collected by the pressure transducer. The shape of the waveform as well as the maximum pressure (80mmHg) stay constant as the rate is increased. Irregularities in the waveforms seen in the image is due to the sampling frequency that causes different points to be measured in each period. When calculating actual values for pulsatility, flow rate and wall shear stress the time-averaged method was used to determine the peak and average pressure values for a ratio that would then be used to determine the wall shear stresses.

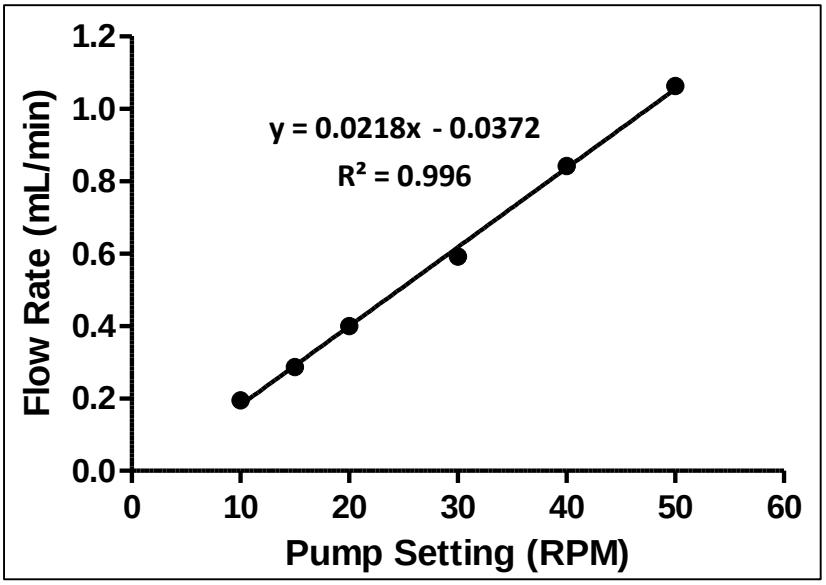

Figure 8. *Plot of the relationship between revolutions per minute (RPM) setting on the pump and the corresponding flow rate (mL/min). The relationship is linear and defined by the given equation.*

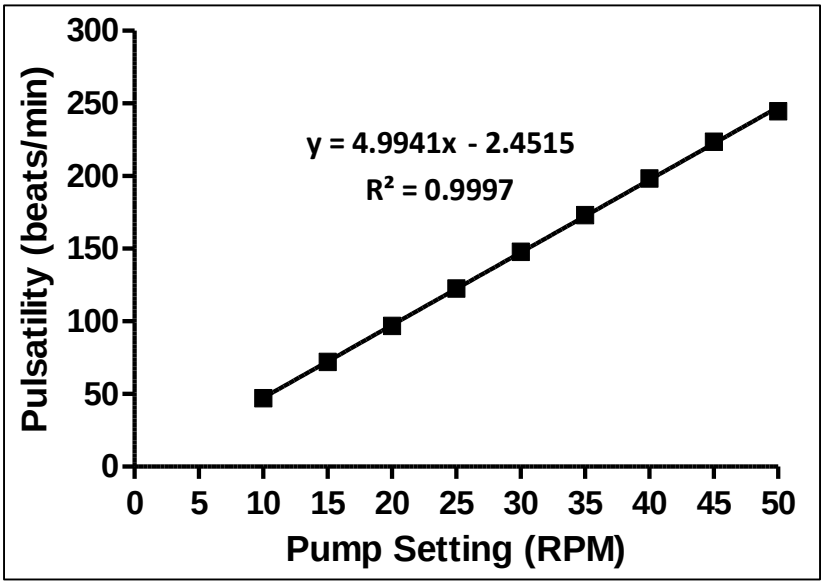

Figure 9. *Pulsatility as defined as beats per minute from the data collected via the pressure transducer and matlab. Specifically Pulsatility was calculated as being equal to frequency which is equal to 1/period. The relationship between RPM and pulsatility is linear and defined by the given equation*

```
filename = uigetfile('*.xls','*.xlsx');     % Choose specific excel file
excelfile=filename;
time = xlsread(excelfile, 'A:A');           % Read first column in Excel
pressure = xlsread(excelfile, 'B:B');       % Read second column in Excel

Fs = 240/12;                    % Sampling frequency
T = 1/Fs;                       % Sample time
L = length(pressure);           % Length of signal
t = (0:L-1)*T;                  % Time vector
M=max(pressure);
N=min(pressure);

subplot(2,1,1)
plot(time,pressure)
axis([0 30 N-10 M+10])
title('Pressure Wave')
xlabel('Time (seconds)')
ylabel('Pressure (mmHg)')

NFFT = 2^nextpow2(L);           % Next power of 2 from length of y
Y = fft(pressure,NFFT)/L;
Y(1)=[];                        % The first component of Y is the sum of..
Z=2*abs(Y(1:NFFT/2+1));         % the data and can be removed
f = Fs/2*linspace(0,1,NFFT/2+1);

subplot(2,1,2)
plot(f,2*abs(Y(1:NFFT/2+1)))    % Plot single-sided amplitude spectrum.
title('Single-Sided Amplitude Spectrum of Y(t)')
xlabel('Frequency (Hz)')
ylabel('|Y(f)|')
datacursormode on
```

Figure 10. *Matlab code for data acquisition from pressure transducer for defining pulsatility of roller pump used to induce pulsatile flow data output outputs original waveform and frequency spectrum, and an excel worksheet with raw values for post-analysis.*

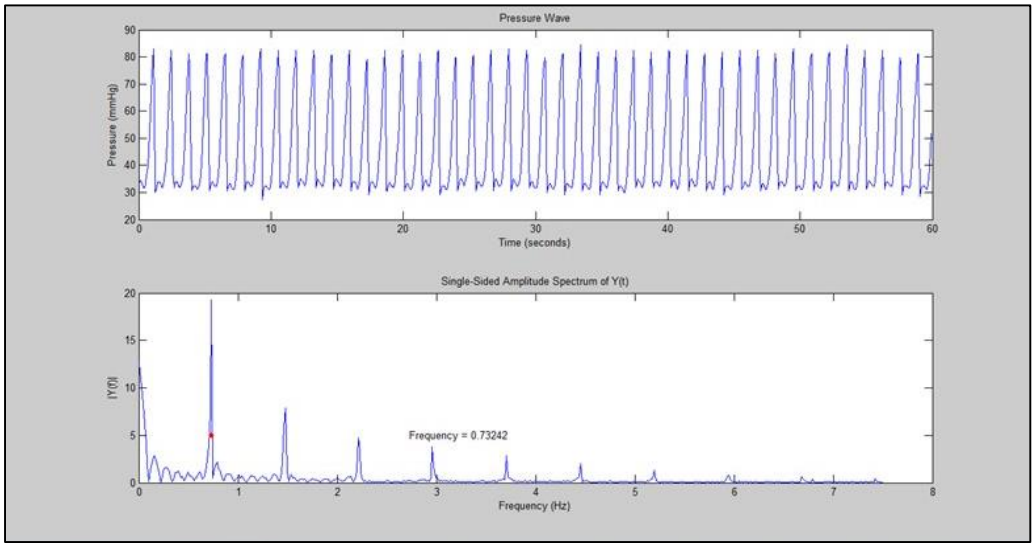

Figure 11. *Representative Matlab output of pressure wave and frequency analysis. The sampling rate available creates a raw values data sheet where there are different points on each wave per period reported*

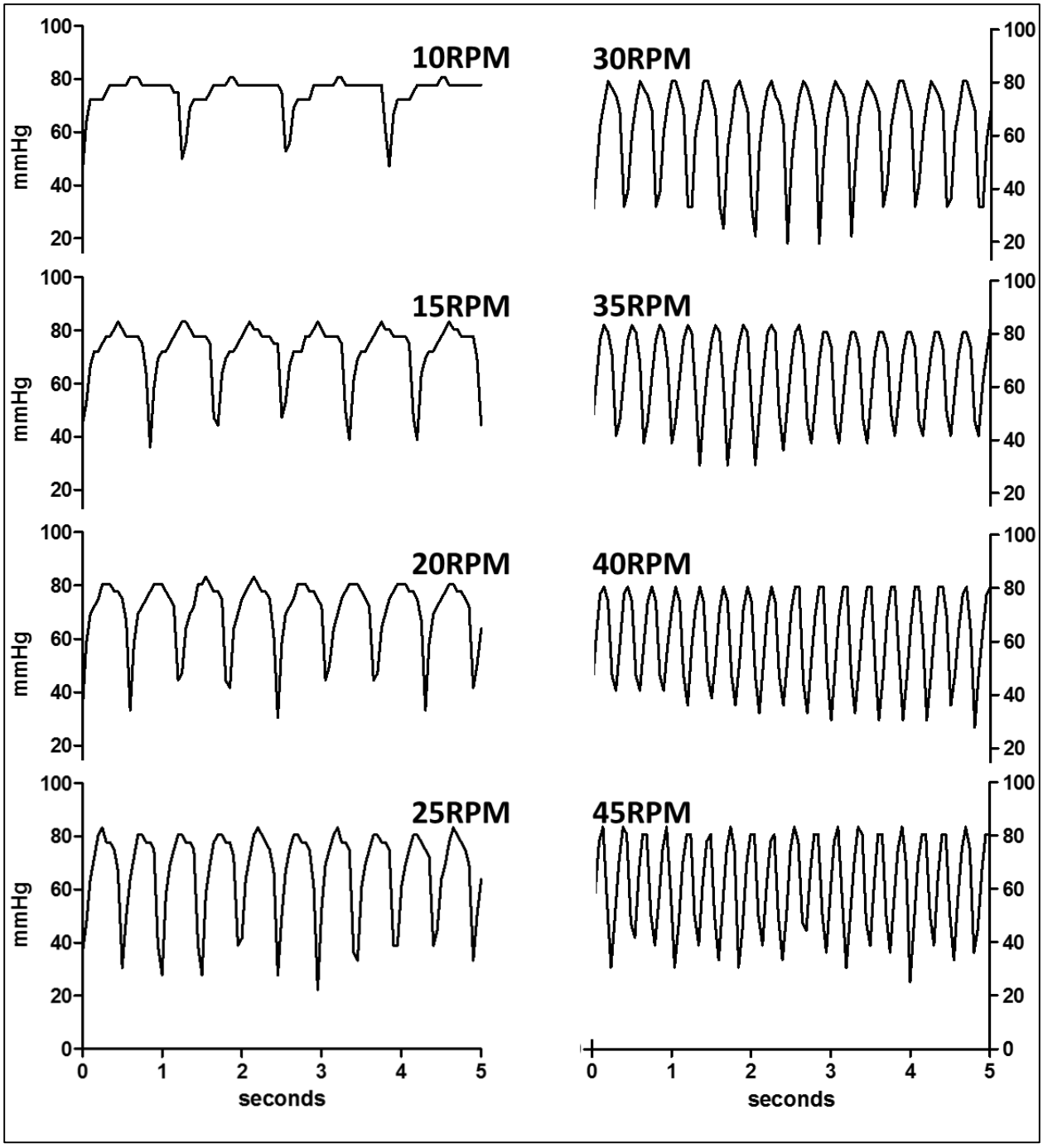

Figure 12. *Waveforms of the pulsatile flow from the watson marlow pulsatile roller pump as a function of pump RPM setting. The correcponding flow rate to the RPM can be caluclated from figure 8. Waforms were drawn by analyzing the excel output from the MatLab program that provided a pressure vaule for each sampled timepoint. The period was determined by the peak-to-peak distance and the pressure values then fit into the period . Irregularities are due to the sampling frequency sampling different points in the wave for each period. This is sufficient to get an image of the waveform, and the time-averaged method was used to determine actual values for peak and average pressure in order to calculate peak shear stress.*

Flow Rate Calculation

For the perfusion of the perfusion media (above) to maintain physiological WSS in the excised vessel was calculated using the peak flow rate in the iliac branch of an average C57BL/6 mouse as determined by Huo et. al., which was found to be Q_{max}= 0.12mL/min[91], coupled with the equation for wall shear stress *(1)*. Specifically,

$$\tau_\omega = \frac{4\eta\dot{Q}}{\pi R^3} \quad (1)$$

τ_ω= WSS, η= viscosity, $\dot{Q}$= flow rate, ρ= density, R= internal radius of the vessel, and D= 2R. Given that $\dot{Q}_{invivo}$= 0.12mL/min for the iliac artery *in vivo*, η_{blood}= 4.0x10^{-3} Pa·s (0.03 Poise), and $D_{femoral}$= 0.20mm[91], the peak τ_ω (WSS) in the femoral artery of an average mouse is 10.18 Pa (101.8 dynes/cm^2). We want to induce this same τ_ω *ex vivo.* To determine the peak flow rate required to maintain this shear in the *ex vivo* model we will simply solve for $\dot{Q}_{exvivo}$ where τ_ω= 10.18 Pa and η_{DMEM}= 8.9x10^{-4}Pa·s. Solving equation *(1)* peak $\dot{Q}_{exvivo}$= 0.53mL/min[83].

The pump needs to be set at average flow rate that will impart the peak flow and WSS equivalent to the vessel, which can be determined by dividing the average flow rates from *figure 8* by the corresponding ratio of average to max pressure (*figure 13b*). This is possible because the ratio of max and min pressure will be equivalent to the ratio of max and min flow rates. Max and average pressure were empirically measured by the pressure transducer at each RPM setting and calculated using the time-averaged method, respectively. The RPM to max flow rate relationship is seen in *figure 13a,* and is 0.5393, 0.7551, and 1.0787mL/min for physiological, 1.4x physiological, and 2x physiological flow. From this line equation RPM is calculated to be 21.5, 27.8, and 37.1 for the same experimental conditions. This corresponds to average flow rates of 0.4319, 0.5682 and 0.7727 mL/min respectively. *Table 2* shows the comparison of parameters between *in vivo* and *ex vivo. Table 3* shows the parameters for each of the experimental setting in detail.

C57BL/6 mice Femoral Artery	In Vivo	Ex Vivo
Peak Wall Shear Stress (τ_ω; Pa)	10.18	10.18
Internal Radius (D; mm)	0.20	0.20
Viscosity (η; Pa·s)	η_{blood}= 4.0x10-3	η_{DMEM}= 8.9x10-4
Peak Flow Rate (Q; mL/min)	Q_{invivo}=0.12	Q_{exvivo}= 0.53

Table 2. *Chart of in vivo versus ex vivo parameters. In order to model the appropriate wall shear stress ex vivo the system needs to compensate for the lower density of perfusion media. To do this, this model will use an increased flow rate as indicated.*

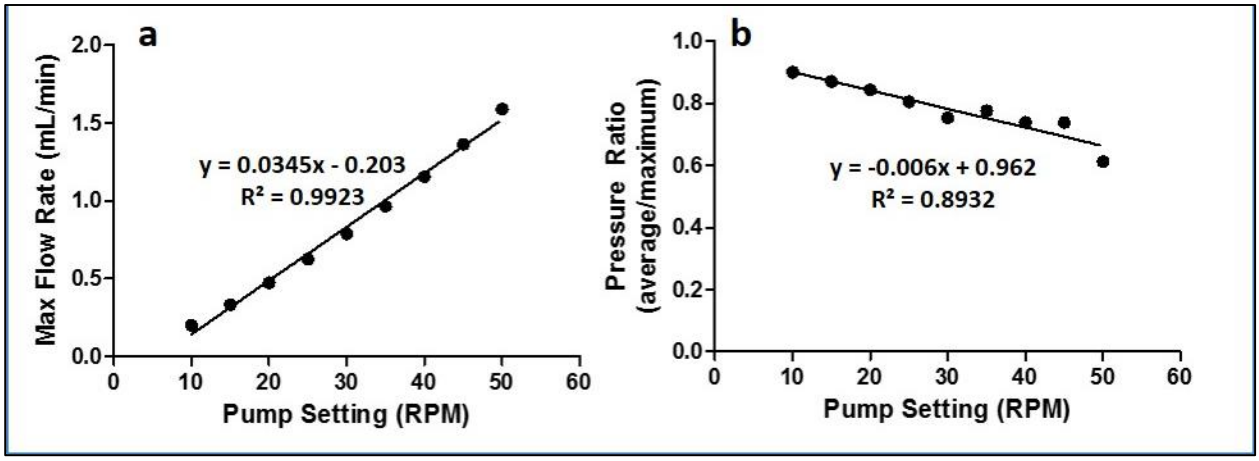

Figure 13. a) *Relationship between RPM and max flow for the Watson-Marlow pulsatile pump.* The relationshop is *linear wih R^2= 0.9923 and is defined by the given equation. From this equation RPM for physiological, 1.4x physiological and 2x physiological flow rate for corresponding peak WSS were calculated to be 21.5, 27.8 and 37.1RPM respectively.* ***b)*** *Relationship between RPM and the ratio for the average pressure to max pressure for the pulsatile pump. The relationship is linear with R^2= 0.8932 and is defined by the given equations. This relationship is used to find the RPM to max flow rate relationship.*

	Pump RPM	MEAN/PEAK pressure ratio	Mean Q̇ (mL/min)	Peak Q̇ (mL/min)	Peak V (cm/s)	Peak WSS (Pa)	Peak WSS (dynes/cm^2)	Mean V (cm/s)	Mean WSS (Pa)	Mean WSS (dynes/cm2)
physiological	21.5	0.8329	0.4492	0.5393	28.6121	10.1859	101.8592	23.8310	8.4838	84.8385
1.4x physiological	27.8	0.7954	0.6006	0.7551	40.0570	14.2603	142.6028	31.8606	11.3424	113.4237
2x physiological	37.1	0.7391	0.7972	1.0787	57.2242	20.3718	203.7183	42.2947	15.0569	150.5690

Table 3. *Table of three experimental conditions and corresponding pump RPM, pressure ratio, mean and peak flow rate (Q), mean and peak velocity (V) and mean and peak wall shear stress (WSS). The above graphs and equations were used to calculate all of these values as described.*

Peak Pressure

Peak pressure in the vessel was simply maintained at 80mmHg by changing the height of the output. The required height of the output for any given RPM was measured using a pressure transducer. The observed relationship between RPM and height required to maintain pressure at 80mmHg is linear, as seen in *figure 14*. For this study the heights were 45.72, 35.66, and 20.5cm above the chamber for physiological, 1.4x physiological and 2x physiological flow respectively.

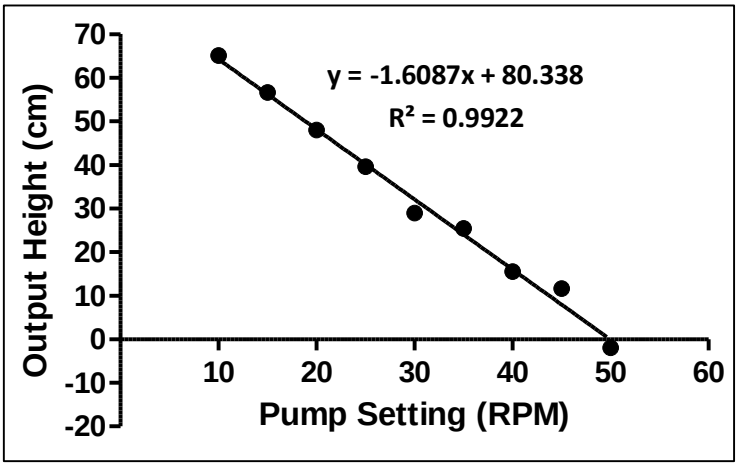

Figure 14. *Relationship between RPM and output height (cm) required to maintain a maximum perfusion pressure in the vessel of 80mmHg.*

Femoral Artery and Branch Isolation

From C57BL/6 mice anesthetized with 2% isoflurane and euthanized by cervical dislocation. Prior to removal, the *in vivo* length of the artery was recorded from the inguinal ligament to the popliteal artery bifurcation so that it could be stretched to physiological length *ex vivo.* There are three standard branches off the main artery that were measured and isolated as well (*figure 15*). The artery was cannulated from the iliac artery so that the cannula comes just proximal to the inguinal ligament and tied into place with suture, the femoral was severed below the popliteal artery branch and the blood flushed from the aorta with saline. After this step the femoral artery was either; 1) cannulated using a second cannula below the popliteal artery branch and the vessel removed to be

used in perfusion chamber described above, 2) excised and placed in TRIzol for RNA analysis, 3) perfusion and immersion fixed with 4% paraformaldehyde for histological analysis or 4) excised and splayed open exposing the endothelial cell surface for immunohistochemistry.

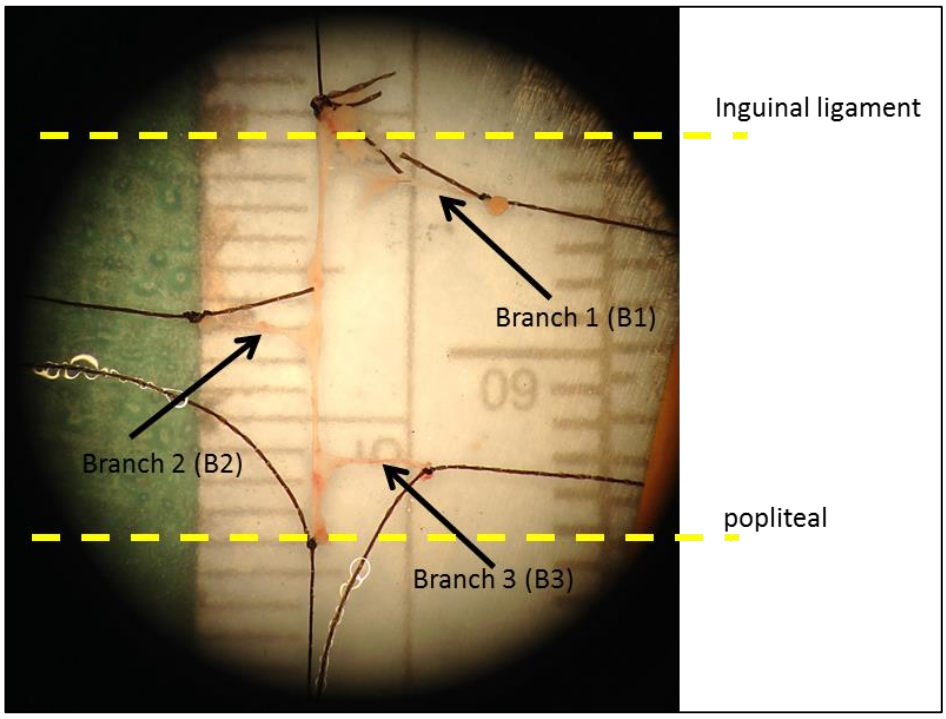

Figure 15. *Representative excised femoral artery. In this image it is indicated that the proximal end of the artery is excised at the inguinal ligament (hip) and the distal end by the popliteal branch (knee). Three distinct branches are also excised bluntly. After cannulation the effective length of the femoral artery on average is 0.85cm.*

Histology

Sections were be taken from vessels immediately excised from *in vivo* as well as vessels maintained *ex vivo* for 24 hours. The femoral arteries were fixed in 4% paraformaldehyde (PFA) and embedded longitudinally in paraffin to allow for cross sectional sectioning of the tissue. After processing the arteries average ~.6cm in length. Serial sections were obtained from the proximal, center, and distal portions of each artery. 3 sections from each location were stained with hematoxylin and eosin (HE), smooth muscle actin (SMA) and Factor VIII (endothelium marker).

Together, these stains verified that the gross morphology of the vessel after being *ex vivo* is comparable to that *in vivo.*

Glycocalyx

Integrity of *in vivo* and *ex vivo* vessels were evaluated with confocal microscopy as previously described[92]. Specifically, the femoral artery was quickly excised or removed from the chamber and flayed open longitudinally to expose the endothelial cell surface. After removal they were placed in 4-2-hydroxyethyl-1-piperazineethanesulfonic acid (HEPES)-buffered salt solution (HBSS, in mmol/L: 5.55 glucose, 114 NaCl, 10 KCl, 1.18 KH2PO4, 1.17 MgSO4·7H2O, 0.5 CaCl2, 25 NaHCO3, 5.0 HEPES, 0.025 EDTA; pH 7.41±0.03) containing 0.1% bovine serum albumin at room temperature. The tissues were then incubated with biotinlylated hyaluronan binding protein (HABP) and mouse anti-heparan sulfate (HS) IgM antibody. After washing, they were incubated with Alexa Fluor 488 conjugated streptavidin (Molecular Probes) that binds to the biotinlylated HABP (US Biologics) and Alexa Fluor 594 conjugated goat-anti mouse IgM secondary (Molecular Probes) to bind to the HS antibody. All incubations were performed in HBSS-BSA for 30 minutes at room temperature. The vessel segments were then placed in a tissue culture dish with a glass bottom in the presence DAPI (nuclear stain) in a soft mount and imaged with a confocal microscope. The glycocalyx thickness was then quantitatively measured as the distance between the HS- or HA-stained luminal boundary focal plane and peak EC nuclear position[92].

mRNA Expression

Extracted and analyzed via qPCR using same primers and methodology as chapter 2. Same markers analyzed as *in vivo*; TNFα, IL-2, MCP-1 as cytokines, VCAM-1, ICAM-1, P-selectin as

endothelial adhesion molecules, and TGFβ, FGF, VEGF, Egr-1 as vascular growth markers. mRNA analysis compared *in vivo* to *ex vivo* physiological flow as well as no flow. Separately, the three branches (B1, B2, B3) of the femoral artery (*figure 15*) were compared to the main femoral artery pre and post *ex vivo* perfusion.

Statistical analysis

Performed between *in vivo* and No Flow *ex vivo* and physiological *ex vivo* conditions using a one-way and two-way student t-test, respectively with Welch's correction to account for different variances. Using n=4 experiments were calculated to have a power of 85% for determining significance at $p<0.05$.

RESULTS

Baseline structure is maintained *ex vivo* compared to *in vivo,* and baseline inflammatory phenotype is characterized at *ex vivo* physiological WSS

Established by comparing tissue structure and endothelial cell markers from arteries analyzed immediately after isolation and arteries perfused under physiological conditions for 24 hours.

Histology

Figure 16. *Histology sections of the mouse femoral artery immediately after in vivo excision. H&E stain shows basic gross morphology. SMA shows smooth muscle cell layer, and the thickness of it. Factor VII shows the endothelium as a complete undisrupted sheath on the inner most later.*

Histology images show that structural integrity is maintained after the femoral artery is perfused *ex vivo*. *In vivo* images are seen in *figure* 16, with a clearly marked thick SMC layer and a thin continuous endothelium. When analyzing the corresponding images of vessels after 24 hours of physiological flow no shearing of the endothelium us seen, and the thickness of the endothelium and VSMC is maintained as well (data not shown).

Glycocalyx

Thickness of the glycocalyx was analyzed using confocal microscopy. Both HABP and syndecan-1 were stained in an effort to identify the mechanosensing layer. However, only syndecan-1 staining proved to be effective in this case. The green colored florescence in *figure 17* represents the protein in the glycocalyx layer that is above the nuclei of the cells (blue). The thickness of the layer was comparable in both the *in vivo* and *ex vivo* samples.

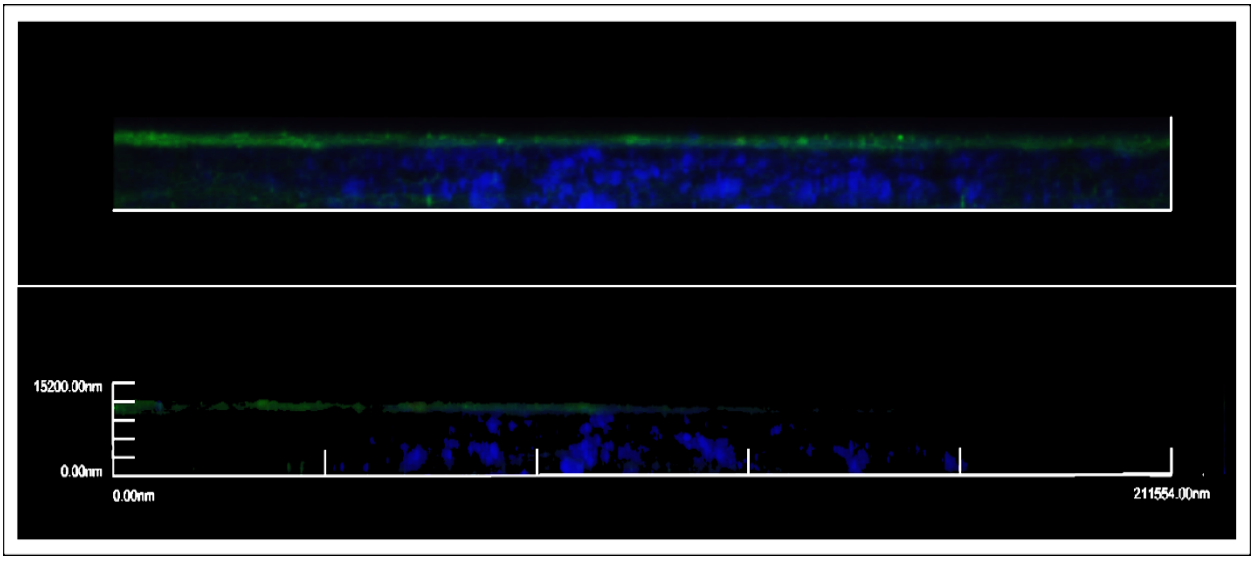

Figure 17. *Confocal image of glycocalyx staining of mouse femoral artery endothelium immediately after in vivo excision (60x). Green fluorescent layer on top represents the glycocalyx protein syndecan-1. Blue Fluorescence is DAPI staining of the nuclei. This image is representative of all images taken both in vivo and ex vivo, image brightness has been altered to allow for better visualization.*

Wall Shear Stress RNA analysis

qPCR analysis shows the level of inflammation based on cytokines, adhesion molecule and growth factor expression levels after physiological vessel perfusion. In *figure 18* there are statistically significant increases in expression of MCP-1, P-selectin and ICAM-1 under physiological WSS. These changes are similar to that seen under no WSS. Fold changes are with respect to *in vivo* ± standard error. Specifically, MCP-1 is increased by 53.49±20.4 fold and 59.19±20.72 fold under No Flow and physiological, respectively which is significantly greater than the 5 fold increase seen in the *in vivo* samples ($p<0.05$). P-selectin increased by 9.46±1.98 fold and 9.35±1.69 fold in No Flow and physiological, again significantly greater than *in vivo* ($p<0.01$). These changes are not seen however in the case of TNFα and VCAM-1 where there is a significant increase with No Flow (16.02± 5.87 fold and 3.96± 1.45 fold) conditions that is absent in the case of physiological WSS.

In *figure 19* the expression of growth factors is displayed. FGF-2, VEGF and Egr-1(transcription factor) are upregulated under No Flow by 2.45±0.82, 1.58±0.43, and 3.86±1.32 fold. A less robust response than the cytokine but significant ($p<0.05$). FGF-2 is similarly upregulated under physiological WSS (2.37±0.66 fold). Egr-1 also shows a lesser but significant upregulation (2.67±0.42 fold).

All changes of mRNA expression at physiological WSS will be incorporated into the analysis moving forward as a baseline inflammatory phenotype for this model.

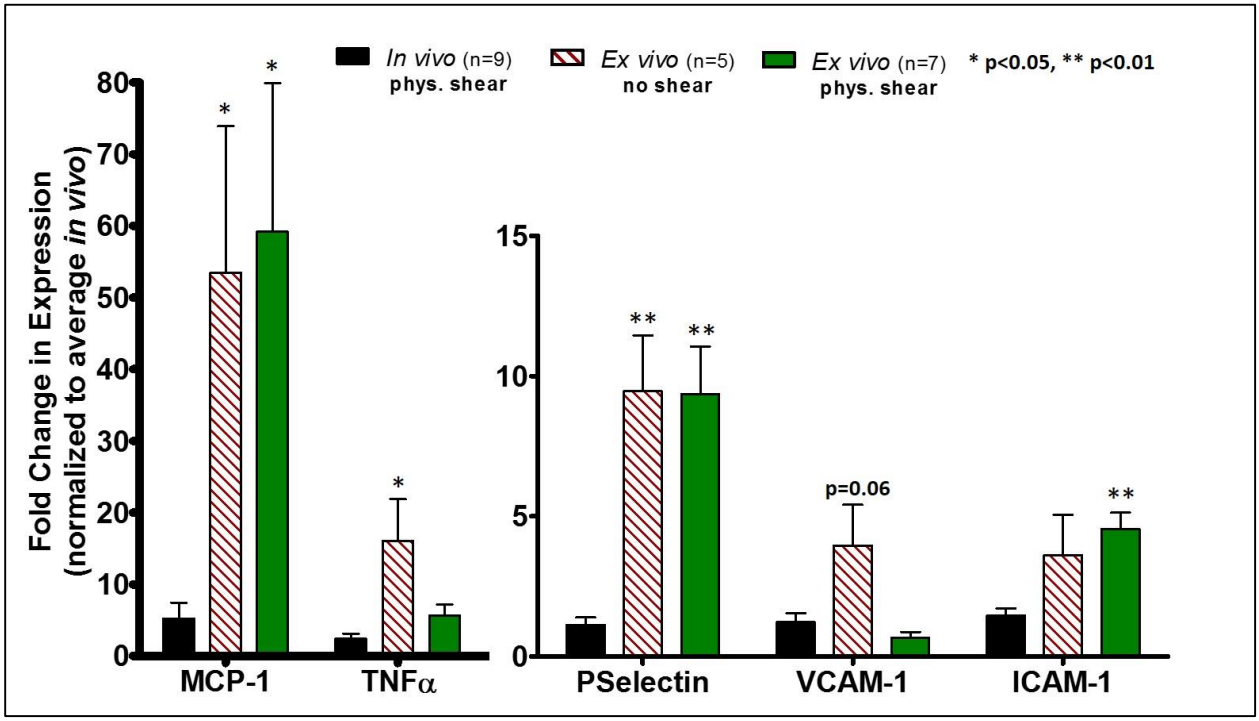

Figure 18. *Bar graph of cytokine and adhesion molecule mRNA expression in vivo, with no WSS, and physiological WSS. No WSS shows an inflammatory response across the board. Physiological WSS does induce an inflammatory response in all except TNFα and VCAM-1. This level of inflammation will be considered as baseline. Data is normalized to housekeeing gene GAPDH and fold change is expressed as* $2^{-\Delta\Delta CT}$ *with respect to in vivo samples. *p<0.05, **p<0.01*

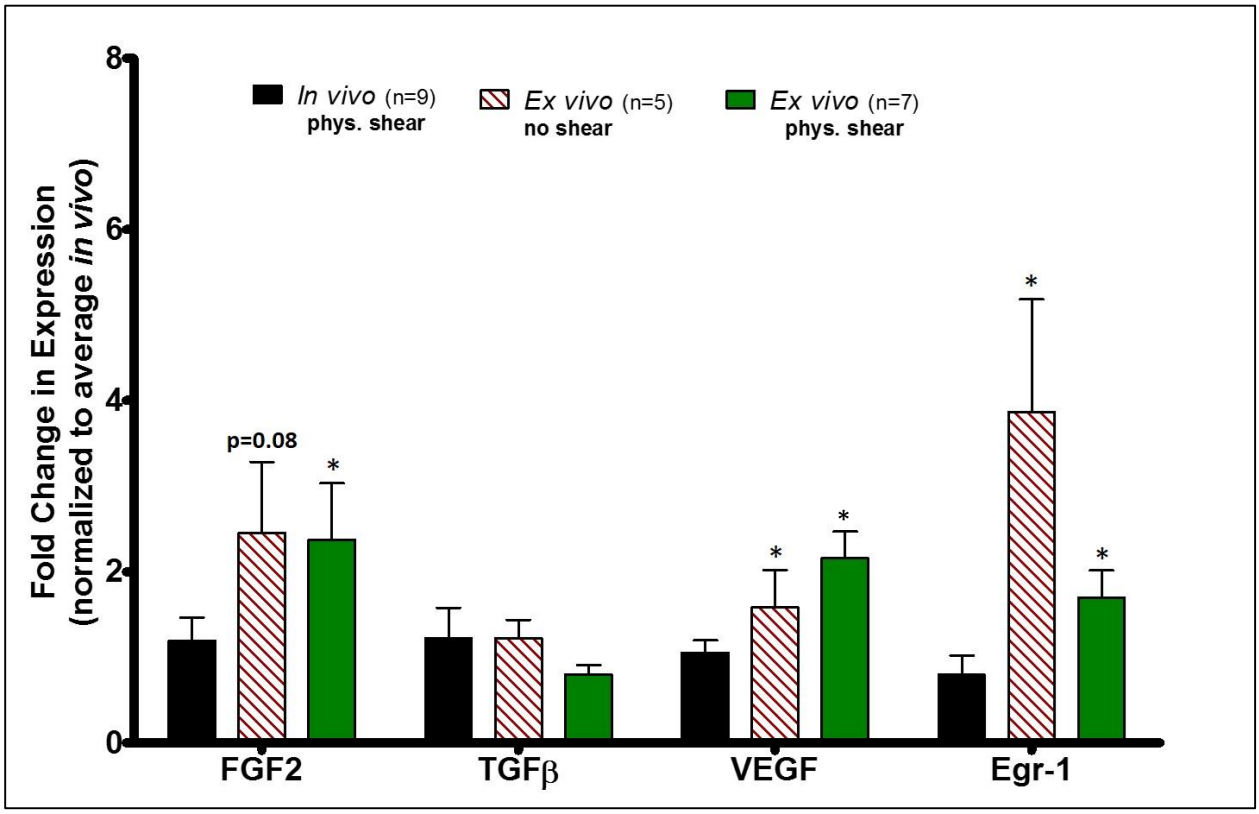

Figure 19. *Bar graph of growth factor and transcription factor (Egr-1) mRNA expression in vivo, with no WSS, and physiological WSS. Under No Flow conditions all factors are upregulated significantly except for TGFβ. Under physiological WSS, FGF2 and Egr-1 show a significant upregulation. Data is normalized to housekeeing gene GAPDH and fold change is expressed as* $2^{-\Delta\Delta CT}$ *with respect to in vivo samples. *p<0.05, **p<0.01*

Main Femoral Artery and Branches Show No Significant Differences

Branch RNA analysis shows expression of all markers in each of the three branches as fold change= $2^{-\Delta\Delta CT}$ with respect to the main femoral artery (*figure 20*). For three conditions, *in vivo*, *ex vivo* 1.4x physiological flow and *ex vivo* no flow, differences were noted in each branch expression (B1, B2, B3) compared to the main femoral artery (FA) for each marker. Differences were analyzed with multiple paired t-tests. There are no significant differences seen in inflammatory marker expression in any branches when compared to FA, except with ICAM expression where B1 with No Flow was significantly upregulated by 6.11±1.40 fold ($p<0.05$).

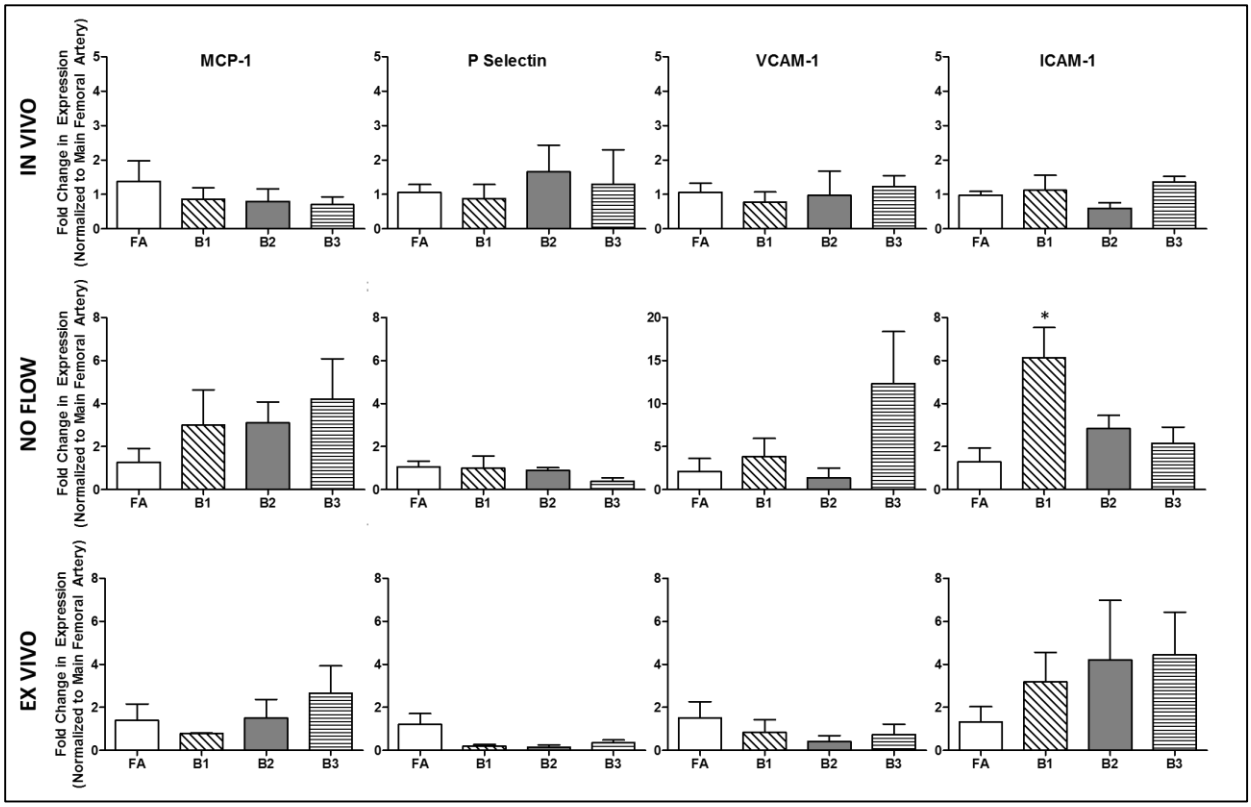

Figure 20. *Bar graphs reresenting mRNA expression of MCP-1, P-selectin, VCAM-1 and ICAM-1 in the three branches of the femoral artery, with respect to the main femoral artery. Analysis is shown for in vivo, no flow and ex vivo vessel. Ex-vivo vessel in this case was perfused at 1.4x physiological WSS. In all cases there were minimal differences seen in expression by the branches when compared to the the femoral artery. Data is normalized to housekeeing gene GAPDH and fold change is expressed as* $2^{-\Delta\Delta CT}$ *with respect to Main Femoral Artery for each condition. n=3 for all conditions. *p<0.05.*

DISCUSSION

Through this study, the use of an explanted femoral artery and its branches was evaluated for the first time. Many *ex vivo* vessel studies use coronary arteries, aortic arches and rings, thoracic/abdominal aorta, and microvessels (arterioles)[81,83,86,87,93]. For the study of WSS induced inflammation, *in vivo* occlusion studies are still the most prevalent.

One of the concerns of using the femoral artery for an inflammation model was that it would not respond the same as the branches and smaller vessels that would, *in vivo*, be responsible for flow mediation through vasodilation, constriction or new vessel formation. Specifically, collaterals do not likely form right off of the main femoral artery but rather off the branches. This study shows that, the overall structure of lumen, endothelium and VMSC being the same, the femoral artery can be used to assess changes due to WSS induced inflammation that can be extrapolated to the branches. This is validated quantitatively through the qPCR results stating that the branch expression is overall not significantly different than the main femoral artery under any conditions. Specifically, the femoral artery expression of chemoattractants, adhesion molecules sand growth factors in response to stimuli is comparable to that of the three branches off the femoral artery. The benefits of being able to use the femoral artery for WSS inflammatory studies stem from the simple fact that it is a larger vessel and easier to manipulate in real time, as well as in processing for post-perfusion analysis of RNA expression.

Other existing models of explanted vessels use similar set ups with abilities to control flow rate, pressure, temperature[81,90,83]. One main variability between studies lays in the perfusate, which is for the most part a basic tissue culture media with specific osmolarity, osmolality and pH. Some systems will add a thickening agent to the media to increase the viscosity to match physiological (40 cP or 4.0×10^{-3} Ps). This is of great relevance to perfusion studies, as the viscosity will directly

affect the shear stress imparted upon the endothelium in the lumen. In this study there was the choice to either use physiological flow rate and thicken the media with dextran to induce physiological shear stress, or leave the media less viscous (0.89cP or 8.9 x 10^{-4} Ps) and increase flow rate to induce physiological shear stress—the decision was made to go with the later.

The rationale was to mitigate the side effects of using dextran to thicken the media. Dextran is commonly used clinically to decrease vascular thrombosis. Specifically dextran binds erythrocytes, platelets, increasing their electronegativity so as to inhibit their aggregation and clumping[94]. This is not a major concern for this study as these particles are being excluded. The first major issue is that the osmolality of the media will be changed, in fact dextran is used in osmotic stress techniques to purposely apply osmotic pressure to biological molecules[95,96]. Since ion channels play a large role in the inflammatory state, this is a concern that could not be ignored. Perhaps most concerning is that dextran also binds the factor VIII- Von Willebrand factor on endothelial cells. The endothelium is the first line of sensing and mechanotransduction of WSS changes, any binding to the endothelial cells could be of concern for the expression of adhesion molecules that are critical for expression of the complete inflammatory phenotype[97].

In addition to flow rate, the pulsatility was characterized[90]. The average heart rate of a C57Bl/6 mouse is about 400 beats/min. The pulsatility is imparted by the roller pump in this study was dependent on the RPM setting. As a result the pulsatility was not equal to physiological, but the goal was to impart the correct maximum shear stress that would be felt by the endothelium *in vivo*. It is admittedly a limitation that the pulsatility cannot be consistent in this model. It should be noted however, that in previous perfusion studies laminar flow has been used as well as roller pumps as in this study. The use of the roller pump was selected because it was deemed important

that the vessel experience peak and minimum WSS in both positive and negative directions as would be *in vivo*.

Overall, this study characterizes an *ex vivo* femoral artery perfusion system in relation to its use for WSS dependent inflammation models. The data shows that the femoral artery is structurally maintained through 24 hours of perfusion. At physiological rates, there is inflammation shown, but no-flow shows more significant inflammation. As long as we assess the baseline inflammatory phenotype after physiological perfusion, this system can be confidently used for inducing specific peak WSS, and identifying chemoattractants, adhesion molecules, and growth factors indicating inflammation.

CHAPTER 4
VASCULAR ENDOTHELIUM ACTIVATION IS INCREASED WITH INCREASED FLUID WALL SHEAR STRESS

ABSTRACT

To study the inflammatory response in a femoral artery due to induced increases in wall shear stress in an *ex vivo* femoral artery bioassay chamber. This aim utilizes the validated *ex vivo* system from chapter 3 to induce inflammatory conditions in the femoral artery by increasing WSS and analyze the vessel's response. The baseline control was the physiological WSS determined in chapter 3, and inflammation induced using TNFα is a positive control. The experimental conditions were induced by increasing the flow through the vessel. The flow was specifically be set to induce 1.4x and 2x physiological WSS. The results were analyzed for RNA expression via qPCR.

INTRODUCTION

In vivo studies of arterial occlusions using the FAE model have provided valuable information to the field of study. However in these models, specific conditions at particular vascular sites are difficult to control, and any chemical or surgical interventions inevitably cause systemic changes that cannot be controlled. Using this *ex vivo* model I will be able to control the level of inflammation chemically or mechanically easily with TNFα or increasing the flow rate from the pump.

MATERIAL AND METHODS

Experimental Design

This aim has two groups, TNFα induced inflammation and wall shear stress (WSS) induced inflammation (n=6/group). The TNFα group serves as a positive control for changes induced by inflammation, there were two experimental high WSS conditions of 1.4x and 2x normal. The normal WSS condition from chapter 3 was used as the negative control (n=6).

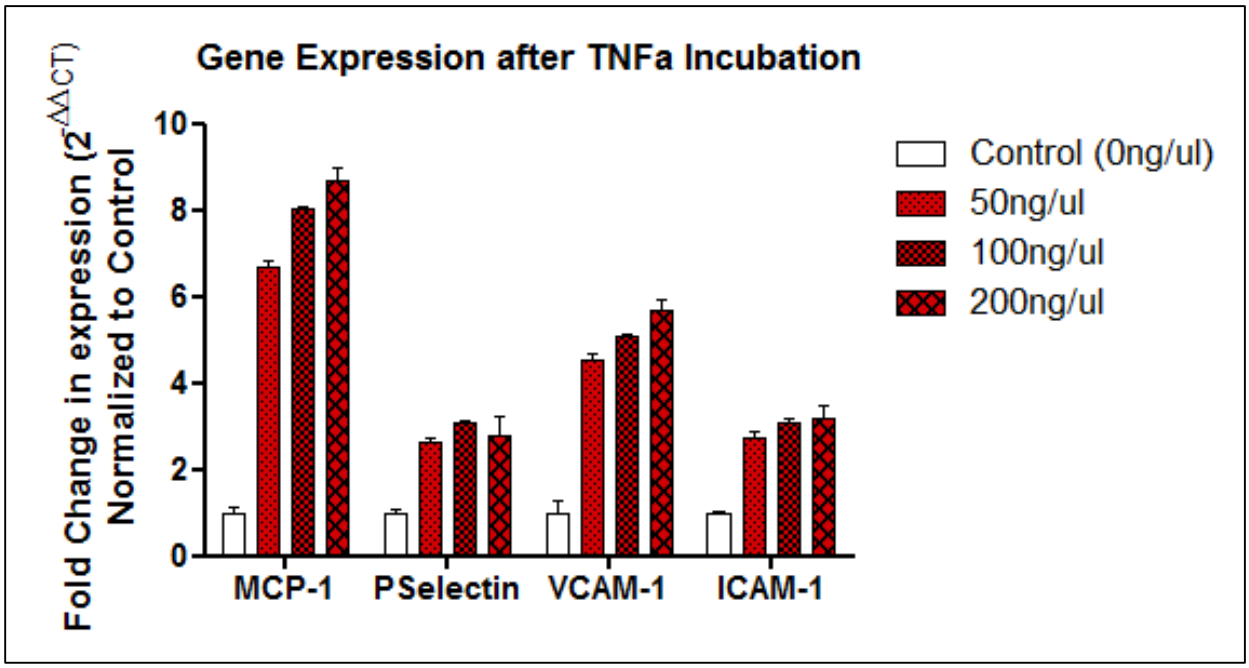

Figure 21. *qPCR results showing inflammatory marker expression of MCECs after incubation with TNFα. Fold changes are with respect to control cells not incubated with any TNFα. There was a response at 50ng/µl and increases as dose increases. At all doses changes were significant compared to control p<0.00. Data is normalized to housekeeing gene GAPDH and fold change is expressed as* $2^{-\Delta\Delta CT}$ *with respect to control.*

TNFα concentration determination

To determine the concentration of TNFα necessary to induce inflammation MCECs (Mouse cardiac endothelial cells) were used. These cells are an immortalized cell line commonly used in in *in vitro* studies of endothelial cells. The cells were plates in a 6 well plate and incubated with varying concentrations of TNFα-mouse (Sigma), 0ng/ul (control), 50ng/ul, 100ng/ul, 200ng/ul, for 1 hour. The cells were then harvested using TriZol reagent, the mRNA isolated and qPCR performed to determine endothelium activation. Cytokine, MCP-1, and endothelial markers P-Selectin, VCAM-1 and ICAM-1 expression was analyzed as done previously using the same primers. The expression is shown as fold change over the control cells (*figure 21*). There is a dose dependent increase in inflammatory marker expression. From this data 50ng/µl will be the concentration of TNFα used to induce activation. Although 200ng/µl results in a more robust

expression change, 50ng/µl is significantly greater than control ($p<0.001$) and is therefore sufficient.

TNFα induced inflammation

TNFα served as the positive control in these studies. Specifically, the perfusate had normal physiological flow rate but will be supplemented with TNF 1µg/mL TNFα (equivalent to 50ng/µl). The vessel was perfused for 24 hours as in chapter 3 and then analyzed for the inflammatory markers.

Induced Wall Shear Stress (WSS)

Controlled by changing the flow rate of the perfusate. Physiological peak WSS was as determined in chapter 3; τ_ω= 10.18 Pa, Medium WSS was 1.4x physiological= 14.26 Pa, and high WSS was 2x physiological= 20.37 Pa. At each WSS setting the vessel was perfused for 24 hours then analyzed for inflammatory markers.

RNA Expression

Extracted and analyzed via qPCR using same primers and methodology as chapter 2. Same markers analyzed as *in vivo*; TNFα, IL-2, MCP-1 as cytokines, VCAM-1, ICAM-1, P-selectin as endothelial adhesion molecules, and TGFβ, FGF, VEGF, Egr-1 as vascular growth markers.

Statistical Analysis

All data is represented as fold change with respect to *in* vivo and statistically analyzed with respect to the physiological peak WSS condition. Multiple t-tests were used to assess differences with Welch's correction to account for unequal variances.

RESULTS

TNFα positive control showed a significant increase in expression of all cytokines and adhesion molecules as seen in *figure 22* ($p<0.05$) except for TNFα ($p=0.07$) and P-selectin ($p=0.06$). Fold changes are given ± standard error. At 1.4x and 2x pWSS fold changes in expression compared to *in vivo* for MCP-1 and P-selectin respectively, were 41.28±15.00 and 95.62±36.48 fold, and 6.47±2.25 and 16.74±8.05 fold (both are not significantly different due to the high expression at pWSS). TNFα is upregulated 30.73±8.26 fold at 1.4x which is significantly greater than pWSS ($p<0.05$). VCAM-1 is significantly upregulated by 10.93±3.95 fold ($p<0.05$) at 1.4x while ICAM-1 is upregulated by 2.98±0.47 ($P=0.05$) at 2x. The results show that there is discernibly increased inflammatory marker expression at both 1.4x and 2x WSS compared to pWSS, even with increased levels at pWSS.

In respect to the growth factors (*figure 23*), with TNFα positive control TGFβ and Egr-1 show a significant increase in expression, though the fold changes are not as robust as the cytokines and adhesion molecules. Specifically a 1.78±0.37 and 2.92±0.69 fold change is seen, respectively ($p<0.05$, $p=0.08$). TGFβ also shows increases at 1.4x and 2x of 2.09±0.56 and 2.16±0.48 fold ($p<0.05$). Transcription factor Egr-1 also shows an increase at 2x of 2.67±0.42 fold and a *significant decrease* of 0.75±0.15 fold ($p<0.05$). FGF-2 and VEGF do not show changes until 2x where there is significant increases of 6.08±1.65 and 4.17±0.85 ($p<0.05$).

We can conclude from both cytokine/adhesion molecule and growth factor data that WSS has an independent role in regulating arterial inflammation.

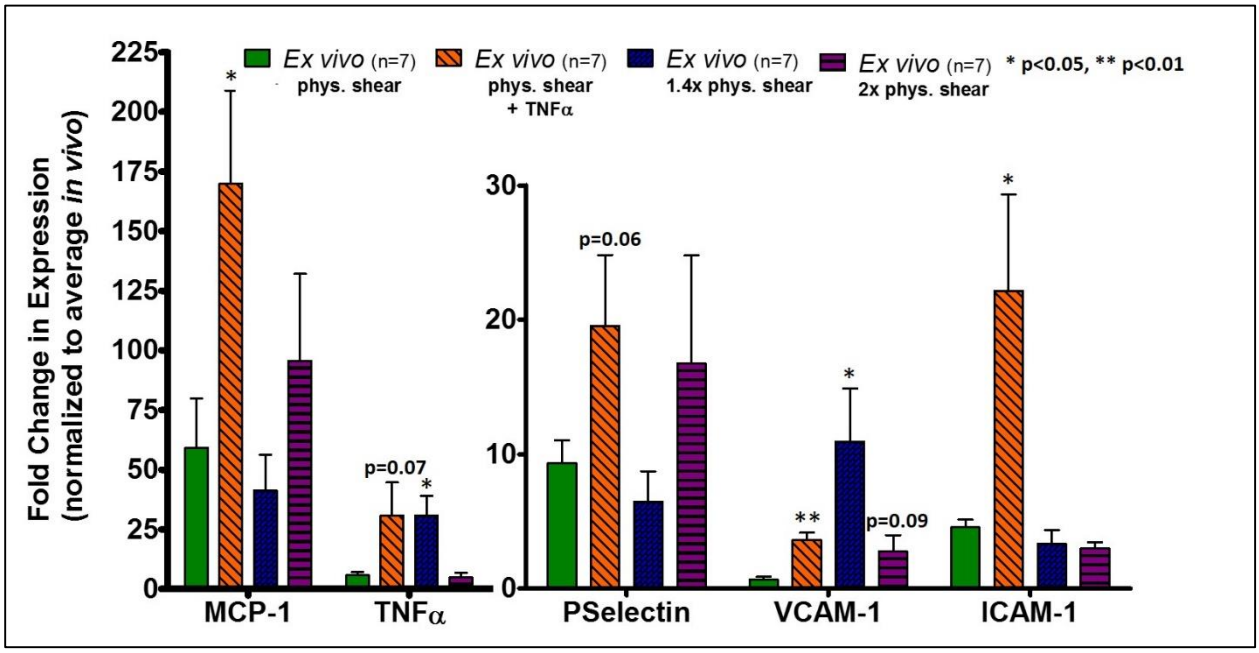

Figure 22. *Bar graphs representing fold change in mRNA expression of cytokins and adhesions molecules after enduring increased WSS and positive control TNFα stimulation. TNFα shows increases in expression across the board. 1.4x pWSS causes an upregulation of TNFα and VCAM-1. 2x pWSS doesn't show significant changes but trends toward upregulation can be seen in MCP-1, P-selectin and VCAM-1. Data is normalized to housekeeing gene GAPDH and fold change is expressed as* $2^{-\Delta\Delta CT}$ *with respect in vivo. *p<0.05, **p<0.01.*

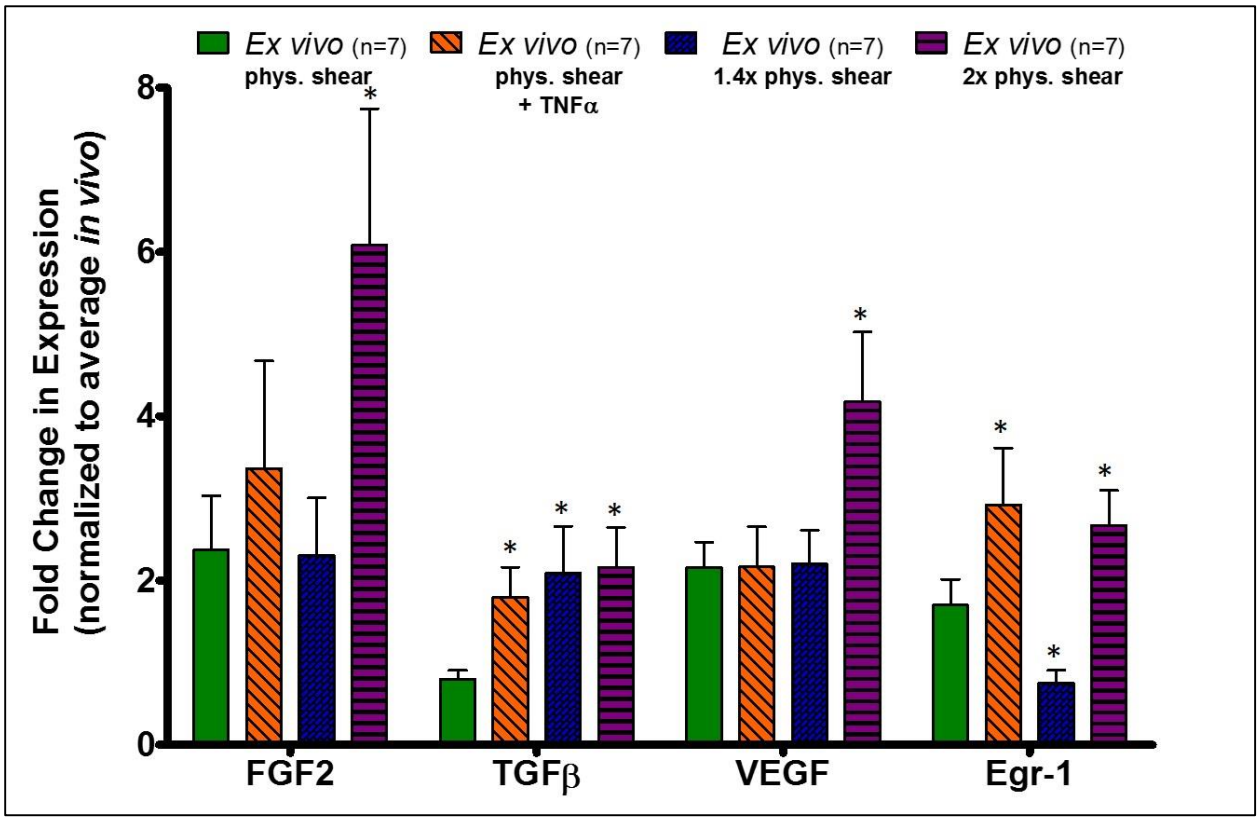

Figure 23. *Bar graphs representing fold change in mRNA expression of growth factors and transcription facto Egr-1 after enduring increased WSS and positive control TNFα stimulation. TGFβ is upregulated under all experimental conditions. 2x WSS presents with significant upregulation of all factors, even when TNFα did not (FGF2, VEGF). 1.4x WSS does not upregulate growth factors, but significantly downregulates Egr-1. Data is normalized to housekeeing gene GAPDH and fold change is expressed as* $2^{-\Delta\Delta CT}$ *with respect in vivo. *p<0.05.*

DISCUSSION

In this study two high WSS conditions were analyzed in respect to the baseline of physiological WSS with TNFα positive control as a reference. Even though physiological wall shear stress elicited an increase in gene expression for many markers, here we see that the increase in WSS provides even greater increases that are discernable beyond the established baseline.

As was hypothesized, MCP-1, TNFα, P-selectin (trend), and VCAM-1 were significantly upregulated with increases in WSS. These markers represent the endothelium's response when initiating an inflammatory response. These same markers are seen to upregulated in *in vivo* occlusion studies[98,80]. It was surprising that ICAM-1 did not present an upregulation as it has been repeatedly shown to be a key factor. However, from chapter 3, we know that the physiological baseline for ICAM-1 already shows an upregulation from *in vivo*. And since the expression of ICAM-1 is known to be early-on it is possible that the upregulation is maxed out at physiological baseline, or any further changes would have been seen prior to the 24 hour time point.

The growth factors analyzed were also selected for their prominence in other studies. It was further hypothesized that there would *not* be an upregulation of growth factors from an increase in shear stress alone. It was expected that the recruitment and influx of leukocytes would be necessary to see any viable increases in growth factor expression[53]. However, here, we see that the selected growth factors do in fact all increase in expression with the increases in WSS.

One theory is that perhaps the upregulation of growth factors is specific to the increases in particular cytokine expression induced by increasing WSS. Specifically, MCP-1 is more

upregulated in 2x WSS than 1.4x and elicits a modest P-selectin and VCAM-1 response. This same parameter results in significant upregulation of FGF-2, TGFb, VEGF and Egr-1. On the other hand, 1.4x WSS shows a significant upregulation of TNFα, while 2x WSS does not. This group then proceeds to not upregulate of P-selectin, though upregulation of VCAM-1 is significant. The growth factors similarly show no upregulation except in TGFβ and actually a significant *downregulation* of Egr-1. This might imply that inducing MCP-1 expression is more relevant to pushing vasculature towards an arteriogenic phenotype than TNFα. This is further supported by the fact that the positive control of TNFα itself illicits a robust MCP-1 response and the subsequent upregulation of almost every marker (except VEGF). However, this theory hits a road block when we see that TNFα expression from the TNFα positive control as well as 1.4x WSS is nearly identical, but the 1.4x does not result in the same phenotypic outcome.

Another, perhaps more promising, idea is that Egr-1 is the driving force. In both 2x WSS and TNFα positive control, Egr-1 is significantly upregulated from physiological WSS. It is known that Egr-1 is a transcriptional factor that plays a role in both pushing the vascular endothelium and VSMCs towards a synthetic phenotype. It is possible that Egr-1 is triggered immediately by the increase in WSS or any other inflammatory activity (TNFα), which then causes a signaling cascade to initiate the inflammatory and synthetic phenotype for the endothelial cells (described in chapter 1). This response progresses through to the VSMC which themselves enter into a synthetic phenotype.

This leads into the question of why, then, does 1.4x pWSS cause a downregulation of Egr-1. While we were expecting a sort of "dose-response" to WSS, it is possible that there is a threshold that needs to be bet in order for Egr-1 to initiate. While a modest inflammatory response is elicited as perhaps indicated by the expression of TNFα, VCAM-1 and TGFβ, a complete response is waiting

for a specific threshold to be met. Also to be considered, is the nature of the pulsatility of the vessel perfusion. The pulsatility at 1.4x WSS is a lower frequency than at 2x WSS, as we know from the pump characterization in chapter 2. Perhaps this plays into the mechanotransduction and signal sensing that the max WSS is being applied at a greater rate at 2x WSS than at 1.4x WSS.

Egr-1 has been shown in recent literature to be a potential "master switch" in arteriogenesis[17,80,80]. Knockout studies have shown that without Egr-1 the arteriogenic response following occlusion is severely blocked[80]. Preliminary studies in our lab have also shown that inflammatory response and monocyte recruitment is diminished in the case of Egr-1 knockouts after femoral artery excision. Further studies using this femoral artery model with Egr-1 knockout arteries could provide valuable information regarding the mechanistic role of Egr-1 in initiating arteriogenic growth.

We can conclude from this study that WSS alone, even without the presence of leukocytes, has the ability to induce an inflammatory phenotype of cytokine, adhesion molecules *and* growth factors. Further, this *ex vivo* femoral artery model is a viable platform for analyzing these changes in a more simplified and easy to access and alter setting. Following studies addressing limitations due to perfusion methods (pulsatility), as well as those assessing multiple time points and more levels of WSS will be able to assess the mechanisms and time frame of the arteriogenic response with respect to WSS.

CHAPTER 5
MONOCYTE RECRUITMENT, ADHESION AND SUBSEQUENT VASCULAR GROWTH FACTOR EXPRESSION INCREASE WITH INCREASED WALL SHEAR STRESS

ABSTRACT

To study monocyte recruitment and progression towards collateral vessel growth in an ex vivo femoral artery bioassay chamber. This aim also utilizes the validated *ex vivo* system from chapter 3, and the experimental samples from chapter 4 will serve as the monocyte-negative controls. In this aim, *ex vivo* femoral arteries were subject to the same wall shear stresses from chapter 4 (physiologically normal, 1.4x higher, and 2x higher). Following the induction of inflammation as predicted in chapter 4, monocytes were fluorescently labeled and introduced into the perfusate. The subsequent adhesion of the monocytes to the endothelial wall was captured by video to allow a time related analysis. The further progression towards arteriogenesis will be analyzed in monocyte (+) vessels as well as the monocyte (-) negative controls (increased wall shear stress only). The results were analyzed for monocyte adhesion by video, immunohistochemistry, and RNA expression via qPCR.

INTRODUCTION

Monocyte recruitment studies are primarily *in vitro* studies, or require the sacrifice of animals at multiple time points to analyze accumulation. With this *ex vivo* model I can observe monocyte behavior in a whole vessel with all the extracellular matrix and structure intact, mimicking the *in vivo* state. Further, the *ex vivo* model will allows monitoring of recruitment and adhesion over multiple time points in the same tissue, reducing the total amount of animals necessary.

MATERIAL AND METHODS

Experimental Design

For this aim the positive control was TNFα induced inflammation + monocytes (n=4), the negative control was the experimental samples from chapter 4 where there is induced inflammation without

monocytes. There were three experimental groups 1) physiological peak WSS (10.18 Pa) + monocytes, 2) 1.4x physiological peak WSS (14.26 Pa) + monocytes and 3) 2 physiological peak WSS (20.37 Pa) + monocytes. All groups were analyzed via immunohistochemistry and RNA analysis separately 24 at (n=4).

Negative Mouse Monocyte Enrichment

The EasySep Monocyte Enrichment Kit from StemCell (cat#19761) was used for this process. Briefly, bone marrow was harvested from both femoral arteries using a total of 4mL of "recommended medium" (PBS + 2% FBS). The sample was spun at 300g for 6 minutes and the supernatant discarded. After resuspending in recommended medium monocyte enrichment cocktail was added, which is a cocktail of biotinlylated antibodies against cell surface antigens on all cells other than specifically monocytes. Following washing, a tetrameric antibody complex was added which recognizes and binds both biotin as well as dextran. The dextran it binds to is in the next reagent which are magnetic dextran iron particles. Finally, placed in the EasySep magnet, the magnetic particles withhold all the labeled unwanted cells, leaving only untouched monocytes in the liquid. The monocytes were then incubated with calcein-AM to tag them for imaging.

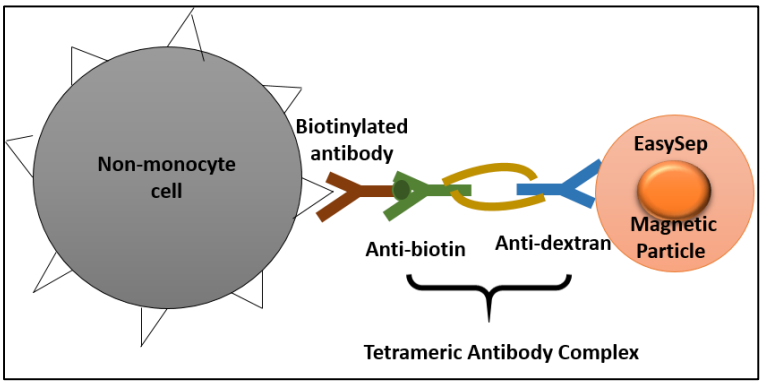

Figure 24. *A schematic of the antibody binding process to remove all unwanted cells for negative isolation of monocytes from bone marrow. Anti-dextran, Biotinlyated antibodies attach to all unwanted cells. Dextran coated magnetic beads then attach to all tagged cells. After placing in a magnet only monocytes are remaining in the suspension.*

Fluorescence-activated cell sorting (FACS)

FACS was used to confirm purity of isolated monocytes. Pelleted cells were resuspended in FACS buffer. The cells were then blocked in the dark for 10 minutes. The antibodies for CD11b+ and Ly6c, specific for primary monocytes were then added at 25µl, incubated in the dark for 8 minutes. Cell aliquots were also stained with CD11b only and Ly6c only, as well as blank for control purposes (plots not shown here). The cells were the washed in FACS buffer and resuspended in PBS + 1% paraformaldehyde for fixation. Cells were then sorted to for double labeled cells and also to measure the intensity of the CD11b and Ly6c staining. From *figure 25* we can see that almost all the cells have been stained for both markers >98%. There appears to be two distinct populations which is consistent with the fact there monocytes are known to exist as both $Ly6c^{hi}$ and $Ly6c^{lo}$ cell types[99]. The cells were also counted using a coulter counter, which showed that from 2 femurs a total of approximately 500,000 monocytes can be isolated using the negative isolation technique.

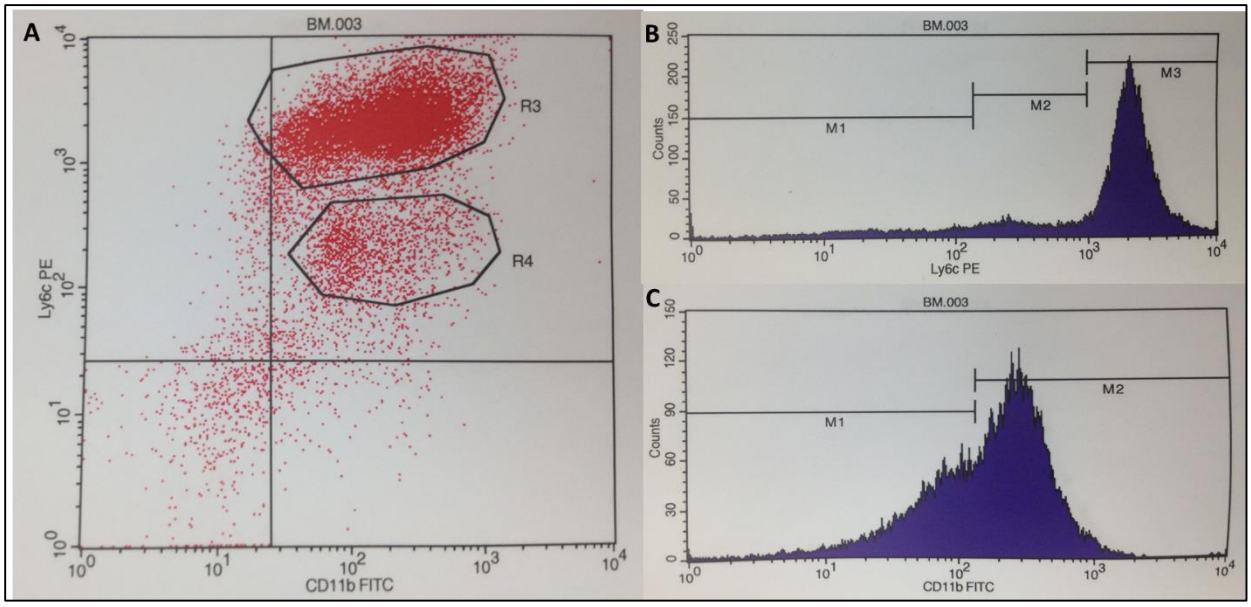

Figure 25. *Results from FACS sorting of negatively isolated monocytes.* ***A)*** *shows the FACS scatter of the double labeled cell population which is in the upper right quadrant that comprised >98% of the cells.* ***B)*** *shoes the intensity of the Ly6c labeling and* ***C)*** *shows the intensity of the CD11b staining.*

Monocyte Activation

Monocytes will be activated using TNFα at the concentrations determined by the MCEC *in vitro* experiment from the chapter 4. Specifically monocytes were exposed to 50ng/mL of TNFα for 30 minutes. Simultaneously, Calcein-AM was added to the monocytes; calcein is a green fluorescent marker that will bind to all live cells, and since there are only monocytes in solution, all the monocytes were tagged green. After 30 minutes the cells were washed by centrifugation at 300g for 3 minutes three times. (This is very important otherwise when perfused in the femoral artery, the residual calcein will attach to the viable cells in the vessel). The cells are now ready to use, they remain viable for a few hours without the addition of any cytokines. The cells were fluorescently imaged to assess the efficacy of the labeling (*figure 26*). It was found by manual counting that 100% of the live cells were labeled with the calcein. These images were also used as a reference point for the size of the monocytes when assessing attachment to the femoral artery.

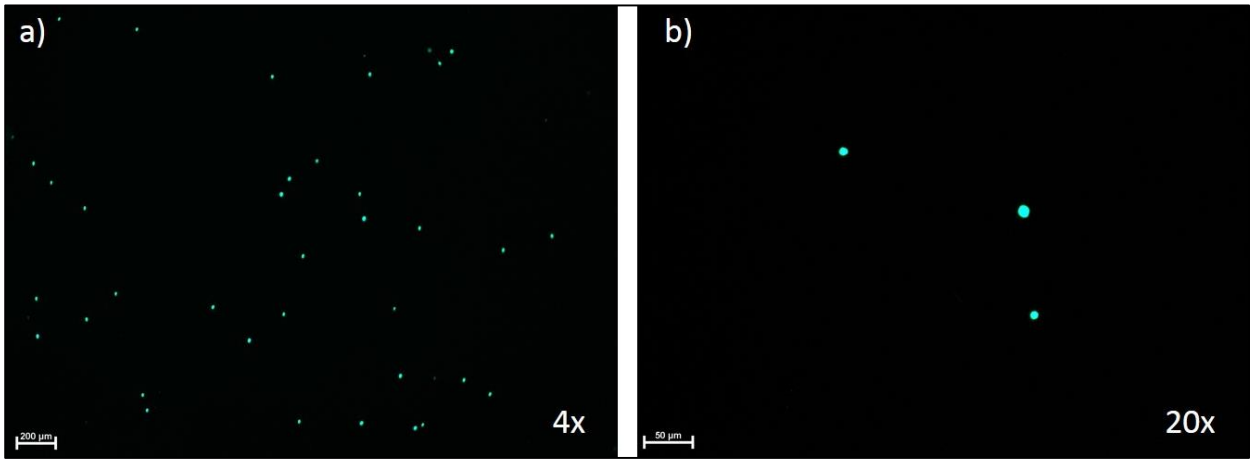

Figure 26. *Negatively isolated monocytes were incubated with calcein-AM for 30 minutes. The cells were then washed and a small drop placed on a glass slide to visualize the effectiveness of the labeling. Shown here are the calcein labeled monocytes.* ***A)*** *Representative size of monocytes when labeled seen at 4x.* ***B)*** *Representative field of labeled monocytes at 20x.*

Monocyte Recruitment and Adhesion

Measured as a function of time by video and immunohistochemistry. Using video the TNFα activated and calcein labeled monocytes perfused through the cannulated artery were monitored. At 24 hours the vessels were fixed and imaged for CD11b to quantify the monocytes that have adhered. RNA was extracted and analyzed via qPCR as in the previous chapters. Looking for the same markers as *in vivo*; MCP-1 and TNFα as cytokines, VCAM-1, ICAM-1, P-selectin as endothelial adhesion molecules, and TGFβ, FGF, VEGF, Egr-1 as vascular growth markers.

RESULTS

Upon perfusing the cannulated femoral arteries with isolated monocytes, it became apparent that the velocity of the monocytes was too high to allow for any rolling, or sticking of the monocytes, and therefore would not allow for any subsequent increases in arteriogenic factors. Through the microscope and video the monocytes can be seen traveling through the vessel but not sticking. *Figure 27* shows vessels with perfused monocytes. Upon flaying open, you can see that there is some evidence of monocytes in the TNFα and physiological WSS groups, but as soon as the WSS is increased to 1.4x WSS, there is no sign of any monocytes.

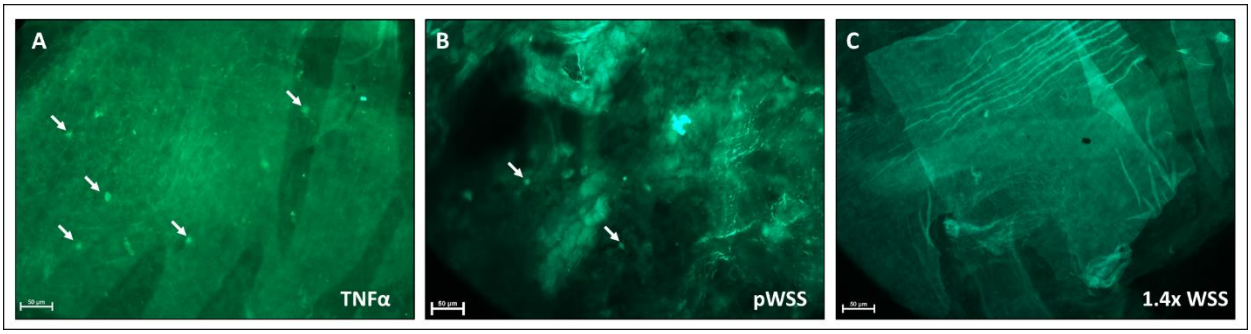

Figure 27. *Femoral arteries were perfused for 24 hours at* ***A)*** *pWSS with TNFα in the last hour,* ***B)*** *pWSS alone and* ***C)*** *1.4x WSS Calcein labeled TNFα activated monocytes were then introduced into the perfusate for 1 hour. The vessels were then harvested, flayed open, washed and fixed for imaging. The images here are taken at 20x. The white arrows indicate any possible adhered monocytes.* ***A)*** *TNFα vessels seem to have some monocyte attachment.* ***B)*** *pWSS had some evident of monocytes though much less than TNFα.* ***C)*** *1.4x WSS perfusion did not allow for any monocyte adherence. Further 2x WSS also did not allow monocytes to adhere (data not shown).*

Static Monocyte Adhesion

To test the endothelium activation of the artery after 24 hour perfusion and its ability to adhere monocytes, I flayed open the vessels post 24 hour perfusion and statically incubated them with activated monocytes for 1 hour. The vessels were then gently washed, fixed and imaged for any adherent cells. Vessels were fixed and mounted with DAPI so as to show the cellular vascular lumen. *Figure 28* shows a vessel incubated with monocytes after pWSS perfusion. There were no monocytes seen to attach under these conditions. *Figure 29* shows a femoral artery incubated with monocytes after TNFα endothelium activation. There is some evidence of monocyte attachment as indicated by the white arrows. This is a representative picture, there are some regions of the vessel that had more or less accumulation of monocyte labeling. *Figure 30* shows a femoral artery incubated with monocytes after 1.4x WSS perfusion. Here, like in the TNFα vessel you see an accumulation of monocytes along the vessel that is representative of the accumulation along the whole vessel. Finally *figure 31* shows a femoral artery incubated with monocytes after 2x WSS perfusion. Here there are clearly more adherent monocytes than in any other condition as indicated by the white arrows. This increase in representative of what was seen along the whole vessel.

The flaying of the vessel was inconsistent and therefore the amount of monocytes versus the amount of viable surface area was not consistent. This provides a preliminary picture that the increase in WSS does induce an activation that translates to monocyte adhesion, but more controlled studies need to be performed.

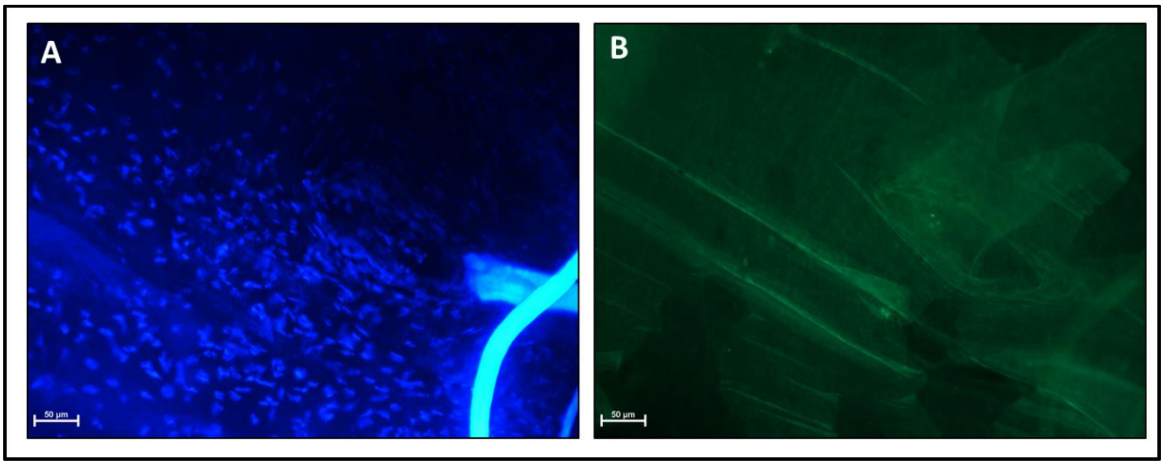

Figure 28. *Femoral arteries were perfused at pWSS for 24 hours. The vessels were then harvested, flayed open and incubated with static, activated, calcein labeled monocytes for 1 hour. The vessels were then washed, fixed and mounted with DAPI to visualize the endothelium. The vessels were imaged at 20x for any adherent monocytes. Representative images are shown here.* ***A)*** *DAPI stained vessel, indicating the cell lined vessel.* ***B)*** *Complete lack of adherent monocytes along the whole femoral artery.*

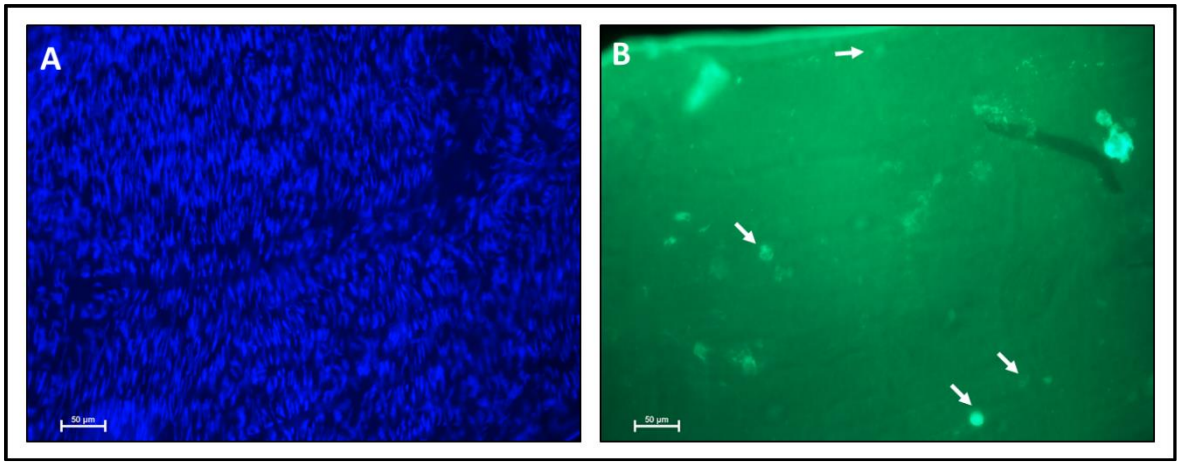

Figure 29. *Femoral arteries were perfused at pWSS for 24 hours then activated with TNFα in the perfusate for 1 hour. The vessels were then harvested, flayed open and incubated with static, activated, calcein labeled monocytes for 1 hour. The vessels were then washed, fixed and mounted with DAPI to visualize the endothelium. The vessels were imaged at 20x for any adherent monocytes. Representative images are shown here.* ***A)*** *DAPI stained vessel, indicating the cell lined vessel.* ***B)*** *Evidence of monocyte adherence along the vessel indicated by the white arrows.*

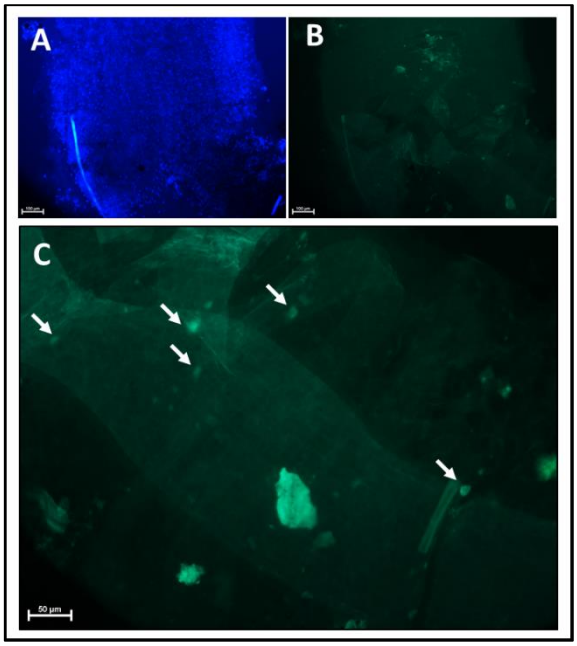

Figure 30. *Femoral arteries were perfused at 1.4x pWSS for 24 hours. The vessels were then harvested, flayed open and incubated with static, activated, calcein labeled monocytes for 1 hour. The vessels were then washed, fixed and mounted with DAPI to visualize the endothelium. The vessels were imaged at 10x and 20x for any adherent monocytes. Representative images are shown here. A) 10x image of DAPI stained vessel, indicating the cell lined vessel. B) 10x image of same location as in image A). C) Evidence of monocyte adherence along the vessel indicated by the white arrows.*

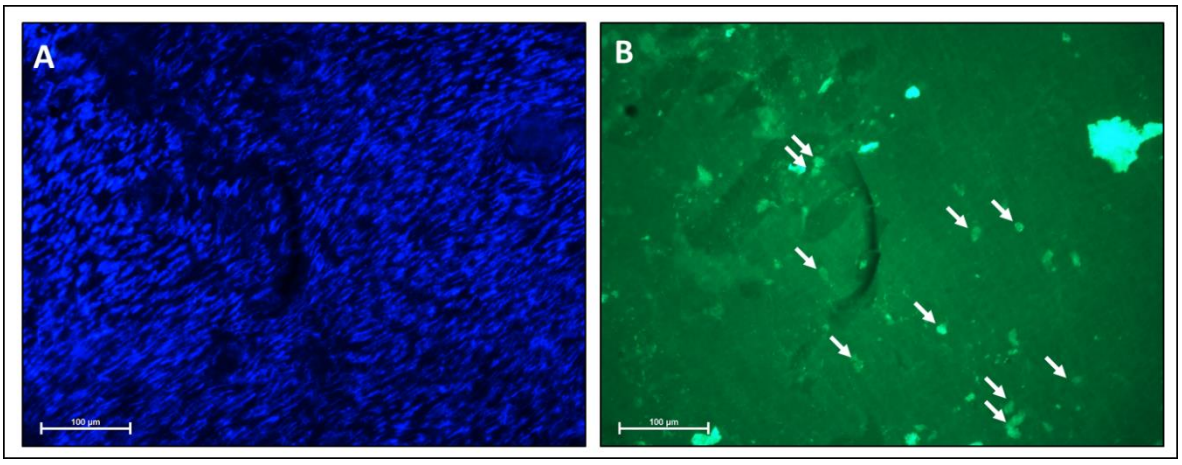

Figure 31. *Femoral arteries were perfused at 2x pWSS for 24 hours. The vessels were then harvested, flayed open and incubated with static, activated, calcein labeled monocytes for 1 hour. The vessels were then washed, fixed and mounted with DAPI to visualize the endothelium. The vessels were imaged at 20x for any adherent monocytes. Representative images are shown here. A) DAPI stained vessel, indicating the cell lined vessel. B) Evidence of monocyte adherence along the vessel indicated by the white arrows.*

DISCUSSION

The perfusion of monocytes through the femoral artery can be seen on video, however, the flow rate requires to induce the experimental WSS is too great to allow for the monocyte adhesion that we expected to see. To increase flow rate as opposed to media viscosity was a justified decision in chapter 3, but was not effective through this portion of the study.

The static monocyte incubation on arteries with the inflammatory phenotype induced by WSS shows that the phenotype is specific to WSS and has direct implications on monocyte adhesion. Specifically, higher WSS means more adhesion molecules and therefore more monocyte adhesion. Previous studies have done this type of static monocyte incubation various on activated endothelial cells. Additionally, referring back to the previous chapter, the 2x WSS showed a more robust inflammatory and growth factor mRNA expression response than 1.4x. This is in line with the increased monocyte adhesion we see after static incubation. In addition to monocyte adhesion, this shows us that the inflammatory phenotype is sustained even after removing the vessel from perfusion, for at least 1 hour.

As a proof of concept we have increased media viscosity using dextran and lowered flow rate and shown that monocytes in this perfusion system do in fact have the ability to roll and adhere to the endothelium dynamically. To make any conclusions using the thickened media, however, the WSS studies to assess inflammatory response would have to be repeated with the increased viscosity perfusate since the presence of dextran is likely to have confounding implications.

As a preliminary look, I perfused one vessel at physiological WSS with perfusate of viscosity increased to that of blood (4.0×10^{-3}Pa·s) using dextran. The vessel was perfused for 24 hours at the 6.8RPM setting to achieve physiological WSS on the pump which corresponds to an average

flow rate of 0.111mL/min and a max flow rate of 0.120mL/min. The arteries were then processed with TriZol for RNA extraction and qPCR analysis. The same cytokines, adhesion molecules and growth factors were analyzed.

The results are shown below in comparison to the vessels perfused with regular low viscosity DMEM at the higher flow rate. With only one vessel, no analysis can be completed. However, as seen in *figure 32*, there may be a trend towards there being an increase in MCP-1, TNFα, and P-selectin with the increase in dextran. *Figure 33* shows the growth factors and transcription factor Egr-1. There is a trend towards an increase with dextran of FGF-2 and TGFβ.

These increases in mRNA expression support the initial decision to *not* increase the viscosity of the perfusate with dextran. As previously reported, dextran can have inflammatory effects on the endothelium which seem to be manifested here[97]. Also, though this data does not show it, previous studies have shown significant increases in VCAM-1 and ICAM-1 expression at both the mRNA and protein levels[97]. Similar to reasons that these cellular adhesion molecules may not have shown a robust response in our other studies, it is likely that the changes caused by the dextran are occurring prior to the 24 hour time point. Clearly, more studies will need to be done, and perhaps dextran can be used but the whole system would have to be characterized.

Ideally, this *ex vivo* system will be able to visualize the rolling, sticking and firm adhesion of monocytes in real-time on video. For this to be possible, the current study has determined that the velocity of the particles must be lower. Increasing viscosity is the logical option, but comes with its own setbacks. Options for increasing viscosity include dextran of varying molecular weights, ficoll, polyvinylpyrrlidone, methylcellulose, dimethylpolysiloxane[100]. Each of these have been previously shown to cause changes related to cell morphology, chemotaxis and diffusion. Using

any of these additives will require a full characterization of the artery phenotype after perfusion with respect morphology and mRNA expression in relation to inflammatory markers.

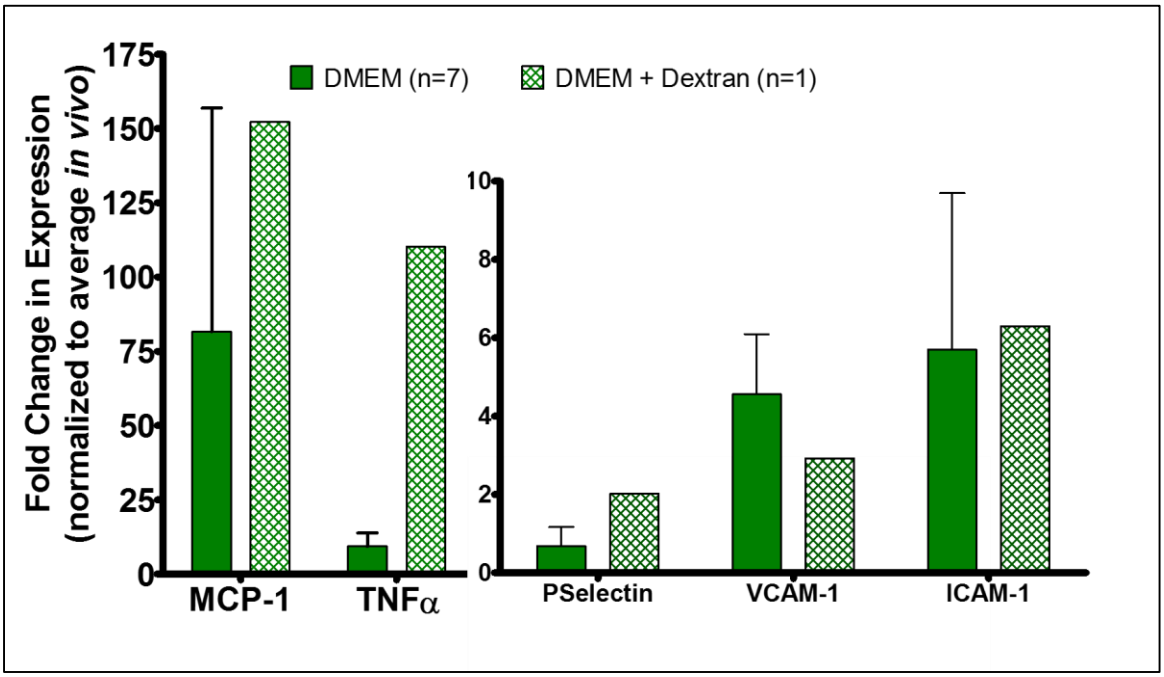

Figure 32. *One femoral artery was perfused at physiological WSS with DMEM+Dextran perfusate to simulate the viscosity of blood. The vessel was analyzed for mRNA expression as previously shown and compared to the DMEM only vessels here. There is a trend towards an increase in MCP-1, TNFα, and P-selectin with the Dextran perfusate.*

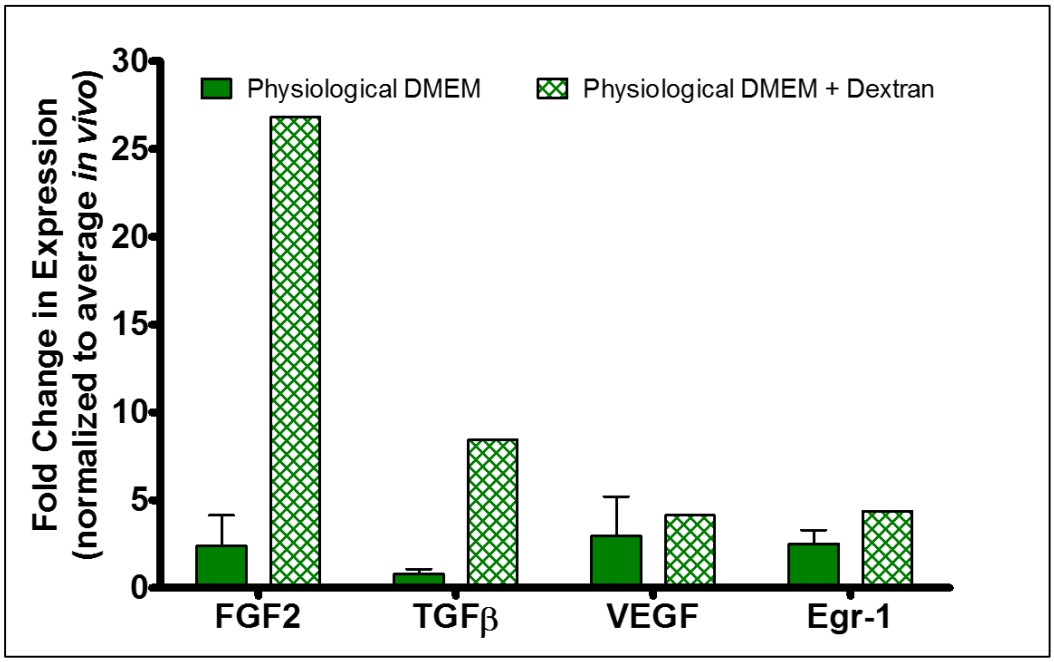

Figure 33. *One femoral artery was perfused at physiological WSS with DMEM+Dextran perfusate to simulate the viscosity of blood. The vessel was analyzed for mRNA expression as previously shown and compared to the DMEM only vessels here. There is a trend towards an increase in FGF2, TGF. VEGF and Egr-1 are too close to make any judgments.*

CHAPTER 6
IMPLICATIONS AND LIMITATIONS

SUCCESSFUL *EX VIVO* FEMORAL ARTERY MODEL

In chapter 3 we demonstrated that the femoral artery is in fact a viable perfusion model for studying inflammation. By assessing the branches along the artery in addition to the main branch, we showed that, at least in terms of inflammatory response, the main femoral artery behaves similarly to the branches and as a larger vessel will allow for easier experimentation and analysis.

The vessel is effectively structurally sustained while maintaining tone and vasoreactivity throughout the 24 hours of perfusion. The model has the capability of being used for many other variables that were not explored in this study. Beyond more conditions of mechanical stimulus, experiments can be designed around pharmacological molecules, pathologically relevant environmental changes, and using femoral arteries of diseased models. In any of these cases this model has the benefits of being able to watch the perfusion in real time, and make changes dynamically throughout a perfusion study. Perfusate, particulates, flow, chemical composition can all be kept constant or changed very specifically. In the case of particulate behavior multiple time points can be assessed using a single vessel.

Specific to the field of arteriogenic study, researchers primarily use *in vivo* occlusion studies or monolayers of cells. Due to animal and vascular variability in any occlusion studies, increases in WSS are assumed but not usually quantified, this model will allow for a more specific analysis of the mechanical effects. When using monolayers of cells, most studies use immortalized human endothelial cell lines. The shear stress that is applied to these cells is usually an average WSS of the vessels in the human vasculature, 10-15dynes/cm^2 which is equal to about 1.0-1.5Pa. The problem with this is that the shear stress felt by arteries of different sizes is very different. Specifically WSS in the carotid artery is 1.1-1.3Pa, in the brachial artery 0.4-0.5Pa and in the femoral artery 0.3-0.5Pa[101]. Further, when translating these *in vitro* findings to *in vivo* models, it

has to be considered that the mean WSS in a given artery decreases linearly with body mass[102]. For example, the average WSS in the mouse femoral artery is 10Pa, which is nearly 30 times greater than in the human femoral artery[103,102].

It is important that when performing studies that have site specific implications in terms of specific arteries or even particular curvature or branch points, that the correct WSS is considered. Using an average WSS is not accurate and translating such *in vitro* results to animal or human models is grossly inaccurate. In this respect, the mouse femoral artery model described here takes into account specific flow rates and WSS at the particular part of the artery being considered. The WSS is calculated considering the diameter of the vessel and applied accordingly allowing for an accurate representation of the magnitude of the WSS that would be felt by the endothelial sheath of a mouse femoral artery *in vivo.*

THE ROLE OF SHEAR STRESS

Through the history of research regarding vascular growth the role of WSS has been debated both in angiogenesis and arteriogenesis. Some studies even argue that it is the circumferential forces that cause increases in pressure that result in the vasculogenic phenotypes and that WSS is not relevant. In this study, however, we kept maximum arterial pressure constant at 80mmHg and changed only the flow rate to increase WSS. Even with constant peak pressure, we showed that increased in WSS have a direct effect on the mRNA expression of endothelial inflammatory markers as well as arteriogenic growth factors. The later finding of changes in growth factors was surprising, since the hypothesis was that this would not occur without the presence of leukocyte, and specifically monocyte, recruitment and adhesion.

As suggested by previous studies, the mechanical signal imparted by the shear stress is likely transduced by either calveoli, Ca^{+} channels, glycocalyx, or a combination thereof to ultimately trigger eNOS and disrupt the osmotic regulation of the endothelium and result in the leukocyte specific chemoattractants and adhesion molecules. Through this explanation which is expanded in the cascade shown in *figure 2*, our data supported hypothesis of endothelium activation by WSS is further validated.

The expression of growth factors as a result of WSS, however, brings in the discussion of the role of Egr-1, and also of how the signal is translated to the smooth muscle cells from the endothelium. From the data we know that when WSS elicits a robust expression of Egr-1, it results in the overexpression of TGFβ, VEGF and even FGF-2. FGF-2 overexpression is a curious find since our proposed mechanism is that FGF-2 is a ligand that is brought in by leukocytes. Since our model did not introduce any leukocytes, it begs the question of where the FGF-2 came from. It is expected that FGFR (receptor) is largely upregulated in the case of arteriogenesis, but FGF-2 has not been found to be very significant[21].

Our study suggest though, that the ligand is also upregulated, though the mechanism is unclear. One hypothesis has to do with the activity of heparan-sulfate in the endothelial glycocalyx. In conditions of wound repair it has been found that heparan-sulfate is broken down by heparanase which in turn activates FGF-2[96]. In this particular condition of high WSS, it can be postulated that the mechanical signal is translated as trauma and triggers heparanase activity. The resulting increase in FGF-2 is what our assays may be detecting.

Overall, our studies indicate that there is a WSS dependent response of the vascular cells towards the arteriogenic, synthetic phenotype. Though it may be the case that leukocytes are necessary to

actually result in outward remodeling and sprouting, through this model we show that the progression can and does begins with just the mechanical stimuli.

LIMITATIONS OF *EX VIVO* CONDITIONS

A main limitation of this model, thus far, is that there is an inflammatory response that was defined by the study that occurs even under physiological conditions. This could be mitigated by assessing what could be altered to make the perfusion more physiologic, perhaps by controlling pulsatility or controlling the gaseous environment better. But even as is, this model has been shown to be able to provide discernable data in relation to inflammatory and vascular markers.

Another consideration is that this model removes particulates and circulating cells from the perfusate that would be present in *in vivo* circulation. While most *ex vivo* vascular perfusion models also follow this practice, it has to be noted that key physiological factors have been removed. That being said, due to the nature of the system, one could design a study that conditionally adds these parts back into the perfusate, or even use whole (anti-coaguated) blood. A virtue of this *ex vivo* system is the ability to treat variables independently to tease out specific mechanistic properties.

Finally, it must be considered, that the vessel has been removed from its native environment and detached from any interstitial tissue and the adventitia disrupted. While the artery is stretched to *in vivo* length to the best of our ability, it is still not spatially positioned exactly as it was *in vivo.* And further, any branches will also be out of sync from their original x-y-z positioning.

As with any model there are limitations, but as long as they are kept in mind, and the proper controls and baselines maintained, this femoral artery model can had a variety of far reaching applications.

CHAPTER 7
FUTHER WORK: EARLY GROWTH RESPONSE PROTEIN-1 (EGR-1) AS A POTENTIAL "MASTER SWITCH" IN ARTERIOGENESIS

INTRODUCTION

Egr-1 is highly associated with cardiovascular disease such as atherosclerosis. Studies in the field, and now this current study, have shown that Egr-1 likely plays a critical role in vascular growth, specifically arteriogenesis following vascular occlusion and resulting collateral growth[80,21,17]. There is also data of support Egr-1's role in the regulation of the genes involved in leukocyte recruitment[17]. Further, it has been shown that Egr-1 is critical for switching SMCs from contractile phenotype to the proliferative type by downregulating a particular splicing factor[80]. To study all of these mechanisms further Egr-1 knockout ($Egr\text{-}1^{-/-}$) mice have been used to help conditionally study its role *in vivo*. Through *in vivo* femoral artery ligation studies it has been shown that perfusion recovery is greatly hindered in $Egr\text{-}1^{-/-}$ mice[80]. In our lab we have performed preliminary femoral artery excision studies on knockout mice followed by mRNA analysis at 24, 48 and 72 hours. The ability to complete these studies have been dictated by limitations of the model.

KNOCKOUT LIMITATIONS

Female $Egr^{-/-}$ mice have been found to be sterile and therefore cannot be used to breed more knockouts. Due to this, the propagation of the $Egr^{-/-}$ genotype is only possible by breeding $Egr^{-/-}$ males with $Egr^{-/+}$ females. As such the probability of producing a knockout offspring is only 50%. Of these 50% we can also presume that the gender split will also be 50%. Ideally, all studies would be performed on the male knockouts to eliminate any variation in results due to female estrus. However, due to the slow rate at which make knockouts are made available, being able to use the female knockouts could prove to be an asset. Knowing that the female knockouts are sterile, we know that the lack of the Egr-1 gene is having some effect on the endocrine system. Previous studies have shown that there is a developmental effect on the pituitary which is critical in the hormone cycle of females[104]. Therefore, to be able to use these mice for any experiments we must

investigate how their cycle differs from a wild-type animal, and what that would mean for our studies.

USE OF FEMALE EGR-1 KNOCKOUTS

Previous studies have shown that there is a developmental effect on the pituitary by knocking out Egr-1 which is critical in the hormone cycle of females[105]. Since Egr-1 is being extensively studied for its role in arteriogenesis and vascular remodeling related to peripheral cardiovascular disease and injury, the effect of estrogen cannot be ignored when using a female model. Specifically, estrogen has known beneficial effects on arterial wall function[106,107] and protective effects in cases of vascular injury or disease[108,109,] such as during trauma hemorrhage[110,111,112], protecting against atherosclerosis[113], as well as aiding in healing after vascular injury[114,115,116].

A normal wild-type female mouse exhibits a predictable estrus cycle of 4-5 days and consists of 4 distinct phases: proestrus, estrus, metaestrus, diestrus in that order. This consistent cycling allows researchers to be confident of the hormonal state of the animal during experimentation, or use random sampling of large animal numbers. Studies have shown, however, that a knockout model will often adversely affect the estrous cycle of a mouse[105]. Proper cycle mediation is dependent on the function of the hypothalum-pituitary-gonads axis[117]. Specifically, gonadotropin-releasing hormone (GnRH) reaches the pituitary which stimulated the secretion of luteinizing hormone (LH) and follicle-stimulating hormone (FSH)[117]. These hormones in turn stimulate ovarian cells leading to ovulation and estrogen modulation; estrogen and progesterone are the two main hormones that mediate the estrus cycle. Egr-$1^{-/-}$ mice have decreased levels of LH released by the pituitary, which inherently causes their estrogen and progesterone mediation to be different.

We propose that simple vaginal smears will help us determine the utility of these animals. Key factors in experimentation using these animals is to know 1) whether they are still cycling at all, 2) if they are cycling how is it different, and finally 3) decide which stage in the cycle you will perform your experiments. Studies to date have reported that Egr-1$^{-/-}$ females are sterile, and therefore anestrous. However, from behavioral observation we believed that the mice were in fact cyclically becoming more aggressive- a behavioral indication of the onset of estrous. It is also possible that the estrus cycle of some females may have arrested due to lack of male presence and mating.

Experimental Design

The estrus cycle in the mouse was monitored by obtaining a vaginal smear on a daily basis for two weeks and microscopic analysis after hematoxylin and eosin (HE) staining[118]. Smear was obtained by using a mini-cotton swab that is soaked in saline. The mouse was handled as previously described[117]; briefly, the mouse was lifted from the base of the tail, and the opposite hand used to grasp the nape of the neck. The mouse was then inverted in the palm of the handlers hand and restrained by holding tail between fingers- which effectively exposes the vaginal opening. The area was cleaned with a saline soaked gauze. The pre-wet cotton swab was then inserted into the vaginal opening and the wall swabbed around once and then rolled onto a microscope slide. The sample was then stained using the HE protocol below. This method allows the prediction of the estrous cycle by the types of cells present; specifically the proportions of epithelial cells, cornified cells, and leukocytes[117]. The identification of cell type is made easy by the HE stain in which the hematoxylin stains nuclei while the eosin stains other cellular parts.

Vaginal Smear Staining

The slides were first fixed in 95% ethanol for 10 seconds then rinsed in tap water. They were then stained with Gills III Hematoxylin for two minutes and then rinsed in two changes of tap water. The samples were then blued in Lithium carbonate. The slides were then placed in 95% ethanol for 5 seconds and stained with eosin for 1 minute. Slides were finally dehydrated with ethanol and xylene and mounted with mounting media.

Vaginal Smear Analysis

The pre-ovulatory day corresponds to the proestrus phase when estrogen increases (progesterone decreases). Proestrus is identified by a predominance of nucleated epithelial cells, some cornified cells may be present. After the surge of estrogen, ovulation occurs and estrogen remains elevated into the start of the next phase which is estrus. Estrus is identified by distinctively cornified cells that that have no nucleus and irregular shape, these are the only cells present in estrus. At the end of the estrus day, the estrogen levels drop to basal levels as the cycle enters into metaestrus. Metaestrus is essentially a transition between estrus and diestrus where there is a mix of cell types including nucleated or cornified epithelial cells but a predominance of leukocytes. Estrogen levels are low and progesterone levels are on the rise[105]. Diestrus is characterized by a strong leukocyte presence and a peak of progesterone levels. Smears were analyzed visually and by cell count. Each smear was imaged systematically in four locations and all the cells counted in each image, and reported as total cell type with standard deviation.

Results

As an assessment of mouse estrus in $Egr^{-/-}$ females, we monitored wild-type and three knockout mice 12-14 weeks of age. Initially all mice were exposed to male urine in their bedding to "jump-start" any arrested estrus cycles. All mice were monitored daily by vaginal smears for 15 days at

the same time of day. Shown below are representative images of the estrus phases for one wild-type and one knockout. From hematoxylin and eosin staining and analysis of the vaginal swabs the wild-type cycle displays four clear stages, the estrus cycle is 4-5 days long (*figure 32*). Egr-1$^{-/-}$ mice also displayed cycling but with elongated phases, resulting in a cycle averaging 7 days. Over the 7 days changes in cell type occurred as in the wild-type, but the cell types present at each stage vary. In the wild-type the estrus stage is very distinct with only cornified cells and no nucleated cells or leukocytes. As shown in *figure 33*, the Egr-1$^{-/-}$ cycle exhibits the presence of leukocytes in every stage that never disappear.

The presence of leukocytes is very striking in the comparison of the two estrus phases, where the wild-type displays an absence of any nuclear staining at all, but the knockouts show a strong presence of leukocytes. This is indicative of hormone deficiency where estrogen and progesterone balances are altered, not allowing the mouse to fully enter estrus. This likely due to the fact that it has been shown that the transcription of LH-β is dependent on Egr-1[119]. Percentage of each cell type; cornified, epithelial, leukocytes, in four stages was counted and is shown as bar graphs in *figure 34*. WT vs. Egr-1$^{-/-}$Cell types were counted in n=4 randomized image windows.

At this stage we can conclude that the Egr-1 deficiency distinctly effects the estrus cycle in a visually identifiable way, but that there is a distinct cycling meaning that they are not anestrous as previously described. By coupling this type of estrus mapping with hormone levels previously described, the female Egr-1 -/- mice can be effectively use for experimentation as any fluctuations due to cycling will be noted.

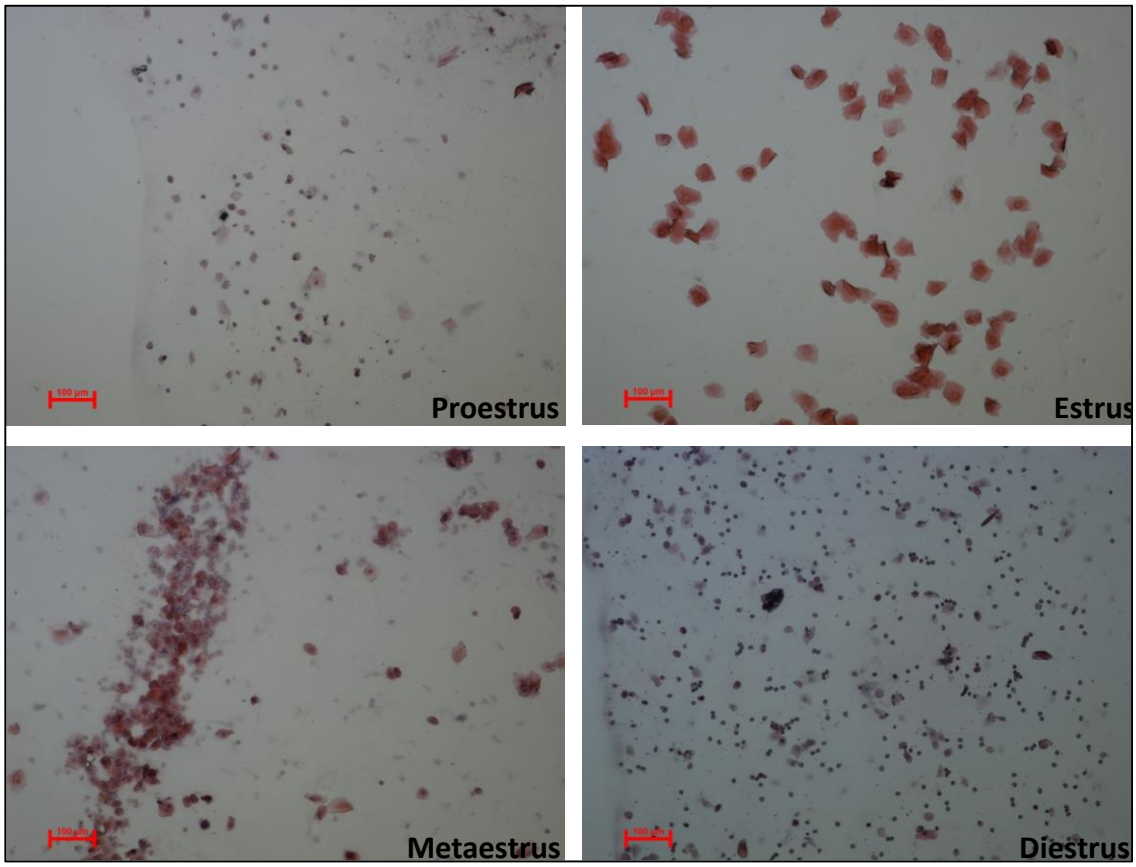

Figure 34. *Wild-type female mice were vaginally swabbed daily and imaged to see what cell types were present. Cell populations present are used to identify which phase of the cycle the mouse is in. Representative images of wild-type mouse vaginal smears depicted as 4 phases of the estrus cycle.* ***Proestrus*** *shows characteristic epithelial cells.* ***Estrus*** *then shows only cornified cells, with a distinct absence of nuclear staining.* ***Metaestrus*** *is a transitional phase that includes all cell types, but importantly shows the emergence of leukocytes, which dominate the final phase of* ***Diestrus.***

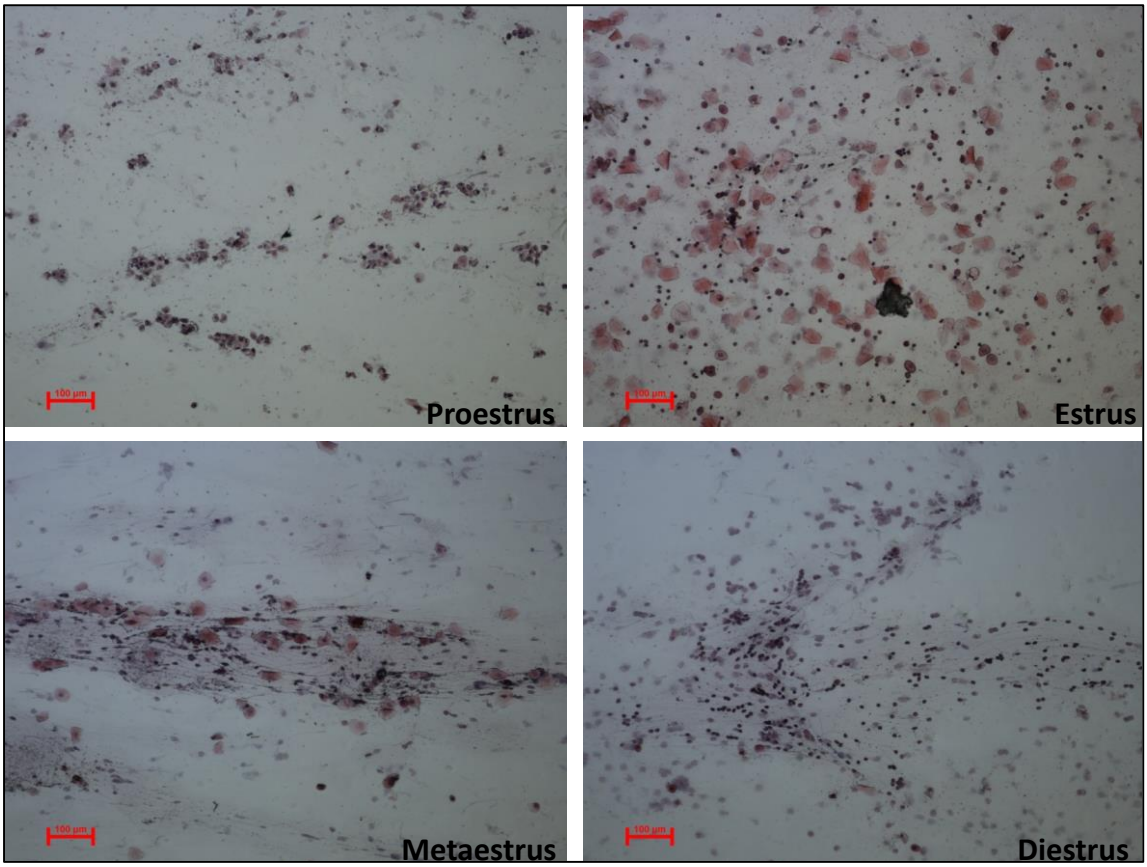

Figure 35. *Egr-1$^{-/-}$ female mice were vaginally swabbed daily and imaged to see what cell types were present. Cell populations present are used to identify which phase of the cycle the mouse is in. Representative images of Egr-1-null mouse vaginal smears depicted as 4 phases of the estrus cycle.* ***Proestrus****shows characteristic epithelial cells.* ***Estrus*** *then shows cornified cells, but unlike the wild type there is a distince presence of nucleated cells—leukocytes.****Metaestrus*** *is still a transitional phase that includes all cell types, but importantly shows the emergence of leukocytes, which dominate the final phase of* ***Diestrus.***

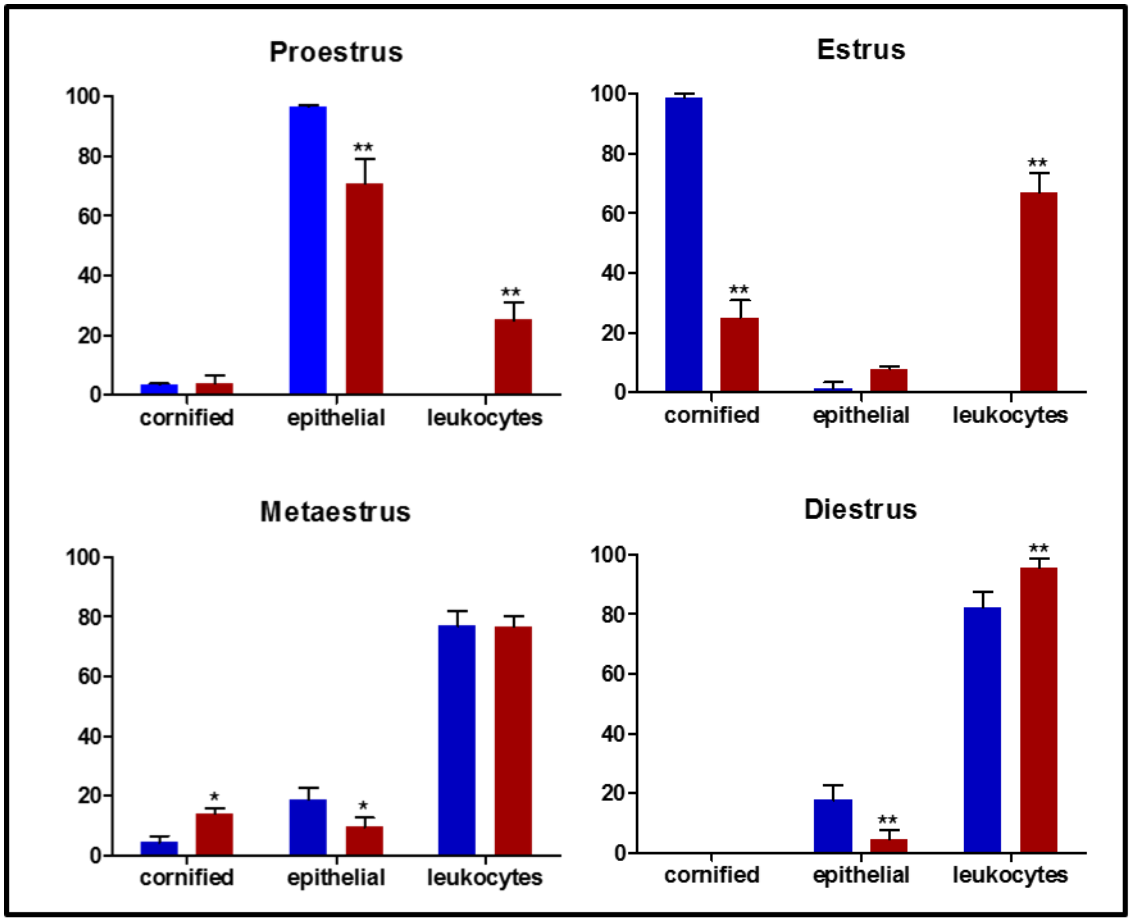

Figure 36. *Percentage of each cell type; cornified, epithelial, leukocytes, in four stages WT vs. Egr-1-/- cell types were counted in n=4 randomized image windows. Significant differences of Egr-1-/-compared to WT shown as*<0.01, **<0.001.*

REFERENCE LIST

1. Limbourg, A. *et al.* Evaluation of postnatal arteriogenesis and angiogenesis in a mouse model of hind-limb ischemia. *Nat. Protocols* **4**, 1737-1748 (2009).
2. Hirschi, K.K., Skalak, T.C., Peirce, S.M. & Little, C.D. Vascular Assembly in Natural and Engineered Tissues. *Annals of the New York Academy of Sciences* **961**, 223-242 (2002).
3. Members, W.G. *et al.* Heart Disease and Stroke Statistics—2012 Update. *Circulation* **125**, e2-e220 (2012).
4. Berliner, J.A. *et al.* Atherosclerosis: Basic Mechanisms. *Circulation* **91**, 2488-2496 (1995).
5. Witztum, J.L. The oxidation hypothesis of atherosclerosis. *The Lancet* **344**, 793-795 (1994).
6. Brown, M.S. & Goldstein, J.L. Scavenging for receptors. *Nature* **343**, 508-509 (1990).
7. Demer, L.L. Effect of calcification on in vivo mechanical response of rabbit arteries to balloon dilation. *Circulation* **83**, 2083-93 (1991).
8. National Heart, L., and Blood Institute. Explore Atherosclerosis. (2011).
9. Staff, M.C. Arteriosclerosis / atherosclerosis. Vol. 2013 (2012).
10. Melillo, G. *et al.* Gene therapy for collateral vessel development. *Cardiovascular Research* **35**, 480-489 (1997).
11. Wenger, A. *et al.* Modulation of in vitro angiogenesis in a three-dimensional spheroidal coculture model for bone tissue engineering. *Tissue Engineering* **10**, 1536-1547 (2004).
12. Cross, M.J. & Claesson-Welsh, L. FGF and VEGF function in angiogenesis: signalling pathways, biological responses and therapeutic inhibition. *Trends in Pharmacological Sciences* **22**, 201-207 (2001).
13. Arras, M. *et al.* Monocyte activation in angiogenesis and collateral growth in the rabbit hindlimb.
14. Chalothorn, D., Zhang, H., Clayton, J.A., Thomas, S.A. & Faber, J.E. Catecholamines augment collateral vessel growth and angiogenesis in hindlimb ischemia. *American Journal of Physiology - Heart and Circulatory Physiology* **289**, H947-H959 (2005).
15. Ito, W.D. *et al.* Angiogenesis but not collateral growth is associated with ischemia after femoral artery occlusion. *The American journal of physiology* **273**, H1255-65 (1997).
16. Lee, C.W. *et al.* Temporal patterns of gene expression after acute hindlimb ischemia in mice: insights into the genomic program for collateral vessel development. *Journal of the American College of Cardiology* **43**, 474-482 (2004).
17. Sarateanu, C.S. *et al.* An Egr-1 master switch for arteriogenesis: Studies in Egr-1 homozygous negative and wild-type animals. *The Journal of thoracic and cardiovascular surgery* **131**, 138-145 (2006).
18. Schalch, P. *et al.* Homozygous deletion of early growth response 1 gene and critical limb ischemia after vascular ligation in mice: Evidence for a central role in vascular homeostasis. *The Journal of thoracic and cardiovascular surgery* **128**, 595-601 (2004).
19. Scholz, D. *et al.* Ultrastructure and molecular histology of rabbit hind-limb collateral artery growth (arteriogenesis). *Virchows Archiv* **436**, 257-270 (2000).
20. Scholz, D. *et al.* Contribution of Arteriogenesis and Angiogenesis to Postocclusive Hindlimb Perfusion in Mice. *Journal of Molecular and Cellular Cardiology* **34**, 775-787 (2002).

21. Schaper, W. & Scholz, D. Factors Regulating Arteriogenesis. *Arteriosclerosis, Thrombosis, and Vascular Biology* **23**, 1143-1151 (2003).
22. Dvorak, H.F., Brown, L.F., Detmar, M. & Dvorak, A.M. Vascular permeability factor/vascular endothelial growth factor, microvascular hyperpermeability, and angiogenesis. *Am J Pathol* **146**, 1029-39 (1995).
23. Helisch, A. & Schaper, W. Arteriogenesis: the development and growth of collateral arteries. *Microcirculation (New York, N.Y.: 1994)* **10**, 83-97 (2003).
24. White, F.C., Bloor, C.M., McKirnan, M.D. & Carroll, S.M. Exercise training in swine promotes growth of arteriolar bed and capillary angiogenesis in heart. *J Appl Physiol* **85**, 1160-8 (1998).
25. Hansen-Smith, F., Egginton, S., Zhou, A.L. & Hudlicka, O. Growth of arterioles precedes that of capillaries in stretch-induced angiogenesis in skeletal muscle. *Microvasc Res* **62**, 1-14 (2001).
26. Cheng, C.P., Parker, D. & Taylor, C.A. Quantification of wall shear stress in large blood vessels using Lagrangian interpolation functions with cine phase-contrast magnetic resonance imaging. *Ann Biomed Eng* **30**, 1020-32 (2002).
27. Wootton, D.M. & Ku, D.N. Fluid mechanics of vascular systems, diseases, and thrombosis. *Annual review of biomedical engineering* **1**, 299-329 (1999).
28. Conway, D.E. *et al.* Expression of CYP1A1 and CYP1B1 in human endothelial cells: regulation by fluid shear stress. *Cardiovasc Res* **81**, 669-77 (2009).
29. Resnick, N. *et al.* Fluid shear stress and the vascular endothelium: for better and for worse. *Progress in Biophysics and Molecular Biology* **81**, 177-199 (2003).
30. Kamiya, A. & Togawa, T. Adaptive regulation of wall shear stress to flow change in the canine carotid artery. *The American journal of physiology* **239**, H14-21 (1980).
31. Unthank, J.L., Fath, S.W., Burkhart, H.M., Miller, S.C. & Dalsing, M.C. Wall remodeling during luminal expansion of mesenteric arterial collaterals in the rat. *Circ Res* **79**, 1015-23 (1996).
32. Zarins, C.K., Zatina, M.A., Giddens, D.P., Ku, D.N. & Glagov, S. Shear stress regulation of artery lumen diameter in experimental atherogenesis. *J Vasc Surg* **5**, 413-20 (1987).
33. Heil, M. & Schaper, W. Influence of Mechanical, Cellular, and Molecular Factors on Collateral Artery Growth (Arteriogenesis). *Circulation Research* **95**, 449-458 (2004).
34. Langille, B.L. & O'Donnell, F. Reductions in arterial diameter produced by chronic decreases in blood flow are endothelium-dependent. *Science* **231**, 405-7 (1986).
35. Ngai, C.Y. & Yao, X. Vascular Responses to Shear Stress: The Involvment of Mechanosensors in Endothelial Cells. *The Open Circulation and Vascular Journal*

3, 85-94 (2010).
36. Reitsma, S., Slaaf, D., Vink, H., van Zandvoort, M. & oude Egbrink, M. The endothelial glycocalyx: composition, functions, and visualization. *Pflügers Archiv European Journal of Physiology* **454**, 345-359 (2007).
37. Forstermann, U., Pollock, J.S., Schmidt, H.H., Heller, M. & Murad, F. Calmodulin-dependent endothelium-derived relaxing factor/nitric oxide synthase activity is present in the particulate and cytosolic fractions of bovine aortic endothelial cells. *Proc Natl Acad Sci U S A* **88**, 1788-92 (1991).
38. Nilius, B. & Droogmans, G. Ion channels and their functional role in vascular endothelium. *Physiol Rev* **81**, 1415-59 (2001).

39. Gouverneur, M., Berg, B., Nieuwdorp, M., Stroes, E. & Vink, H. Vasculoprotective properties of the endothelial glycocalyx: effects of fluid shear stress. *J Intern Med* **259**, 393-400 (2006).
40. Pries, A.R., Secomb, T.W. & Gaehtgens, P. The endothelial surface layer. *Pflugers Archiv : European journal of physiology* **440**, 653-66 (2000).
41. Ihrcke, N.S., Wrenshall, L.E., Lindman, B.J. & Platt, J.L. Role of heparan sulfate in immune system-blood vessel interactions. *Immunol Today* **14**, 500-5 (1993).
42. Gouverneur, M., Spaan, J.A., Pannekoek, H., Fontijn, R.D. & Vink, H. Fluid shear stress stimulates incorporation of hyaluronan into endothelial cell glycocalyx. *Am J Physiol Heart Circ Physiol* **290**, H458-2 (2006).
43. van den Berg, B.M., Spaan, J.A., Rolf, T.M. & Vink, H. Atherogenic region and diet diminish glycocalyx dimension and increase intima-to-media ratios at murine carotid artery bifurcation. *Am J Physiol Heart Circ Physiol* **290**, H915-20 (2006).
44. Hartmannsgruber, V. *et al.* Arterial Response to Shear Stress Critically Depends on Endothelial TRPV4 Expression. *PLoS One* **2**, e827 (2007).
45. Liedtke, W. & Kim, C. Functionality of the TRPV subfamily of TRP ion channels: add mechano-TRP and osmo-TRP to the lexicon! *Cell Mol Life Sci* **62**, 2985-3001 (2005).
46. Kohler, R. *et al.* Evidence for a functional role of endothelial transient receptor potential V4 in shear stress-induced vasodilatation. *Arterioscler Thromb Vasc Biol* **26**, 1495-502 (2006).
47. Troidl, C. *et al.* Trpv4 induces collateral vessel growth during regeneration of the arterial circulation. *Journal Of Cellular And Molecular Medicine* **13**, 2613-2621 (2009).
48. Lloyd, P.G., Yang, H.T. & Terjung, R.L. Arteriogenesis and angiogenesis in rat ischemic hindlimb: role of nitric oxide. *American Journal of Physiology - Heart and Circulatory Physiology* **281**, H2528-H2538 (2001).
49. Cai, W.J., Kocsis, E., Luo, X., Schaper, W. & Schaper, J. Expression of endothelial nitric oxide synthase in the vascular wall during arteriogenesis. *Mol Cell Biochem* **264**, 193-200 (2004).
50. Tzima, E. *et al.* A mechanosensory complex that mediates the endothelial cell response to fluid shear stress. *Nature* **437**, 426-31 (2005).
51. Cai, W. & Schaper, W. Mechanisms of arteriogenesis. *Acta Biochim Biophys Sin (Shanghai)* **40**, 681-92 (2008).
52. Schaper, W. & Schaper, J. *Arteriogenesis*, (Kluwer Academics Publisher, London, 2004).
53. Ley, K., Laudanna, C., Cybulsky, M.I. & Nourshargh, S. Getting to the site of inflammation: the leukocyte adhesion cascade updated. *Nat Rev Immunol* **7**, 678-89 (2007).
54. McEver, R.P. & Cummings, R.D. Role of PSGL-1 binding to selectins in leukocyte recruitment. *J Clin Invest* **100**, S97-103 (1997).
55. Eriksson, E.E., Xie, X., Werr, J., Thoren, P. & Lindbom, L. Importance of primary capture and L-selectin-dependent secondary capture in leukocyte accumulation in inflammation and atherosclerosis in vivo. *J Exp Med* **194**, 205-18 (2001).
56. Alon, R., Hammer, D.A. & Springer, T.A. Lifetime of the P-selectin-carbohydrate bond and its response to tensile force in hydrodynamic flow. *Nature* **374**, 539-42 (1995).
57. Lawrence, M.B., Kansas, G.S., Kunkel, E.J. & Ley, K. Threshold levels of fluid shear promote leukocyte adhesion through selectins (CD62L,P,E). *The Journal of cell biology* **136**, 717-27 (1997).

58. Marshall, B.T. *et al.* Direct observation of catch bonds involving cell-adhesion molecules. *Nature* **423**, 190-3 (2003).
59. Chesnutt, B.C. *et al.* Induction of LFA-1-dependent neutrophil rolling on ICAM-1 by engagement of E-selectin. *Microcirculation* **13**, 99-109 (2006).
60. Shaw, S.K., Bamba, P.S., Perkins, B.N. & Luscinskas, F.W. Real-time imaging of vascular endothelial-cadherin during leukocyte transmigration across endothelium. *J Immunol* **167**, 2323-30 (2001).
61. Muller, W.A. Leukocyte–endothelial-cell interactions in leukocyte transmigration and the inflammatory response. *Trends in Immunology* **24**, 326-333 (2003).
62. Mamdouh, Z., Chen, X., Pierini, L.M., Maxfield, F.R. & Muller, W.A. Targeted recycling of PECAM from endothelial surface-connected compartments during diapedesis. *Nature* **421**, 748-53 (2003).
63. Carman, C.V. & Springer, T.A. A transmigratory cup in leukocyte diapedesis both through individual vascular endothelial cells and between them. *The Journal of cell biology* **167**, 377-88 (2004).
64. Mamdouh, Z., Mikhailov, A. & Muller, W.A. Transcellular migration of leukocytes is mediated by the endothelial lateral border recycling compartment. *The Journal of Experimental Medicine* **206**, 2795-2808 (2009).
65. Feng, D., Nagy, J.A., Pyne, K., Dvorak, H.F. & Dvorak, A.M. Neutrophils emigrate from venules by a transendothelial cell pathway in response to FMLP. *J Exp Med* **187**, 903-15 (1998).
66. Hoefer, I.E. *et al.* Leukocyte subpopulations and arteriogenesis: Specific role of monocytes, lymphocytes and granulocytes. *Atherosclerosis* **181**, 285-293 (2005).
67. Ito, W.D. *et al.* Monocyte chemotactic protein-1 increases collateral and peripheral conductance after femoral artery occlusion. *Circ Res* **80**, 829-37 (1997).
68. Schaper, J., Konig, R., Franz, D. & Schaper, W. The endothelial surface of growing coronary collateral arteries. Intimal margination and diapedesis of monocytes. A combined SEM and TEM study. *Virchows Arch A Pathol Anat Histol* **370**, 193-205 (1976).
69. Frenette, P.S. & Wagner, D.D. Adhesion Molecules. *New England Journal of Medicine* **334**, 1526-1529 (1996).
70. Zimmerman, G.A., McIntyre, T.M. & Prescott, S.M. Adhesion and signaling in vascular cell--cell interactions. *J Clin Invest* **98**, 1699-702 (1996).
71. Celi, A. *et al.* P-selectin induces the expression of tissue factor on monocytes.
72. Frenette, P.S. & Wagner, D.D. Adhesion molecules--Part II: Blood vessels and blood cells. *N Engl J Med* **335**, 43-5 (1996).
73. Fujimoto, T. & McEver, R. The cytoplasmic domain of P-selectin is phosphorylated on serine and threonine residues. *Blood* **82**, 1758-1766 (1993).
74. Huo, Y. & Ley, K. Adhesion molecules and atherogenesis. *Acta physiologica Scandinavica* **173**, 35-43 (2001).
75. Hoefer, I.E. *et al.* Arteriogenesis Proceeds via ICAM-1/Mac-1- Mediated Mechanisms. *Circulation Research* **94**, 1179-1185 (2004).
76. Ley, K. & Huo, Y. VCAM-1 is critical in atherosclerosis. *The Journal of Clinical Investigation* **107**, 1209-1210 (2001).
77. Hoefer, I.E., van Royen, N., Buschmann, I.R., Piek, J.J. & Schaper, W. Time course of arteriogenesis following femoral artery occlusion in the rabbit. *Cardiovascular Research* **49**, 609-617 (2001).

78. Couffinhal, T. *et al.* Impaired Collateral Vessel Development Associated With Reduced Expression of Vascular Endothelial Growth Factor in ApoE-/- Mice. *Circulation* **99**, 3188-3198 (1999).
79. Livak, K.J. & Schmittgen, T.D. Analysis of Relative Gene Expression Data Using Real-Time Quantitative PCR and the 2−ΔΔCT Method. *Methods* **25**, 402-408 (2001).
80. Pagel, J.I. *et al.* Role of early growth response 1 in arteriogenesis: impact on vascular cell proliferation and leukocyte recruitment in vivo. *Thromb Haemost* **107**, 562-74 (2012).
81. Rubenstein, D. *et al.* Bioassay Chamber for Angiogenesis with Perfused Explanted Arteries and Electrospun Scaffolding. in *Microcirculation* Vol. 14 723-737 (Taylor & Francis Ltd, 2007).
82. Koller, A., Sun, D. & Kaley, G. Role of shear stress and endothelial prostaglandins in flow- and viscosity-induced dilation of arterioles in vitro. *Circulation Research* **72**, 1276-1284 (1993).
83. Yamawaki, H., Lehoux, S. & Berk, B.C. Chronic Physiological Shear Stress Inhibits Tumor Necrosis Factor–Induced Proinflammatory Responses in Rabbit Aorta Perfused Ex Vivo. *Circulation* **108**, 1619-1625 (2003).
84. Hofmann, A. *et al.* Combined targeting of lentiviral vectors and positioning of transduced cells by magnetic nanoparticles. *Proceedings of the National Academy of Sciences* **106**, 44-49 (2009).
85. Shintani, Y. *et al.* Hepatocyte growth factor promotes an anti-inflammatory cytokine profile in human abdominal aortic aneurysm tissue. *Atherosclerosis* **216**, 307-312 (2011).
86. Laurindo, F. *et al.* Vascular free radical release. Ex vivo and in vivo evidence for a flow-dependent endothelial mechanism. *Circulation Research* **74**, 700-709 (1994).
87. Myers, P.R. *et al.* Release of EDRF and NO in ex vivo perfused aorta: inhibition by in vivo E. coli endotoxemia. *American Journal of Physiology - Heart and Circulatory Physiology* **268**, H955-H961 (1995).
88. Zhou, X., Izumi, Y., Burg, M.B. & Ferraris, J.D. Rac1/osmosensing scaffold for MEKK3 contributes via phospholipase C-γ1 to activation of the osmoprotective transcription factor NFAT5. *Proceedings of the National Academy of Sciences* **108**, 12155-12160 (2011).
89. Dickinson, H., Moritz, K., Wintour, E.M., Walker, D.W. & Kett, M.M. A comparative study of renal function in the desert-adapted spiny mouse and the laboratory-adapted C57BL/6 mouse: response to dietary salt load. *American Journal of Physiology - Renal Physiology* **293**, F1093-F1098 (2007).
90. Dougherty, F.C., Donovan, F.M., Jr. & Townsley, M.I. Harmonic analysis of perfusion pumps. *J Biomech Eng* **125**, 814-22 (2003).
91. Huo, Y., Guo, X. & Kassab, G.S. The flow field along the entire length of mouse aorta and primary branches. *Annals of Biomedical Engineering* **36**, 685-99 (2008).
92. van den Berg, B., Spaan, J. & Vink, H. Impaired glycocalyx barrier properties contribute to enhanced intimal low-density lipoprotein accumulation at the carotid artery bifurcation in mice. *Pflügers Archiv European Journal of Physiology* **457**, 1199-1206 (2009).
93. Chesler, N.C., Ku, D.N. & Galis, Z.S. Transmural pressure induces matrix-degrading activity in porcine arteries ex vivo. *American Journal of Physiology - Heart and Circulatory Physiology* **277**, H2002-H2009 (1999).
94. Zeerleder, S., Mauron, T., Lämmle, B. & Wuillemin, W.A. Effect of low-molecular weight dextran sulfate on coagulation and platelet function tests. *Thrombosis Research* **105**, 441-446 (2002).

95. Kamler, M., Pizanis, N., Hagl, S., Gebhard, M.M. & Jakob, H. Extracorporal circulation induced leukocyte/endothelial cell interaction is inhibited by Dextran. *Clinical Hemorheology and Microcirculation* **31**, 139-148 (2004).
96. Webb, A.R., A., B.S. & D., B.E. In vitro colloid osmotic pressure of commonly used plasma expanders and substitutes: a study of the diffusibility of colloid molecules. *Intensive Care Medicine* **15**, 116-120 (1988).
97. Rouleau, L., Rossi, J. & Leask, R. Concentration and Time Effects of Dextran Exposure on Endothelial Cell Viability, Attachment, and Inflammatory Marker Expression In Vitro. *Annals of Biomedical Engineering* **38**, 1451-1462 (2010).
98. Schaper, W. & Ito, W.D. Molecular Mechanisms of Coronary Collateral Vessel Growth. *Circ Res* **79**, 911-919 (1996).
99. Lin, S.L., Castaño, A.P., Nowlin, B.T., Lupher, M.L. & Duffield, J.S. Bone Marrow Ly6Chigh Monocytes Are Selectively Recruited to Injured Kidney and Differentiate into Functionally Distinct Populations. *The Journal of Immunology* **183**, 6733-6743 (2009).
100. KHORSHID, F.A. The Effect of the Medium Viscosity on the Cells Morphology in Reaction of Cells to Topography- I. *Proc. 2nd Saudi Sci. Conl,Fac. Sci.*, (2005).
101. Reneman, R. & Hoeks, A.G. Wall shear stress as measured in vivo: consequences for the design of the arterial system. *Medical & Biological Engineering & Computing* **46**, 499-507 (2008).
102. Cheng, C. *et al.* Large variations in absolute wall shear stress levels within one species and between species. *Atherosclerosis* **195**, 225-35 (2007).
103. Wang, C.H. *et al.* Assessment of mouse hind limb endothelial function by measuring femoral artery blood flow responses. *J Vasc Surg* **53**, 1350-8 (2011).
104. Huang, W., Fernando, S., Allard, L.F. & Sun, Y.-P. Solubilization of Single-Walled Carbon Nanotubes with Diamine-Terminated Oligomeric Poly(ethylene Glycol) in Different Functionalization Reactions. *Nano Letters* **3**, 565-568 (2003).
105. Fata, J.E., Chaudhary, V. & Khokha, R. Cellular Turnover in the Mammary Gland Is Correlated with Systemic Levels of Progesterone and Not 17β-Estradiol During the Estrous Cycle. *Biology of Reproduction* **65**, 680-688 (2001).
106. Mendelsohn, M.E. & Karas, R.H. Estrogen and the blood vessel wall. *Current Opinion in Cardiology* **9**, 619-626 (1994).
107. Stumpf, W.E. Steroid hormones and the cardiovascular system: Direct actions of estradiol, progesterone, testosterone, gluco- and mineralcorticoids, and soltriol [vitamin D] on central nervous regulatory and peripheral tissues. *Cellular and Molecular Life Sciences* **46**, 13-25 (1990).
108. Farhat, M.Y., Lavigne, M.C. & Ramwell, P.W. The vascular protective effects of estrogen. *Faseb Journal* **10**, 615-624 (1996).
109. Mendelsohn, M.E. & Karas, R.H. The Protective Effects of Estrogen on the Cardiovascular System. *New England Journal of Medicine* **340**, 1801-1811 (1999).
110. Blair, M.L. & Mickelsen, D. Plasma protein and blood volume restitution after hemorrhage in conscious pregnant and ovarian steroid-replaced rats. *American Journal of Physiology - Regulatory, Integrative and Comparative Physiology* **290**, R425-R434 (2006).
111. Slimmer, L.M. & Blair, M.L. Female reproductive cycle influences plasma volume and protein restitution after hemorrhage in the conscious rat. *American Journal of Physiology - Regulatory, Integrative and Comparative Physiology* **271**, R626-R633 (1996).

112. Yang, S. *et al.* Estrus cycle: influence on cardiac function following trauma-hemorrhage. *American Journal of Physiology - Heart and Circulatory Physiology* **291**, H2807-H2815 (2006).
113. Losordo, D.W., Kearney, M., Kim, E.Z., Jekanowski, J. & Isner, J.M. VARIABLE EXPRESSION OF THE ESTROGEN-RECEPTOR IN NORMAL AND ATHEROSCLEROTIC CORONARY-ARTERIES OF PREMENOPAUSAL WOMEN. *Circulation* **89**, 1501-1510 (1994).
114. Iafrati, M.D. *et al.* Estrogen inhibits the vascular injury response in estrogen receptor [alpha]-deficient mice. *Nat Med* **3**, 545-548 (1997).
115. Krasinski, K. *et al.* Estradiol Accelerates Functional Endothelial Recovery After Arterial Injury. *Circulation* **95**, 1768-1772 (1997).
116. Lindner, V. *et al.* Increased expression of estrogen receptor-beta mRNA in male blood vessels after vascular injury. *Circulation Research* **83**, 224-229 (1998).
117. Caligioni, C.S. Assessing Reproductive Status/Stages in Mice. in *Current Protocols in Neuroscience* (John Wiley & Sons, Inc., 2001).
118. Longo, G.M. *et al.* Matrix metalloproteinases 2 and 9 work in concert to produce aortic aneurysms. *The Journal of Clinical Investigation* **110**, 625-632 (2002).
119. Lee, S.L. *et al.* Luteinizing Hormone Deficiency and Female Infertility in Mice Lacking the Transcription Factor NGFI-A (Egr-1). *Science* **273**, 1219-1221 (1996).